



Calhoun: The NPS Institutional Archive
DSpace Repository

Theses and Dissertations

1. Thesis and Dissertation Collection, all items

1990-06

Error probabilities of frequency-hopped MFSK with self-normalization combining in a fading channel with partial-band interference

Briske, Michael W.

Monterey, California: Naval Postgraduate School

<http://hdl.handle.net/10945/27721>

This publication is a work of the U.S. Government as defined in Title 17, United States Code, Section 101. Copyright protection is not available for this work in the United States.

Downloaded from NPS Archive: Calhoun



<http://www.nps.edu/library>

Calhoun is the Naval Postgraduate School's public access digital repository for research materials and institutional publications created by the NPS community. Calhoun is named for Professor of Mathematics Guy K. Calhoun, NPS's first appointed -- and published -- scholarly author.

Dudley Knox Library / Naval Postgraduate School
411 Dyer Road / 1 University Circle
Monterey, California USA 93943

2

NAVAL POSTGRADUATE SCHOOL

Monterey, California

AD-A232 467



THESIS

DTIC
ELECTE
MAR 12 1991
S B D

ERROR PROBABILITIES OF FREQUENCY HOP
MFSK WITH SELF-NORMALIZATION COMBINING
IN A FADING CHANNEL WITH
PARTIAL-BAND INTERFERENCE

by

Michael W. Briske

June 1990

Thesis Advisor:

Tri T. Ha

Approved for public release; distribution is unlimited

91 3 06 039

UNCLASSIFIED

SECURITY CLASSIFICATION OF THIS PAGE

REPORT DOCUMENTATION PAGE				Form Approved OMB No 0704-0188	
1a REPORT SECURITY CLASSIFICATION UNCLASSIFIED			1b RESTRICTIVE MARKINGS		
2a SECURITY CLASSIFICATION AUTHORITY			3 DISTRIBUTION / AVAILABILITY OF REPORT Approved for public release; distribution is unlimited		
2b DECLASSIFICATION / DOWNGRADING SCHEDULE					
4 PERFORMING ORGANIZATION REPORT NUMBER(S)			5 MONITORING ORGANIZATION REPORT NUMBER(S)		
6a NAME OF PERFORMING ORGANIZATION Naval Postgraduate School		6b OFFICE SYMBOL (If applicable) EC	7a NAME OF MONITORING ORGANIZATION Naval Postgraduate School		
6c ADDRESS (City, State, and ZIP Code) Monterey, California 93943-5000			7b ADDRESS (City, State, and ZIP Code) Monterey, California 93943-5000		
8a NAME OF FUNDING / SPONSORING ORGANIZATION		8b OFFICE SYMBOL (If applicable)	9 PROCUREMENT INSTRUMENT IDENTIFICATION NUMBER		
8c ADDRESS (City, State, and ZIP Code)			10 SOURCE OF FUNDING NUMBERS		
			PROGRAM ELEMENT NO	PROJECT NO	TASK NO
					WORK UNIT ACCESSION NO.
11 TITLE (Include Security Classification) ERROR PROBABILITIES OF FREQUENCY-HOP MFSK WITH SELF-NORMALIZATION COMBINING IN A FADING CHANNEL WITH PARTIAL-BAND INTERFERENCE					
12 PERSONAL AUTHOR(S) BRISKE, Michael W.					
13a TYPE OF REPORT Engineer's Thesis		13b TIME COVERED FROM _____ TO _____		14 DATE OF REPORT (Year, Month, Day) 1990 June	
15 PAGE COUNT 123					
16 SUPPLEMENTARY NOTATION The views expressed in this thesis are those of the author and do not reflect the official policy or position of the Department of Defense or the U.S. Government.					
17 COSATI CODES			18 SUBJECT TERMS (Continue on reverse if necessary and identify by block number)		
FIELD	GROUP	SUB-GROUP	MFSK; self-normalization receiver; Reed-Solomon Coding; convolutional coding; fading path; partial-band interference		
19 ABSTRACT (Continue on reverse if necessary and identify by block number) Research entails derivation of statistical description of output from an MFSK receiver which uses self-normalization of the output from quadratic detectors. The system uses fast frequency hopping to provide diversity and assumes independent channels for each hop when the signal is recombined. The effects of fading channels are investigated for both Rayleigh and Rician fading channel descriptions. Probability of bit error is plotted for various signal-to-noise ratios (SNR) and different levels of diversity versus worst-case partial-band jamming. Analysis for Forward Error Correction coding is included for rate 1/2 and 1/3 convolutional codes and (n,k) Reed-Solomon Block codes. Probability of bit error is plotted for each code with various signal-to-noise ratios and diversity levels 1 to 4 versus worst-case partial-band jamming.					
20 DISTRIBUTION / AVAILABILITY OF ABSTRACT <input type="checkbox"/> UNCLASSIFIED/UNLIMITED <input type="checkbox"/> SAME AS RPT <input checked="" type="checkbox"/> DTIC USERS			21 ABSTRACT SECURITY CLASSIFICATION UNCLASSIFIED		
22a NAME OF RESPONSIBLE INDIVIDUAL HA, Tri T.			22b TELEPHONE (Include Area Code) 408-646-2788		22c OFFICE SYMBOL EC/Ha

DD Form 1473, JUN 86

Previous editions are obsolete

SECURITY CLASSIFICATION OF THIS PAGE

S/N 0102-LF-014-6603

UNCLASSIFIED

Approved for public release: distribution is unlimited

**ERROR PROBABILITIES OF FREQUENCY-HOPPED MFSK WITH
SELF-NORMALIZATION COMBINING IN A FADING CHANNEL WITH
PARTIAL-BAND INTERFERENCE**

by

Michael W. Briske
Captain, United States Army
BSEE, Rose-Hulman Institute of Technology, 1981

Submitted in partial fulfillment of the
requirements for the degree of

**MASTER OF SCIENCE IN ELECTRICAL ENGINEERING
AND ELECTRICAL ENGINEER**

from the

NAVAL POSTGRADUATE SCHOOL

June 1990

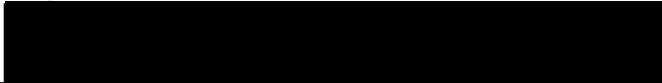
Author:



Michael W. Briske

Approved by:


Tri T. Ha, Thesis Advisor


Glen A. Myers, Co-advisor


John P. Powers, Chairman,
Department of Electrical and
Computer Engineering


Gordon E. Schacher,
Dean of Science and Engineering

ABSTRACT

Research entails derivation of statistical description of output from an MFSK receiver which uses self-normalization of the output from quadratic detectors. The system uses fast frequency hopping to provide diversity and assumes independent channels for each hop when the signal is recombined. The effects of fading channels are investigated for both Rayleigh and Rician fading channel descriptions. Probability of bit error for the uncoded performance is plotted for various signal-to-noise ratios (SNR) and different levels of diversity versus worst-case partial-band jamming. Analysis for Forward Error Correction coding is included for rate 1/2 and 1/3 convolutional codes and (n,k) Reed-Solomon Block codes. Probability of bit error is plotted for each code with various signal-to-noise ratios and diversity levels 1 to 4 versus worst-case partial-band jamming.



Accession For	
NTIS GRA&I	<input checked="checked" type="checkbox"/>
DTIC TAB	<input type="checkbox"/>
Unannounced	<input type="checkbox"/>
Justification	
By	
Distribution/	
Availability Codes	
Dist	Avail and/or Special
A-1	

TABLE OF CONTENTS

I.	INTRODUCTION	1
II.	BACKGROUND INFORMATION	3
	A. LOW-ALTITUDE SATELLITE SYSTEM	3
	B. THE COMMUNICATION CHANNEL	7
	C. DIVERSITY TECHNIQUES AND FREQUENCY-HOPPING SPREAD SPECTRUM	13
	D. THE SELF-NORMALIZATION RECEIVER	17
	E. ERROR CORRECTION CODING	19
	F. METHOD OF RESEARCH	20
III.	THE COMMUNICATION CHANNEL	21
	A. DESCRIPTION OF THE SIGNAL	21
	B. BINARY FREQUENCY SHIFT KEYING	31
	C. M-ARY FREQUENCY SHIFT KEYING	34
	D. NUMERICAL PROCEDURE	36
VI.	FORWARD ERROR CORRECTION	39
	A. REED-SOLOMON NON-BINARY BLOCK CODES	44
	B. CONVOLUTIONAL CODES	45
V.	DISCUSSION OF RESULTS	47
	A. UNCODED SYSTEM PERFORMANCE	49
	B. CODED SYSTEM PERFORMANCE	60

VI. CONCLUSIONS AND RECOMMENDATIONS	72
A. CONCLUSIONS	72
B. RECOMMENDATIONS	73
APPENDIX A - DERIVATION OF EQUATION (3.14)	74
APPENDIX B - DERIVATION OF EQUATION (3.28)	77
APPENDIX C - ADDITIONAL ILLUSTRATIONS	79
REFERENCES	110
INITIAL DISTRIBUTION LIST	112

LIST OF FIGURES

Figure 1.	Comparison of Geostationary Satellite Earth Coverage versus LASAT Earth Coverage	4
Figure 2.	The Portion of Low-altitude Satellite orbit with Satellites visible to an Earth Station	6
Figure 3.	Typical FH Transmitter and Receiver	15
Figure 4.	FH-MFSK Transmitter	16
Figure 5.	Self-Normalization FH-MFSK Receiver	18
Figure 6.	FH-MFSK Transmitter and Receiver Modified for FEC Coding .	40
Figure 7.	System Performance for various Partial-Band Jamming Ratios in a Rician-fading channel with $E_b/N_c = 13.35$ dB.	48
Figure 8.	System Performance for various Partial-Band Jamming Ratios in a Rician-fading channel with $E_b/N_o = 20$ dB.	48
Figure 9.	Uncoded System Performance for BFSK in a deeply-faded Rayleigh channel with $E_b/N_o = 20$ dB.	50
Figure 10.	Uncoded System Performance for BFSK in a moderately-faded Rayleigh channel with $E_b/N_o = 20$ dB.	51
Figure 11.	Uncoded System Performance for BFSK in a Rician-faded channel with $E_b/N_o = 20$ dB.	51
Figure 12.	Uncoded System Performance for BFSK in a nonfaded channel with $E_b/N_o = 20$ dB.	52
Figure 13.	Uncoded System Performance for BFSK in a Rician-faded channel with $E_b/N_o = 13.35$ dB.	53
Figure 14.	Uncoded System Performance for BFSK in a nonfading channel with $E_b/N_o = 13.35$ dB.	53

Figure 15. Uncoded Performance for 4-ary FSK in a Rayleigh-faded channel with $E_b/N_o = 20$ dB.	54
Figure 16. Uncoded Performance for 4-ary FSK in a Rician-faded channel with $E_b/N_o = 20$ dB.	55
Figure 17. Uncoded Performance for 4-ary FSK in a deeply-faded Rayleigh channel with $E_b/N_o = 20$ dB.	55
Figure 18. Uncoded Performance for 4-ary FSK in a Rician-faded channel with $E_b/N_o = 20$ dB.	57
Figure 19. Uncoded Performance for MFSK, $M = 2$ to 32, in a deeply-faded Rayleigh channel with $E_b/N_o = 20$ dB.	57
Figure 20. Uncoded Performance for MFSK, $M = 2$ to 32, in a moderately-faded Rayleigh channel with $E_b/N_o = 20$ dB.	58
Figure 21. Uncoded Performance for MFSK, $M = 2$ to 32, in a Rician-faded channel with $E_b/N_o = 20$ dB.	58
Figure 22. Uncoded Performance for MFSK, $M = 2$ to 32, in a nonfaded channel with $E_b/N_o = 20$ dB.	59
Figure 23. Uncoded Performance for a Noise-normalization Receiver, for $M = 2$ to 32, in a Rayleigh-faded channel, with $E_b/N_o = 20$ dB. .	59
Figure 24. Uncoded Performance for a Noise-normalization Receiver, for $M = 2$ to 32, in a Rician-faded channel, with $E_b/N_o = 20$ dB. ...	60
Figure 25. Reed-Solomon (7,3) Coded Performance for BFSK in a Rayleigh-faded channel with $E_b/N_o = 20$ dB.	61
Figure 26. Reed-Solomon (7,3) Coded Performance for BFSK in a Rician-faded channel with $E_b/N_o = 20$ dB.	61
Figure 27. Reed-Solomon (15,5) Coded Performance for BFSK in a Rayleigh-faded channel with $E_b/N_o = 20$ dB.	62
Figure 28. Reed-Solomon (15,5) Coded Performance for BFSK in a Rician-faded channel with $E_b/N_o = 20$ dB.	62
Figure 29. Rate 1/2 Convolutional Coded BFSK in a Rayleigh-faded channel with $E_b/N_o = 20$ dB.	64

Figure 30. Rate 1/2 Convolutional Coded BFSK in a Rician-faded channel with $E_b/N_o = 20$ dB.	64
Figure 31. Rate 1/3 Convolutional Coded BFSK in a Rayleigh-faded channel with $E_b/N_o = 20$ dB.	65
Figure 32. Rate 1/3 Convolutional Coded BFSK in a Rician-faded channel with $E_b/N_o = 20$ dB.	65
Figure 33. Coded Performance for BFSK, $L=2$ (solid) and $L=3$ (dashed) in a Rayleigh-faded channel with $E_b/N_o = 20$ dB.	66
Figure 34. Coded Performance for BFSK, $L=2$ (solid) and $L=3$ (dashed) in a Rician channel with $E_b/N_o = 20$ dB.	67
Figure 35. Coded Performance for 4-ary FSK, $L=2$ (solid) and $L=3$ (dashed) in a Rayleigh-faded channel with $E_b/N_o = 20$ dB.	67
Figure 36. Coded Performance for 4-ary FSK, $L=2$ (solid) and $L=3$ (dashed) in a Rician channel with $E_b/N_o = 20$ dB.	68
Figure 37. Coded Performance for 4-ary FSK, $L=2$ (solid) and $L=3$ (dashed) in a Rayleigh channel with $E_b/N_o = 20$ dB.	69
Figure 38. Coded Performance for 4-ary FSK, $L=2$ (solid) and $L=3$ (dashed) in a Rician-faded channel with $E_b/N_o = 20$ dB.	69
Figure 39. Coded Performance for 8-ary FSK, $L=2$ (solid) and $L=3$ (dashed) in a Rayleigh-faded channel with $E_b/N_o = 20$ dB.	71
Figure 40. Coded Performance for 8-ary FSK, $L=2$ (solid) and $L=3$ (dashed) in a Rician-faded channel with $E_b/N_o = 20$ dB.	71

ACKNOWLEDGEMENT

I would like to thank Professor Tri T. Ha for the opportunity to accomplish the research on my own with minimal guidance only when required to provide a better finished product. Many thanks go to Professor R. Clark Robertson, whose help all through the research was invaluable. Special thanks are extended to LT Chris Kmiecik, USCG, whose computer programming and debugging talents allowed me to graduate on time. Finally, a big thank you to Karen Callaghan, Code 32 Admin. Asst., whose helpfulness and sense of humor has made life bearable here at NPS.

DEDICATION

This thesis is dedicated to two people; my wife and my Father. To my wife, Kathy, for having tolerated my many mood swings over the last two quarters at NPS, I love you. And to my Father, your quiet strength has guided me to excel in all that I have ever pursued. Thank you both, for being there when I needed you.

I. INTRODUCTION

Military satellite communications systems currently rely on geostationary satellites as their means of connectivity. The greatest advantage afforded by the stationary orbit is that a relatively small number of satellites provide communication coverage for the entire earth's surface. The disadvantages include extremely high cost (hundreds of millions of dollars), requirement of telemetry and tracking systems for station keeping and accurate alignment of antenna systems, and the presentation of stationary targets for counter-measure operations.

A major concern is the vulnerability of the geostationary satellite to anti-satellite (ASAT) systems. Since the communication network is comprised of a relatively small number of satellites, the loss of even one could severely degrade the effectiveness of the system. At present, their 22,000-mile orbits make them relatively safe from countermeasures; however, developing technology ensures a future threat of destruction or disruption.

The development of a low-altitude-satellite (LASAT) communication system could alleviate many of the problems mentioned above. The design methodology is to build relatively low-cost (several million dollars) satellites that would be put into low-altitude random orbits. The proposed usage would be as an emergency restoral system in which a large number of satellites are launched in rapid succession. The

large number of satellites would essentially preclude any ASAT system, no matter how sophisticated, from totally disrupting the network.

This document provides a general overview of the LASAT proposal and analysis of a self-normalization receiver to be used in the proposed LASAT system. Chapter II provides a LASAT overview and a detailed discussion of the communication channel and problems associated with use of multiple repeaters in a single network. The analysis of the communication link in Chapter III includes:

- effects of multipath fading on the signal,
- derivation of the probability of bit error for a Frequency-hopped Binary Frequency shift Keyed (FH-BFSK) signal, and
- derivation of the probability of bit error for a Frequency-hopped M-ary Frequency Shift Keyed (FH-MFSK) signal using a union bound.

Chapter IV discusses application of forward error correction (FEC) coding on the bit stream. The results of all analyses are presented in Chapter V and conclusions are discussed in Chapter VI.

II. BACKGROUND INFORMATION

A. LOW-ALTITUDE SATELLITE SYSTEM

The primary mission of Low-Altitude Satellites (LASAT) is emergency restoral or short-term crisis communications. As such, the satellites will be expected to provide communication support for no longer than several weeks. The system will consist of a large number of satellites placed in random low orbits, thereby eliminating the need for station-keeping and telemetry subsystems. The satellite will provide access for digitized voice and encrypted data between major ground force commanders.

The satellites will use broad-beam antennas that provide coverage of the entire visible portion of the earth relative to its orbital location. Due to the physics of the low orbit, the area of coverage will be considerably smaller than that associated with a geostationary satellite (see Figure 1), and the window for communications with any particular satellite will be on the order of minutes [Ref. 1:p. 44]. This will require a high density of satellites to provide continuous communications to the users. The only control system required for the satellite is a gyroscope and earth sensor to keep its antenna pointed radially at the center of the Earth's surface directly beneath it. There is no requirement in this application for satellite-to-satellite communications, since they will be used strictly as repeaters.

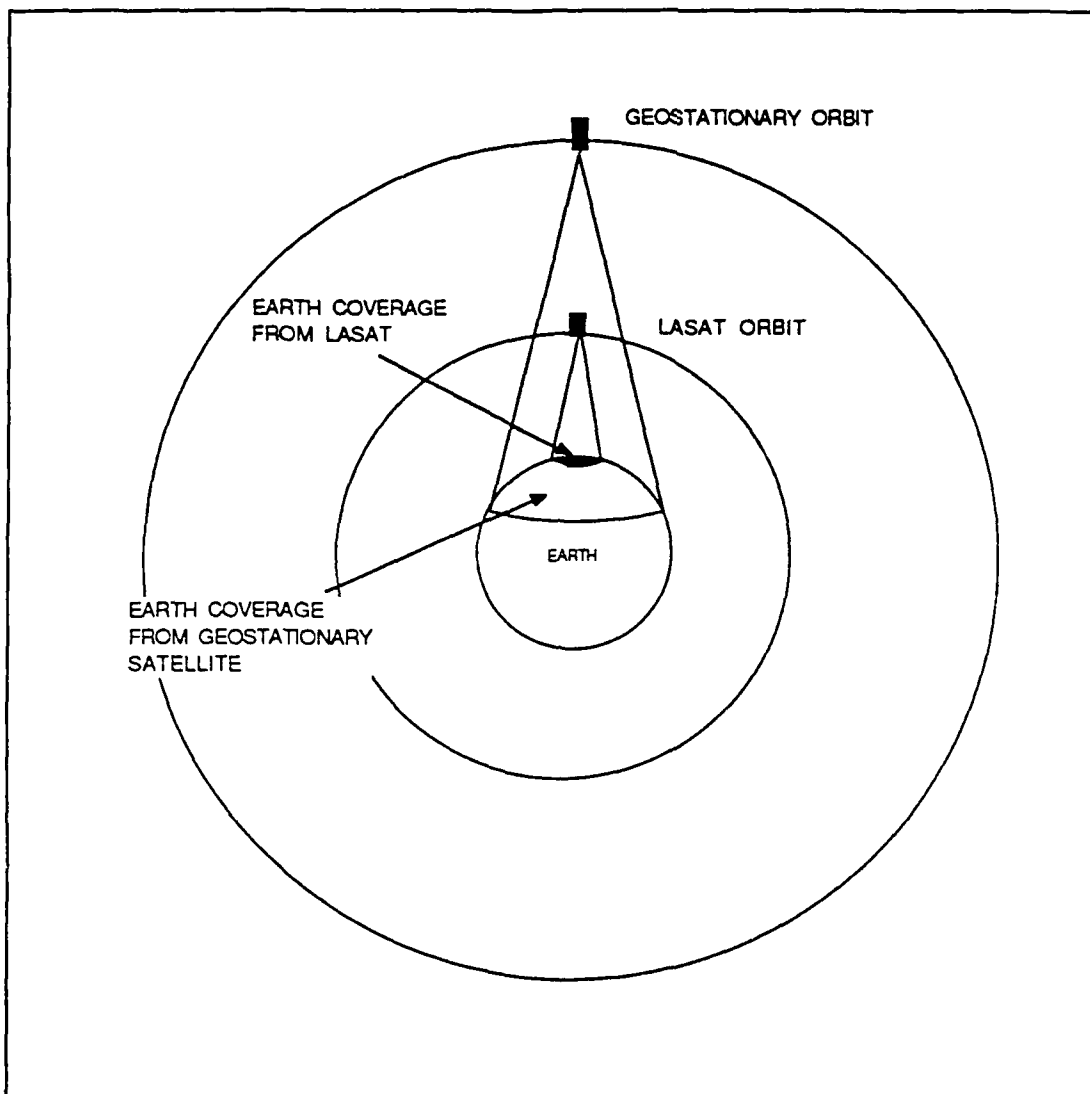


Figure 1. Comparison of Geostationary Satellite Earth coverage versus LASAT Earth coverage.

Although the use of random orbits and multiple satellites lessens the threat against them, it also necessitates employment of omni-directional antennas for the ground stations. These antennas have inherently low gain, so it is expected that the system must operate at fairly large values of input signal powers. An additional

drawback is that the antenna will accept signals from any satellite within view and from any direction. Multiple signals, originating from several satellites and/or multipath reflections, create fading effects on the desired signal. This is discussed further in Chapter II.B.

Finally, the use of some type of access-restriction coding may be required to prevent unauthorized use or to enhance anti-jamming capabilities of the satellites. This, however, is beyond the scope of this research. This section concentrates on the distribution of satellites in random orbits and the average number that will be seen by a particular ground station.

The satellites are assumed to be contained within the volume of a shell between altitudes h_1 and h_2 above the Earth's surface with volume

$$V = \frac{4}{3} \pi (R_2^3 - R_1^3) \quad (2.1)$$

where

$$\begin{aligned} R_1 &= R_e + h_1 \\ R_2 &= R_e + h_2 \end{aligned} \quad (2.2)$$

and R_e is the radius of the earth. The probability density function (pdf) for the number of satellites in view has been derived [Ref. 2] as a function of the total number of satellites in orbit and a ratio of the volume of space that is observable to a ground station versus the total volume of space surrounding the earth to an altitude of h_2 . This area is shown in Figure 2 as the shaded portion between the two

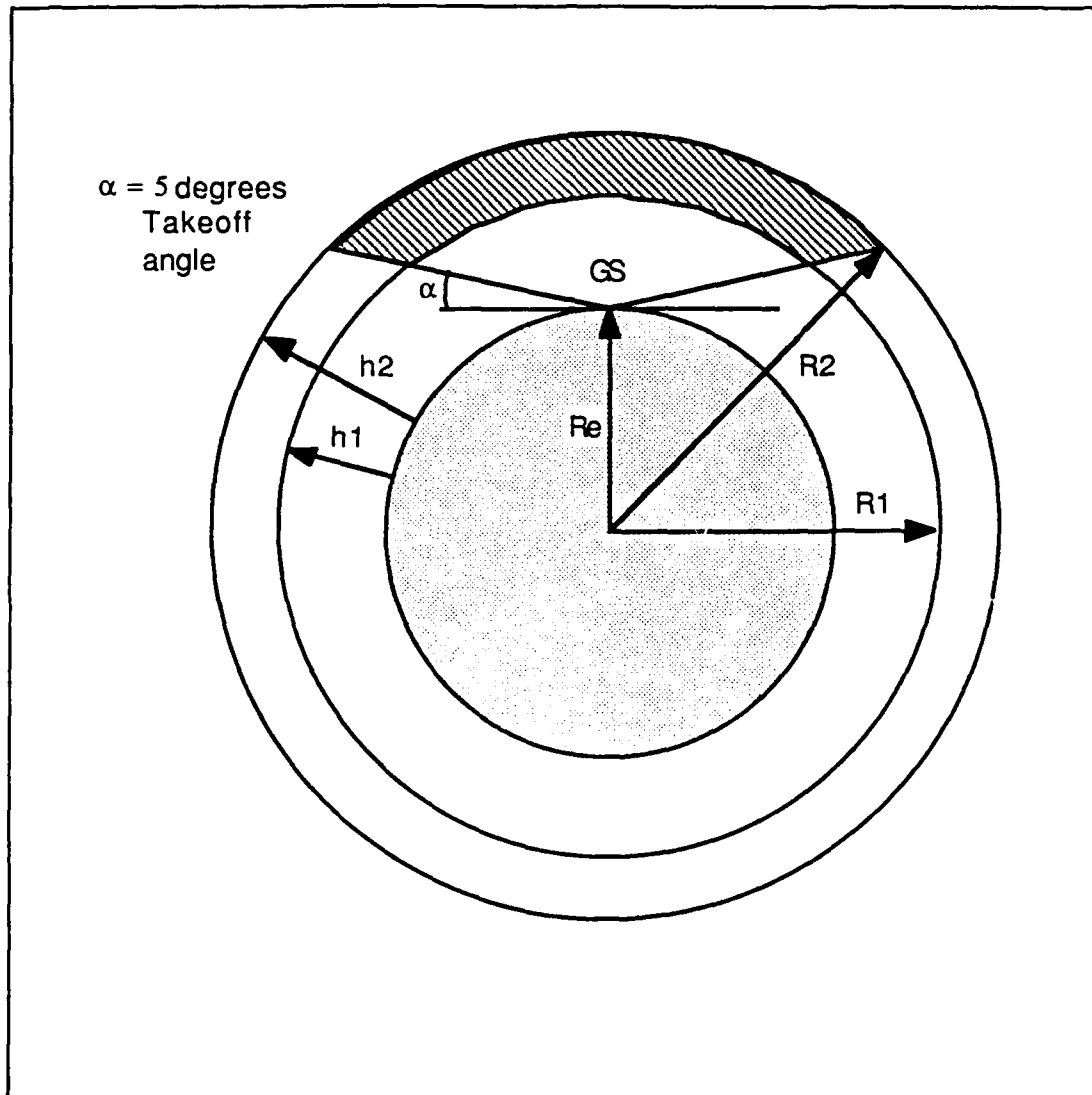


Figure 2. The Portion of Low-altitude Satellite orbit with Satellites visible to an Earth Station.

outermost concentric circles. The pdf for the number n in view results from dividing the area into m small volume elements of volume v and taking the limit as $v \rightarrow 0$ and $m \rightarrow \infty$. The result is a Poisson distribution:

$$f_N(n) = \frac{(\rho v)^n}{n!} e^{-\rho v}, \quad (2.3)$$

where ρ is the density of L satellites in the total volume described by (2.1). The mean and variance of the Poisson random variable are

$$\begin{aligned}\bar{n} &= \rho v = \frac{Lv}{V}, \\ \sigma_n^2 &= \rho v = \frac{Lv}{V}.\end{aligned}\tag{2.4}$$

Therefore, the number of satellites in view will depend directly on the number in orbit and inversely on the altitudes of their orbits.

For $L = 250$ total satellites, assuming $h_1 = 550$ km (300 NM) and $h_2 = 750$ km (400 NM), the number in view averages 11.54; for $L = 150$ satellites, the average is 6.92. Since all satellites in view are expected to receive and retransmit any signal at its input, the ground stations will have to contend with multiple copies of the same information originating from sources at different locations. The combination of multipath signals in the receiver causes the fading phenomenon mentioned above and is elaborated on in the following section.

B. THE COMMUNICATION CHANNEL

The multiple signals arrive at the desired ground station with various arrival times, phases, and amplitudes. The result is similar to the effect of a single transmission that is reflected, refracted and/or delayed by a time-varying channel. In this situation, multiple signals are developed by multiple transmitters and variations in the atmosphere. Since the effects are similar for both cases, the analysis here

simply combines all effects and follows the discussion presented by Proakis [Ref. 3:pp. 454-457] on the effects of a time-varying channel on received signal components. Multipath fading, that is due primarily to the combination of two reflected signals that arrive as mirror images of the intended signal, is referred to as *specular*. When the received signal is the combination of many signals, it produces a noise-like component referred to as *diffuse*. The received signal here will consist of the sum of all signals with different delays and attenuation factors associated with the path to each of the originating transmitters. This can be represented numerically as

$$r(t) = \sum_n \alpha_n(t) s[t - \tau_n(t)] \quad (2.5)$$

where $\alpha_n(t)$ is the attenuation factor for the signal received from the n th source or path and $\tau_n(t)$ is the delay associated with that path. If the transmitted signal were a single sine wave, the attenuation would have to be quite severe to have an appreciable effect on the received vector. However, the overall effect of multiple signals is the result of combining several signals with various phases. The phase of a sine wave changes by 2π radians whenever τ_n changes by $1/f_c$, where f_c is the carrier frequency of the desired signal. Since the system will probably operate in a range from upper Very-high-frequency (VHF) to the Super-high-frequency (SHF) spectrum, $1/f_c$ is a relatively small number. Therefore, small changes in delay or path

length can cause large changes in the signal phase. The wavelength at 100 MHz, for example, is

$$\lambda = \frac{c}{f_o} \approx 3 \text{ m}, \quad (2.6)$$

where f_o is an average carrier frequency and $c = 3 \times 10^8$ m/s is the free space speed of light. Thus, a difference of only 1.5 m between two path lengths would result in destructive interference at the receiver. The numerous phases, or corresponding delays, of the multiple received signals can be due to path length differences to the various satellites, fluctuations in the atmospheric conditions between transmitter and receiver, or reflections from objects in the path. Regardless of the cause, the effect at the input to the receiver is a signal that appears to fade at random times due to destructive addition of the sine waves with unequal phases. The phase changes can be viewed as uniformly distributed from 0 to 2π . The summation of multiple samples, by means of the Central Limit Theorem, leads to a Gaussian random variable. The fading signal phenomenon affects the amplitude of the received composite signal, which can be viewed as the envelope of the process (this is important later since a noncoherent envelope detector will be used). Therefore, the amplitude of the faded signal can be represented as a Rayleigh-distributed random variable. Assuming that the received signal contains both a direct (or specular) and some number of indirect (or diffuse) signal components leads to a Rayleigh distribution with a mean value

other than zero, or (more often termed) a Rician random variable. The amplitude of the received signal can be described statistically [Ref. 4:p. 108] by the pdf,

$$f_A(a) = \frac{a}{\sigma^2} \exp\left[-\frac{a^2 + \alpha^2}{2\sigma^2}\right] I_0\left(\frac{a\alpha}{\sigma^2}\right) \quad a > 0, \quad (2.7)$$

where α^2 is the power in the direct component, $2\sigma^2$ is the power of the diffuse components, and $I_0(x)$ is the zeroth-order modified Bessel function of the first kind. When the direct component power goes to zero, which occurs in times of deep fading on the channel, the function reverts to the Rayleigh function described above and the pdf becomes

$$f_A(a) = \frac{a}{\sigma^2} \exp\left[-\frac{a^2}{2\sigma^2}\right] \quad a > 0. \quad (2.8)$$

The expected fading distribution is averaged over the receiver output samples to obtain a probabilistic description of the most likely transmitted signal that caused the outcome. The fading that occurs on the channel can be defined as slow or fast relative to the signal bandwidth and duration. Slow fading is when the channel remains constant for the duration of a single transmitted signal, while fast fading results in significant change in the channel through a single transmitted signal. The two terms used to describe the effects of fading are the coherence bandwidth and coherence time of the channel [Ref. 3:pp. 464-466].

The coherence bandwidth of the channel is defined as the frequency range over which the amplitude and phase of the transmitted signal are relatively constant (the signal passes undistorted). It is represented as

$$(\Delta f)_c = \frac{1}{T_m}, \quad (2.9)$$

where $(\Delta f)_c$ is the coherence bandwidth and T_m is the multipath spread of the channel. That is, T_m is a measure of the shift allowed to produce a non-zero output for the autocorrelation of a very narrow pulse sent over the channel. If two sinusoids with frequency separation greater than the coherence bandwidth are transmitted simultaneously, they will be affected differently by the channel. In fact, the output for each frequency can be considered as though it were from an independent channel. If the signal bandwidth is small compared to the coherence bandwidth, the channel is described as *frequency non-selective* and vice versa as *frequency selective*. A frequency selective channel is undesirable since the signal is severely distorted during transmission.

The coherence time is defined as

$$(\Delta t)_c = \frac{1}{B_d}, \quad (2.10)$$

where B_d is the Doppler spread of the channel. Doppler spread is the measure of spectral spreading of an impulse sent through the channel. A slowly changing channel has a large coherence time and, correspondingly, a small Doppler spread. This

implies that signals of duration less than the coherence time pass through the channel relatively unaltered. If the transmitted signal has duration longer than the coherence time, distortion in the form of intersymbol interference may result.

The distinction between fast and slow fading can now be expressed in terms of the *spread factor* of the channel as

$$T_m B_d \gtrless 1. \quad (2.11)$$

where the less than criteria holds for slow fading. This implies that if a signal can be found with a bandwidth $W \ll (\Delta f)_c$ and a signal duration $T \ll (\Delta t)_c$, the channel can be modelled as slow fading.

Fast fading, or scintillation, by definition is the rapid variation in the amplitude and phase of the transmitted signal (or when the spread factor > 1). This is caused primarily by turbulence or irregularities in the channel. Lack of a simple model of the effects of fast fading make analysis difficult, if not impossible. However, proper choice of the signals used in the system, as described above, preclude the occurrence of fast fading, so it is ignored in most applications and analyses.

The M-ary FSK signals discussed here are assumed to have a bandwidth less than the channel coherence bandwidth. Additionally, the signal duration is assumed shorter than the channel coherence time (i.e., the signal rate is much greater than the Doppler spread). Selecting signals such that their center frequencies are separated by greater than $(\Delta f)_c$ Hz insures the received signals are independent and some type

of signal processing can be used to improve the ability of the receiver to determine which of the M signals was transmitted.

C. DIVERSITY TECHNIQUES AND FREQUENCY-HOPPING SPREAD SPECTRUM

The most common technique used to improve receiver performance is diversity of some type. Diversity is the action of sending identical information from the source to receiver by L independent means, either simultaneously or sequentially. The receiver gleans the information contained in each of the separate signals, combines the individual channels, and delivers a best estimate of the information sent to the receiver. Diversity is accomplished using one of the following techniques [Ref. 3:p. 463]:

- Frequency Diversity - use of L frequencies to transmit the signal (frequency spacing assumed greater than the coherence bandwidth $(\Delta f)_c$).
- Time Diversity - the signal is sent in L time slots (the slot separation is greater than the coherence time $(\Delta t)_c$).
- Spatial Diversity - the system employs more than one antenna (separated by at least 10 wavelengths of the carrier frequency).
- Polarization Diversity - the signal is transmitted simultaneously over multiple polarizations.

Each of the above schemes offers advantages and disadvantages. Spatial and polarization techniques are not applicable due to the mobility of ground stations and the changing path associated with LASAT systems. Frequency and time diversity offer the simplest methods for implementation. Frequency-hopping (FH) and Direct-sequence (DS) spread spectrum (SS) are the two means to be considered. DS-SS

employs transmission over L frequencies simultaneously, while FH-SS transmits on L single frequencies sequentially. These methods each have advantages and disadvantages and, while either method is suitable for the LASAT system, the emphasis here will be on a frequency-hopping system.

Frequency-hopping (FH) systems use a pseudo-random generator to select sequential carrier frequencies for transmission. A typical FH transmitter-receiver pair is shown in Figure 3 [Ref. 5:p. 349]. Consider here that the information bits with rate R_b are modulated onto the carrier by means of an arbitrary scheme. The goal is to provide multiple independent copies of the same message that can be processed to obtain a best estimate of the transmitted signal. Fast hopping (when the same information is carried on more than one hop) provides the desired frequency and time diversity for improved receiver performance.

A fast hopping FH communication system can be used to offset the effects of both thermal noise and partial band noise jamming, which has been shown to be effective against a FH system [Ref. 5:pp. 570-580]. Provided that the hops are spaced by time intervals

$$T_H = \frac{1}{R_H} , \quad (2.12)$$

where R_H is the hopping rate of the transmitter, and that the adjacent output frequencies are greater than $(\Delta f)_c$, the output of the receiver from each hop is independent of any other hop. This is based on the requirements for independence in terms of the coherence time and bandwidth of the channel.

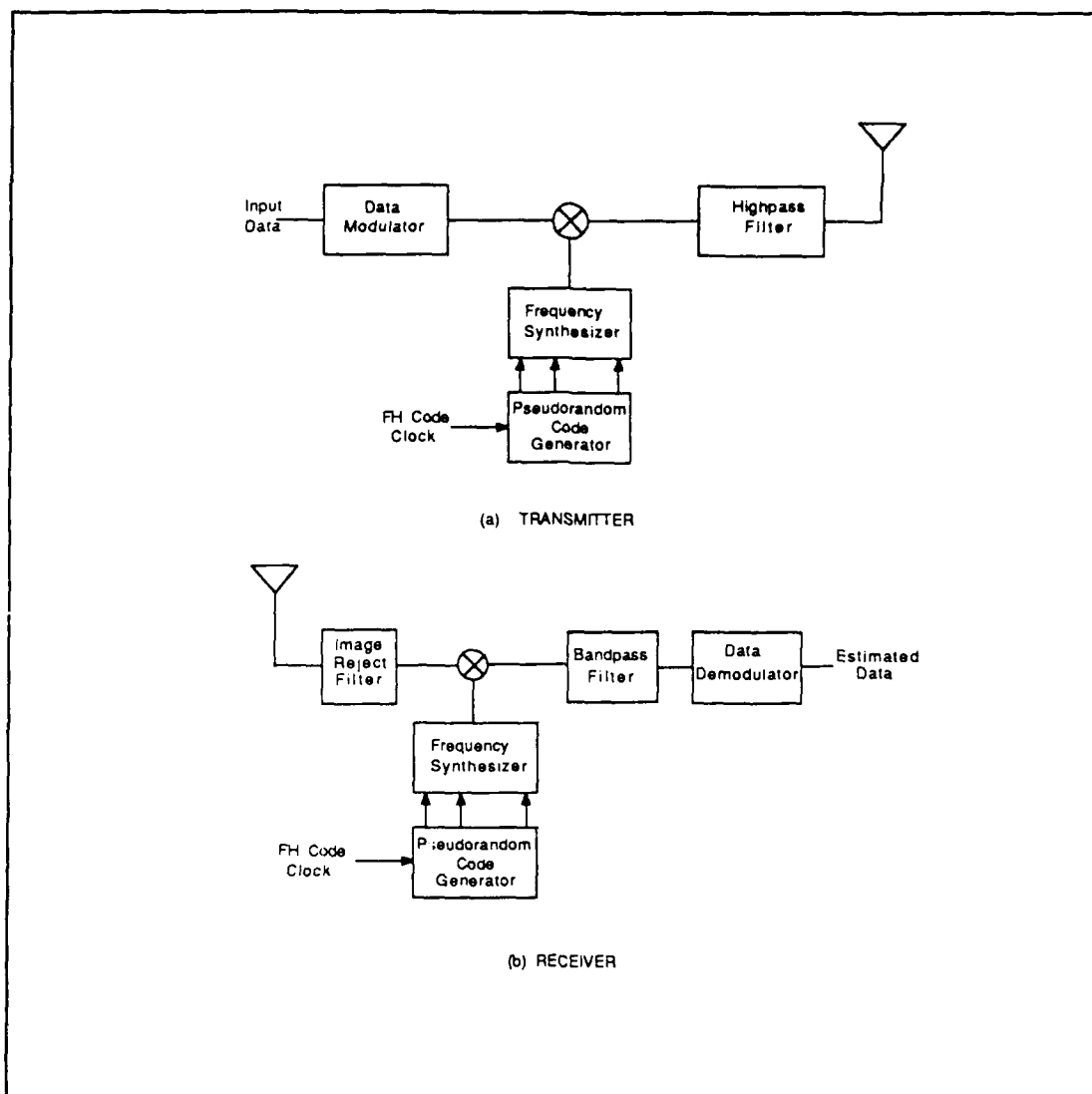


Figure 3. Typical FH Transmitter and Receiver [Ref. 5:p.349].

M-ary frequency-shift-keyed (MFSK) modulation is the usual choice for FH systems. One of M frequencies is chosen to modulate the carrier based on k bits input to the M-ary source coder of Figure 4, where $M = 2^k$. The frequencies are assumed spaced to be orthogonal to all others, which implies they are at least $1/kT_b$

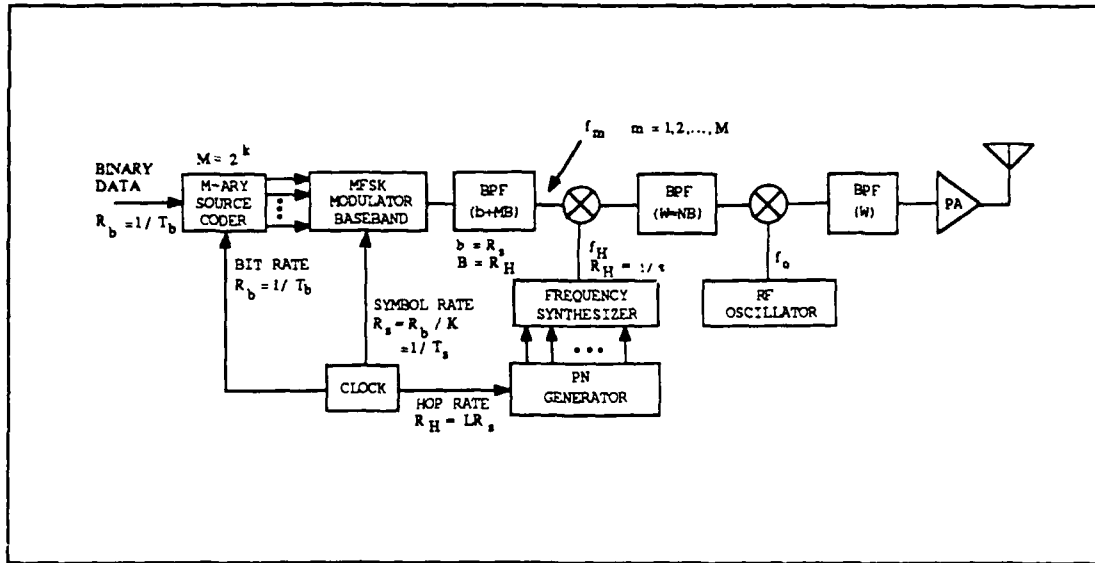


Figure 4. FH-MFSK Transmitter.

Hz apart, where T_b is the bit duration. The information rate R_b and symbol rate R_s are related by

$$R_b = kR_s = \frac{1}{T_b} = \frac{k}{T_s} \quad (2.13)$$

or equivalently,

$$T_s = kT_b \quad (2.13a)$$

where T_s is the symbol duration. Each symbol is divided into L chips for a fast hopping system. Since the chip duration T_H is shorter than the symbol duration T_s , orthogonal signalling now requires that the M frequencies be spaced $B = 1/T_H = L/kT_b$. The total bandwidth for the system now becomes

$$W = N_H MB = \frac{N_H ML}{KT_b}, \quad (2.14)$$

where N_H is the total number of carrier frequencies generated by the frequency synthesizer, and the bandwidth is still constrained by,

$$\frac{ML}{kT_b} > (\Delta f)_c. \quad (2.15)$$

This satisfies both the channel and orthogonality requirements to obtain independent samples and minimizes distortion of the signal over a single hop.

D. THE SELF-NORMALIZATION RECEIVER

The MFSK signal is easily generated by the transmitter in Figure 4, but demodulation at the receiver can be accomplished by a number of different schemes. Coherent detectors have been found to deliver the best performance (lowest error rates) for a given signal-to-noise ratio (SNR) [Ref. 6:pp. 138-152]. However, signals through a fading channel undergo rapid phase changes that make the use of a coherent detector impractical since they rely on the information contained in the phase for demodulation. Use of a noncoherent detector is the best alternative, given that the modulation scheme can be designed to produce orthogonal signals under the constraints in the preceding section. For purposes of the analysis, the receiver (Figure 5) employs a square-Law detector, or synonymously a quadratic detector, to facilitate simulation of the receiver performance. A comparison of the error performance versus SNR for envelope and quadratic detectors used for MFSK systems without

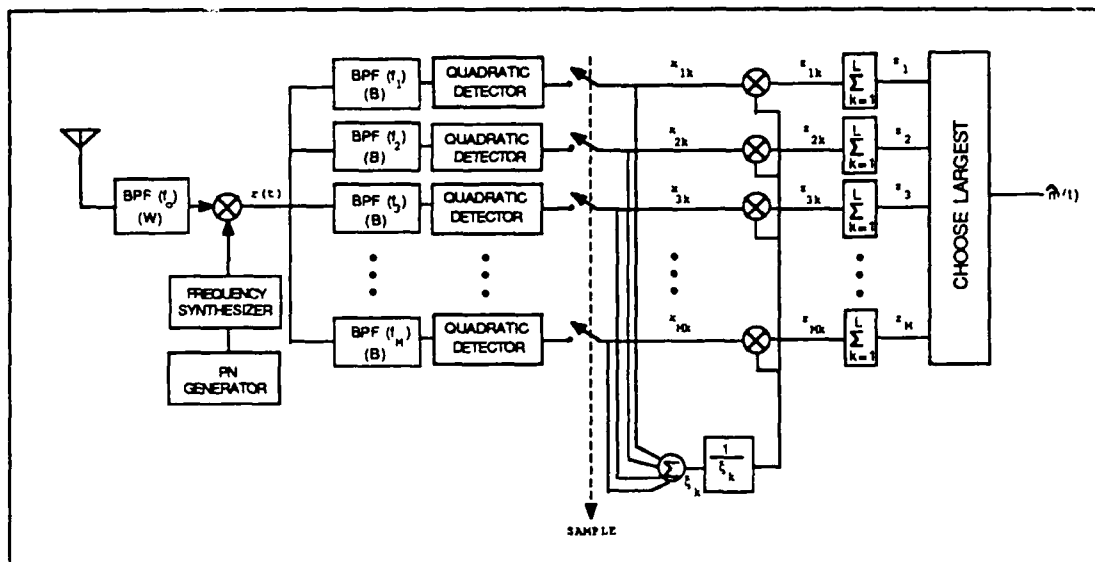


Figure 5. Self-Normalization FH-MFSK Receiver.

normalization has been shown [Ref. 4:p. 263] to be less than 0.2 dB for all values of M . This same assumption is applied here since analysis would not be possible otherwise. The receiver is considered subject to worst-case partial-band jamming: (meaning the jammer concentrates its noise jamming power over a portion η of the total hopping bandwidth, where $0 \leq \eta \leq 1$). The jammer determines the value of η to produce the highest data error ratio in the receiver based on knowledge of the signal-to-noise ratios for both jammer and thermal noise at the receiver. In this respect some of the hops will have both thermal and jamming noise, while others have just thermal noise. In order to neutralize the effects of the noise, the output of the detector is normalized by the sum of the outputs from all M channels. Assuming the noise is a zero-mean Gaussian process, the sum of the M samples will tend toward a constant value when a signal is present in any of the channels since the sum of the Gaussian noise samples will tend toward zero. After normalization, the

channel with a signal present will be averaged toward one and the other channels will be averaged toward zero. Then combining the L independent hops will produce the largest output from the detector with its corresponding signal present at the receiver input. The receiver error performance is found from a probabilistic description of the normalized samples (Chapter III). The assumption that the jammer can find the optimal value of η to cause the highest possible error ratio is not likely, but it does provide an upper bound on error rates for the self-normalization receiver.

E. ERROR CORRECTION CODING

While the system described above is dependent on the received SNR for a given performance level, the actual performance for the system can be significantly improved using various forward error correcting (FEC) coding methods. This increase in performance is called coding gain and is defined as the difference between the SNR required to achieve a given error performance with coding and without. In particular, convolutional codes and Reed-Solomon codes are applied to the data streams in Chapter IV. Convolutional codes were selected for their ease of implementation and Reed-Solomon for the power of their correction capability [Ref. 7:pp. 170,288]. The Reed-Solomon codes are very well suited for correction of burst errors (errors in successive bits), which are highly likely in the case of electrical storms or the energy-saturated electromagnetic environment of the battlefield. Also, transition from satellite-to-satellite may provide periods of missing data if no other satellites are available to retransmit the desired signals. The convolutional codes used are binary codes with constraint length 7, and rates $1/2$ and $1/3$. The rate indicates

the ratio of information bits to total bits transmitted (for a rate 1/2 code, the number of information bits equals the number of overhead bits).

F. METHOD OF RESEARCH

The thesis entails derivation of the equations necessary to obtain system performance of the self-normalizing receiver for varying levels of SNR and signal to jamming ratios. The system equations derived in Chapter III are modelled in a computer simulation and curves plotted for several cases of uncoded and coded performance. Chapter IV provides details of the data coding schemes used to improve system performance and Chapter V the results of the analysis. The final chapter provides conclusions and comments on the results from the simulation and suggested topics for further investigations.

III. THE COMMUNICATION CHANNEL

A. DESCRIPTION OF THE SIGNAL

Analysis of the communications link proceeds from the discussion in Chapter II for the fading channel to derive an analytical expression for the probability of bit error. Derivation of probability of error begins with a description of the signal used as the communications means, M-ary Frequency Shift Keying (MFSK). The received signal will be represented by one of M frequencies occurring one at a time at the input of the receiver. We assume that the frequency has been dehopped with perfect timing. Although this is not a trivial matter, synchronization has been accomplished by many methods and can be assumed available for our purposes. The received signal, assuming the presence of the frequency associated with the first channel, will take the form of:

$$r_k(t) = \sqrt{2S}a_k \cos(\omega_1 t + \theta_k) + n_k(t), \quad k = 1, 2, \dots, L, \quad (3.1)$$

where k is a reference of the hop being received and ω_1 is the frequency of the first channel. This signal can be rewritten in terms of in-phase and quadrature components as:

$$\begin{aligned}
r_k(t) &= \sqrt{2S}a_k(\cos \omega_1 t \cos \theta_k - \sin \omega_1 t \sin \theta_k) \\
&\quad + n_{ck}(t) \cos \omega_1 t + n_{sk}(t) \sin \omega_1 t \\
&= [\sqrt{2S}a_k \cos \theta_k + n_{ck}(t)] \cos \omega_1 t - [\sqrt{2S}a_k \sin \theta_k + n_{sk}(t)] \sin \omega_1 t \\
&= x_{ck}(t) \cos \omega_1 t - x_{sk}(t) \sin \omega_1 t
\end{aligned} \tag{3.2}$$

where $n_{ck}(t)$ and $n_{sk}(t)$ are the independent in-phase and quadrature components of a white Gaussian noise process. The time dependency is dropped based on sampling the output at times kT_H . Then the quadratic detector output for channel 1 provides an envelope squared signal of the form:

$$\begin{aligned}
x_{1k} &= x_{ck}^2 + x_{sk}^2 \\
&= (\sqrt{2S}a_k \cos \theta_k + n_{ck})^2 + (\sqrt{2S}a_k \sin \theta_k + n_{sk})^2
\end{aligned} \tag{3.3}$$

and the other $M-1$ channels

$$x_{ik} = n_{ck}^2 + n_{sk}^2 \quad i=2,3,\dots,M. \tag{3.4}$$

The channels are assumed subject to partial band jamming as described in Chapter II. The jammer concentrates its total power over a fraction η of the bandwidth W , where $0 \leq \eta \leq 1$. Since the jammer has an average spectral density

value of $N_j = J/W$ W/Hz, the jamming spectral density in the fraction of W that is jammed is N_j/η W. The jamming signal is added to the received signal as another Gaussian noise source with variance $\sigma^2 = N_j B/\eta$. The resulting output from the detectors are

$$x_{1k} = (\sqrt{2S}a_k \cos \theta_k + n_{ck} + j_{ck})^2 + (\sqrt{2S}a_k \sin \theta_k + n_{sk} + j_{sk})^2 . \quad (3.5)$$

and for the other channels

$$x_{ik} = (n_{ck} + j_{ck})^2 + (n_{sk} + j_{sk})^2, \quad i=2,3,\dots,M. \quad (3.6)$$

where j_{ck} and j_{sk} are the in-phase and quadrature components of the jamming signal.

The error probability for binary FSK without fading have been derived in previous studies [Ref. 8]. The results are extended here for the MFSK case over a fading channel. Without loss of generality, it is assumed that the signal for channel 1 was sent. Assuming equally likely M-ary symbols, the probability of symbol error, given signal 1 is present, is

$$P_s(e) = \sum_{i=0}^L P_i P_s(e|i) , \quad (3.7)$$

where

$$P_i = \binom{L}{i} \eta^i (1-\eta)^{L-i}, \quad (3.8)$$

is the probability that i out of L hops are jammed, and

$$P_s(e|i) = 1 - P_s(c|i), \quad (3.9)$$

is the probability of an error decision based on i hops out of L total hops jammed. The probability $P_s(c|i)$ in (3.9) is the probability of a correct decision given signal 1 was sent and i hops were jammed.

The probability density function of the output signal is required to calculate the probability of error for the system. When the input to a quadratic detector is a sine wave plus Gaussian noise, the output can be described statistically as a non-central gamma distributed random process. The gamma distribution is the generalized chi-squared distribution for an arbitrary variance where chi-squared has variance normalized to one. The density function for a given amplitude a_k is [Ref. 4:p. 118],

$$f_{x_{1k}|A_k}(x_{1k}|a_k) = \frac{1}{2\sigma_k^2} \exp\left[-\frac{x_{1k} + 2Sa_k^2}{2\sigma_k^2}\right] I_0\left(\frac{\sqrt{2Sx_{1k}}a_k}{\sigma_k^2}\right), \quad (3.10)$$

where

$$\sigma_k^2 = \begin{cases} BN_o & \text{with probability } 1-\eta \\ B(N_o + N_J/\eta) & \text{with probability } \eta \end{cases}, \quad (3.11)$$

which corresponds to non-jammed and jammed hops respectively.

The fading component is considered to be Rician as described in Chapter II, and its probability density is

$$f_{A_k}(a_k) = \frac{a_k}{\sigma^2} \exp\left[-\frac{a_k^2 + \alpha_k^2}{2\sigma^2}\right] I_0\left(\frac{a_k \alpha_k}{\sigma^2}\right), \quad (3.12)$$

where α_k is the relative strength of the direct component and $2\sigma^2$ is the power of the indirect (or diffuse) components as discussed previously. The unconditional pdf is found by evaluating

$$\begin{aligned} f_{x_{1k}}(x_{1k}) &= \int_0^\infty f_{x_{1k}|a_k}(x_{1k}|a_k) f_{A_k}(a_k) da_k \\ &= \int_0^\infty \left[\frac{a_k}{2\sigma_k^2\sigma^2} \right] \exp\left[-\frac{x_{1k} + 2Sa_k^2}{2\sigma_k^2}\right] \exp\left[-\frac{a_k^2 + \alpha_k^2}{2\sigma^2}\right] \times \\ &\quad I_0\left(\frac{\sqrt{2Sx_{1k}}a_k}{\sigma_k^2}\right) I_0\left(\frac{\alpha_k a_k}{\sigma^2}\right) da_k. \end{aligned} \quad (3.13)$$

The integral yields (a complete derivation is given in appendix A)

$$f_{x_{1k}}(x_{1k}) = \frac{1}{2(\sigma_k^2 + 2S\sigma^2)} \exp \left[-\frac{1}{2} \left(\frac{x_{1k} + 2S\alpha_k^2}{\sigma_k^2 + 2S\sigma^2} \right) \right] I_0 \left(\frac{\sqrt{2Sx_{1k}} \alpha_k}{\sigma_k^2 + 2S\sigma^2} \right). \quad (3.14)$$

This is the probability density function of the signal at the output of the quadratic detector shown in Figure 4. After sampling, the outputs from all M channels are summed to produce the self-normalization factor ζ_k as

$$\zeta_k = \sum_{m=1}^M x_{mk}. \quad (3.15)$$

Each of the outputs are divided by ζ_k which yields the desired self-normalized samples z_{mk} . To obtain the pdf of z_{mk} , the new random variable,

$$v_k = \sum_{m=2}^M x_{mk}, \quad (3.16)$$

is introduced as an auxiliary variable. The pdf of each of the $M-1$ channels with only Gaussian noise present is Gamma distributed with one degree of freedom

$$f_{x_{mk}}(x_{mk}) = \frac{1}{2\sigma_k^2} \exp \left[-\frac{x_{mk}}{2\sigma_k^2} \right], \quad (3.17)$$

where σ_k^2 is given in (3.11). The sum of $M - 1$ of these variables is gamma distributed with $M - 1$ degrees of freedom [Ref. 4:p. 112] and the result is

$$f_{v_k}(v_k) = \left(\frac{1}{2\sigma_k^2} \right)^{(M-1)} \frac{1}{\Gamma(M-1)} v_k^{(M-2)} \exp \left[-\frac{v_k}{2\sigma_k^2} \right], \quad (3.18)$$

where

$$\Gamma(M-1) = (M-2)! . \quad (3.19)$$

Now the normalized output from channel one is defined as

$$z_{1k} = \frac{x_{1k}}{x_{1k} + v_k} = \frac{x_{1k}}{\zeta_k} . \quad (3.20)$$

The outputs from all x_{ik} channels are independent as a direct result of using orthogonal signalling waveforms. Therefore, x_{1k} and v_k are independent as well. Since the variables are independent, their joint density is just the product of the two individual densities or

$$\begin{aligned} f_{x_{1k}v_k}(x_{1k}, v_k) &= \frac{1}{2(\sigma_k^2 + 2S\sigma^2)} \exp \left[-\frac{1}{2} \left(\frac{x_{1k} + 2S\alpha_k^2}{\sigma_k^2 + 2S\sigma^2} \right) \right] I_0 \left(\frac{\sqrt{2Sx_{1k}} \alpha_k}{\sigma_k^2 + 2S\sigma^2} \right) \\ &\times \left(\frac{1}{2\sigma_k^2} \right)^{(M-1)} \frac{1}{(M-2)!} v_k^{(M-2)} \exp \left[-\frac{v_k}{2\sigma_k^2} \right]. \end{aligned} \quad (3.21)$$

The density for z_{1k} is obtained by performing a change of variables as follows. The constant S is normalized to 1 without loss of generality. Defining the following transform definitions

$$\begin{aligned}x_{1k} &= \zeta_k z_{1k} , \\v_k &= \zeta_k (1 - z_{1k}),\end{aligned}\tag{3.22}$$

the density transformation becomes

$$f_{z_{1k}, \zeta_k}(z_{1k}, \zeta_k) = f_{x_{1k}, v_k}(\zeta_k z_{1k}, \zeta_k (1 - z_{1k})) \frac{1}{|J|} .\tag{3.23}$$

where $|J|$ is the magnitude of the Jacobian matrix for the transformation. In this case it equals

$$|J| = \begin{vmatrix} \frac{\partial z_{1k}}{\partial x_{1k}} & \frac{\partial z_{1k}}{\partial v_k} \\ \frac{\partial \zeta_k}{\partial x_{1k}} & \frac{\partial \zeta_k}{\partial v_k} \end{vmatrix} = \frac{1}{\zeta_k} .\tag{3.24}$$

The joint density of z_{1k} and ζ_k as can now be written as

$$\begin{aligned}
f_{z_{1k}, \zeta_k}(z_{1k}, \zeta_k) &= \frac{1}{2(\sigma_k^2 + 2\sigma^2)} \exp\left[-\frac{\alpha_k^2}{\sigma_k^2 + 2\sigma^2}\right] I_0\left(\frac{\sqrt{2z_{1k}\zeta_k}\alpha_k}{\sigma_k^2 + 2\sigma^2}\right) \\
&\times \left(\frac{1}{2\sigma_k^2}\right)^{(M-1)} \frac{1}{(M-2)!} \zeta_k^{(M-1)} (1-z_{1k})^{M-2} \\
&\times \exp\left[-\frac{\zeta_k}{2}\left(\frac{z_{1k}}{\sigma_k^2 + 2\sigma_k^2} + \frac{(1-z_{1k})}{\sigma_k^2}\right)\right]. \quad (3.25)
\end{aligned}$$

For simplicity the following substitutions are made in (3.25)

$$\begin{aligned}
\rho_k &= \frac{\alpha_k^2}{\sigma_k^2}, \\
\beta_k &= \frac{2\sigma^2}{\sigma_k^2}, \quad (3.26)
\end{aligned}$$

where ρ_k is the signal-to-noise ratio (SNR) of the direct signal component and β_k is the SNR of the diffuse (or faded) signal component. After the substitutions, the joint density becomes

$$\begin{aligned}
f_{z_{1k}, \zeta_k}(z_{1k}, \zeta_k) &= \frac{1}{(1 + \beta_k)} \left(\frac{1}{2\sigma_k^2}\right)^M \exp\left[-\frac{\rho_k}{1 + \beta_k}\right] \\
&\times (1 - z_{1k})^{M-2} \frac{1}{(M-2)!} \zeta_k^{M-1} \\
&\times \exp\left[-\zeta_k \left(\frac{1 + \beta_k(1 - z_{1k})}{2\sigma_k^2(1 + \beta_k)}\right)\right] I_0\left(\frac{2\sqrt{\frac{z_{1k}\rho_k}{\sigma_k^2} \frac{1}{2}} \sqrt{\zeta_k}}{1 + \beta_k}\right). \quad (3.27)
\end{aligned}$$

The density for z_{1k} is found by integrating out the auxiliary variable ζ_k (details are contained in Appendix L). This yields

$$\begin{aligned}
 f_{z_{1k}}(z_{1k}) &= \frac{M-1}{(1+\beta_k)} (1 - z_{1k})^{M-2} \left[\frac{(1 + \beta_k)}{(1 + \beta_k(1 - z_{1k}))} \right]^M \\
 &\times \exp \left[\frac{\rho_k (1 - z_{1k})}{1 + \beta_k(1 - z_{1k})} \right] \\
 &\times \sum_{m=0}^{M-1} \binom{M-1}{M-1-m} \frac{1}{m!} \left[\frac{z_{1k} \rho_k}{(1 + \beta_k)(1 + \beta_k(1 - z_{1k}))} \right]^m. \quad (3.28)
 \end{aligned}$$

The density for the other $M-1$ channels can be found by setting ρ_k and β_k equal to zero. The resulting density is

$$f_{z_{mk}}(z_{mk}) = (M-1)(1 - z_{1k})^{M-2} \quad \text{for } m=2,3,\dots,M. \quad (3.29)$$

These density functions are normally used to calculate the probability of error using

$$P_s(e|l) = 1 - \int_0^1 \int_0^1 \int_0^1 \dots \int_0^1 f_{z_1, z_2, \dots, z_M}(z_1, z_2, \dots, z_M) dz_1 dz_2 \dots dz_M, \quad (3.30)$$

where

$$f_{z_1, z_2, \dots, z_M}(z_1, z_2, \dots, z_M) = [f_{z_{1k}, z_{2k}, \dots, z_{Mk}}(z_{1k}, z_{2k}, \dots, z_{Mk})]^{\otimes L}, \quad (3.31)$$

represents the L -fold convolution of the joint density function of the z_k 's for the L^{th} level diversity combining. However, this requires the joint density function for the normalized output of all M channels. Since the normalized outputs are no longer independent, the joint density is not obtainable for the general case of arbitrary M because the cross-correlation components are in terms of ζ_k and unknown. The general case can be approximated by solving for a specific case and then applying a union bound to obtain the other cases. The only case that provides an analytical solution is for $M = 2$, i.e., binary frequency shift keying (BFSK).

B. BINARY FREQUENCY SHIFT KEYING

For Binary Frequency Shift Keying (BFSK, $M = 2$) the density functions becomes

$$\begin{aligned}
 f_{z_{1k}}(z_{1k}) &= \frac{1}{(1 + \beta_k)} \left[\frac{(1 + \beta_k)}{(1 + \beta_k(1 - z_{1k}))} \right]^2 \\
 &\times \exp \left[-\frac{\rho_k(1 - z_{1k})}{1 + \beta_k(1 - z_{1k})} \right] \\
 &\times \left[1 + \frac{z_{1k}\rho_k}{(1 + \beta_k)(1 + \beta_k(1 - z_{1k}))} \right] \\
 f_{z_{2k}}(z_{2k}) &= 1
 \end{aligned}
 \tag{3.32}$$

for $0 \leq z_{mk} \leq 1 \quad m=1,2$

Then simplifying, the density for $f_{Z_{1k}}(z_{1k})$ is

$$f_{Z_{1k}}(z_{1k}) = \frac{\rho_k z_{1k} + (1 + \beta_k) [1 + \beta_k (1 - z_{1k})]}{(1 + \beta_k (1 - z_{1k}))^3} \times \exp \left[-\frac{\rho_k (1 - z_{1k})}{1 + \beta_k (1 - z_{1k})} \right]. \quad (3.33)$$

Also, for $M = 2$ the system can be completely defined in terms of one variable.

Using (3.20) with v_k equal to x_{2k} , we obtain the normalized outputs as

$$z_{ik} = \frac{x_{ik}}{x_{1k} + x_{2k}}, \text{ for } i = 1, 2. \quad (3.34)$$

Reworking this for $i = 1$ and 2 yields the variable dependence required to perform the integration in (3.30) as

$$Z_{2k} = 1 - Z_{1k}. \quad (3.35)$$

Defining the output of the diversity combiner in Figure 2 as

$$Z_i = \sum_{k=1}^L Z_{ik}, \text{ for } i=1, 2, \quad (3.36)$$

leads to

$$Z_2 = \sum_{k=1}^L (1 - Z_{1k}) = L - Z_1 , \quad (3.37)$$

where the relationship of (3.35) has been used. Then the probability of error given that i hops contain jamming noise is

$$P_b(i) = \Pr(Z_1 < Z_2 \mid i) = \Pr(Z_1 < L/2 \mid i) . \quad (3.38)$$

This is used in (3.7) to calculate the total probability of error as

$$P_b = \sum_{i=0}^L \binom{L}{i} \eta^i (1-\eta)^{L-i} P_b(i) . \quad (3.39)$$

The calculation of $P_b(i)$ is dependent on the diversity level and the number of hops that are jammed. From (3.38) the probability of error is found through the following integral:

$$P_b(i) = \int_0^{L/2} f_{z_1}(z_1 \mid i) dz_1 , \quad (3.40)$$

where $f_{z_1}(z_1 \mid i)$ is the density function for L th level diversity and i hops jammed of the density for $f_{z_{1k}}(z_{1k} \mid i)$ given in (3.33). This can found by considering the jammed and non-jammed as separate cases. The density function of both are identical except that the noise power is

$$\sigma_k^2 = \left(\frac{N_J}{\eta} + N_p \right) B , \quad (3.41)$$

for the jammed hops and

$$\sigma_k^2 = N_o B , \quad (3.42)$$

for the non-jammed hops. Defining $f_{z_{1k}}^{(j)}(z_{1k})$ as the probability density function when jamming is present and $f_{z_{1k}}^{(n)}(z_{1k})$ when no jamming is present, and using the independence of the individual hops, the combined probability density function is found by convolving these functions with each other as

$$f_{z_1}(z_1 | i) = [f_{z_{1k}}^{(j)}(z_{1k})]^{\otimes i} \otimes [f_{z_{1k}}^{(n)}(z_{1k})]^{\otimes (L-i)} , \quad (3.43)$$

where $\otimes i$ represents an i -fold convolution of the jammed or non-jammed density functions. The value of i ranges from zero to L giving results for all combinations from no hops jammed to all L hops jammed for a single bit. The probability of error is found for each value of i from the integral in (3.40) and then combined in (3.39) to yield the total average probability of error.

C. M-ARY FREQUENCY SHIFT KEYING

The analysis for M-ary Frequency Shift Keying (MFSK) is not obtainable by analytical solution since the Z_{ik} variables are dependent on one another and their joint probability density function is unavailable. The system performance can, however, be evaluated by use of a union bound as mentioned above. The union bound is derived from the following relationship

$$\begin{aligned}
Pr(A \cup B \cup C \cup \dots) &= Pr(A) + Pr(B) + Pr(C) + \dots \\
&- Pr(A \cap B) - Pr(A \cap C) - Pr(B \cap C) - \dots \\
&- Pr(A \cap B \cap C \dots) ,
\end{aligned} \tag{3.44}$$

where A , B and C would represent the cases of $Z_2 > Z_1$, $Z_3 > Z_1$, and $Z_4 > Z_1$ and so forth, depending on the value of M for the system under investigation. The union bound disregards the probabilities of the intersections assuming their values to be small compared with the individual probabilities. The result is

$$Pr(A \cup B \cup C \cup \dots) \leq Pr(A) + Pr(B) + Pr(C) + \dots , \tag{3.45}$$

or in terms of the Z_i 's,

$$\begin{aligned}
&Pr[(Z_1 < Z_2 | i) \cup (Z_1 < Z_3 | i) \cup (Z_1 < Z_4 | i) \dots] \\
&\leq Pr(Z_1 < Z_2 | i) + Pr(Z_1 < Z_3 | i) + Pr(Z_1 < Z_4 | i) + \dots .
\end{aligned} \tag{3.46}$$

The bound equation can be further reduced recognizing that all the Z_i 's for $i=2,3,\dots,M$ are identically distributed and, therefore, the probabilities $Pr(Z_1 < Z_j)$ are of equal value. The bound then reduces to

$$Pr\left[\bigcup_{j=2}^M (Z_1 < Z_j | i)\right] \leq (M-1) \times Pr(Z_1 < Z_2 | i) . \tag{3.47}$$

In the probability of error calculation the value for the bit energy-to-noise ratio is replaced by the symbol energy-to-noise ratio

$$\frac{E_s}{N_T} = \frac{k E_b}{N_T} , \quad (3.48)$$

where N_T is the total noise on a single hop defined by (3.11). The calculations now provide a measure of the symbol error for the system using the equations for the binary system. Because the signalling waveforms were chosen for orthogonality, the probability of bit error is easily calculated as

$$\begin{aligned} P_b(i) &= \frac{M/2}{(M-1)} P_s(i) \\ &\leq \frac{M}{2} \Pr(Z_1 < Z_2 \mid i) \\ &\leq \frac{M}{2} \int_0^{L^2} f_{z_1}(z_1 \mid i) dz_1 , \end{aligned} \quad (3.49)$$

where $f_{z_1}(z_1 \mid i)$ is given in (3.43). The average probability of error is then found using (3.39).

D. NUMERICAL PROCEDURE

Results of the probability of error analysis are provided for $L = 1, 2, 3$, and 4 hops/bit for several signal-to-noise ratios. Direct-to-diffuse component ratios corresponding to Rician fading, Rayleigh fading and nonfading provide an overall

comparison of channel effects on system performance for the self-normalization receiver. In all cases, the solution of (3.40) was accomplished via a numerical integration routine. The average probability of error from (3.39) requires evaluation of $L + 1$ integrals. For example, for $L = 1$ the two cases are one non-jammed hop and one jammed hop. For $L = 2$ there are three cases: both hops non-jammed, one hop jammed/one hop non-jammed, and both hops jammed, etc. Additionally, the worst-case jamming ratio η (the value of η that produced the greatest probability of error for each value of E_b/N_o and E_b/N_j) was used so the curves represent a worst case bound on probability of error.

The solution for $L = 1$ is the evaluation (3.40) using the two signal-to-noise ratios (E_b/N_T) associated with a jammed hop and a non-jammed hop in (3.33) to generate the density function $f_{z_1}(z_1)$. For $L = 2$ and $L = 4$, the conditional probability density functions $f_{z_1}(z_1 | i)$ are found using fast Fourier transforms (FFT) of the probability density functions for each of the jammed and non-jammed cases. Numerical sequences, of length $N = 2^{11} = 2048$, of the densities were generated from (3.31) using the required E_b/N_T for jammed and non-jammed cases. The sequences are zero padded to a total length $(N \times L)$ before the FFT was performed to preserve the desired linear convolution of (3.40). The transformed sequences were multiplied point by point to produce the desired sequence of

$$F_{z_1}(s) = [F_{z_u}^{(j)}(s)]^l \times [F_{z_u}^{(n)}(s)]^{L-l} . \quad (3.50)$$

This result was then inverse fast Fourier transformed to yield the desired sequence for $f_{z1}(z_1)$ to be integrated. The procedure for $L = 3$ was similar to $L = 2$, except that a discrete Fourier transform is used, because padding for a diversity of three can not provide a sequence with a length that is a power of 2. The results are plotted in Chapter IV for the different values of fading ratios and bit energy-to-thermal-noise ratios versus the bit energy-to-jamming-noise ratios.

IV. FORWARD ERROR CORRECTION

Although using fast-frequency-hopping to provide diversity can improve system performance in the presence of partial band jamming, it is representative of a simple repetition code, where the signal is tested against some threshold and the output with a majority count would be selected [Ref. 13]. While diversity by itself does improve system performance, technology today provides use of much more powerful block and convolutional Forward Error Correction (FEC) codes capable of detecting and correcting numerous errors. Diversity, along with coding, will be used to provide performance improvement of anti-jam and low probability-of-intercept capabilities. The FEC coding provides coding gain to the system to decrease the required signal-to-noise plus jamming ratio for a given system performance level, i.e., probability of bit error. In particular, the analysis here will address rate 1/2 and 1/3 constraint length 7 convolutional codes and Reed-Solomon non-binary block codes.

In order to implement the coding scheme, the transmitter and receiver of Figures 4 and 5 must be modified as shown in Figure 6 [Ref. 14]. In the transmitter, the information bits arriving at rate R_b are mapped to Q -ary symbols where $Q = 2^q$ at a rate of $R_q = R_b/q$ and then passed to the encoder. A special case is for $q = 1$, which is called a binary encoder. For a binary encoder, the binary to Q -ary conversion is a straight-through connection. The encoder outputs n Q -ary symbols for every k Q -ary inputs and is defined as an (n,k) coder. The code rate then becomes

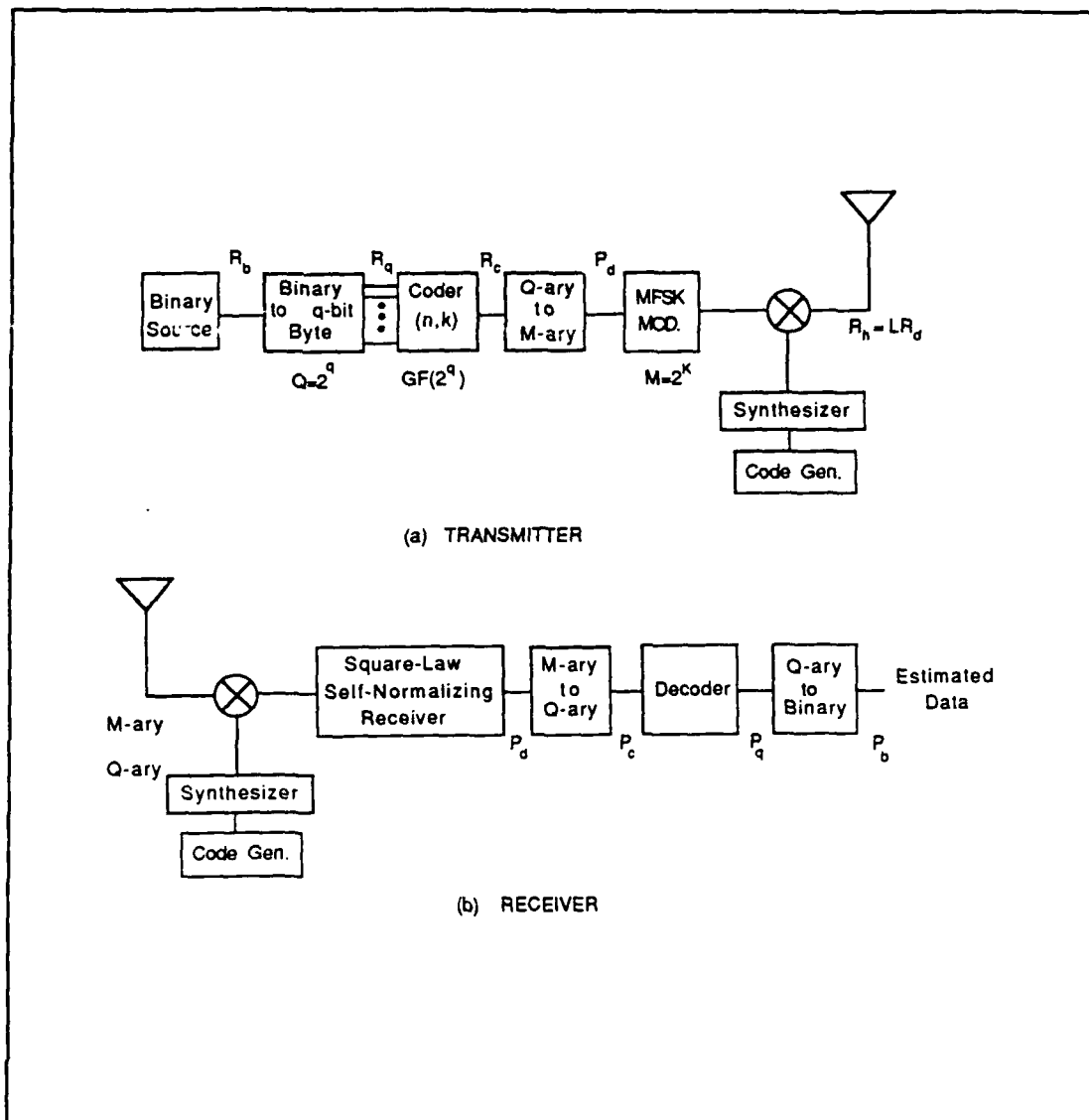


Figure 6. FH-MFSK Transmitter and Receiver Modified for FEC Coding [Ref. 14].

$r = k/n$ and the output symbols are created at $R_c = nR_q/k = nR_b/qk$. The Q -ary coded symbols are then converted to the M -ary symbols, where $M = 2^K$, required by the transmission channel at a rate $R_d = qR_c/K = nR_b/kK$. Another special case exists if $M = Q$; then the connection here is again straight-through. The choice of M and Q , in principle, is arbitrary; however, it is most convenient to choose K and q so

that one is an integer multiple of the other to simplify the analysis. The M -ary words are applied to the MFSK modulator which selects one of M baseband frequencies, the same as for the uncoded transmitter, which mixes the signal onto the frequency-hopping carrier. In order to maintain the orthogonal relationship of the transmitted signals, the M frequencies are spaced B Hz apart, where $B = R_h = LR_d = nLR_b/kK$, with L being the diversity level and R_h the hopping rate. The bandwidth of the M -ary group is $MB = MLR_d = nMLR_b/kK$ [Ref. 14]. This indicates that the improvement in performance requires the bandwidth to be increased by a factor of $1/r$ compared to the uncoded system as indicated in (2.13). Although the cost is more bandwidth in an already overcrowded electromagnetic spectrum, it is actually beneficial in terms of the system bandwidth satisfying the coherence bandwidth requirement of the channel (see Chapter II.B.). The total system bandwidth W is now

$$W = N_h B = \frac{nLN_h R_b}{kK}, \quad (4.1)$$

where N_h is the total number of possible carrier frequencies from the frequency synthesizer of Figure 6a.

The receiver shown in Figure 6b performs the decoding operation in reverse from that of the encoder. The demodulator is the self-normalizing quadratic receiver described in Chapter III. Thus, the performance at the output from the demodulator is described by (3.39) for BFSK and (3.49) for MFSK with $M > 2$. The demodulator makes a soft decision on which of the M -ary symbols was sent and passes it to the M -ary to Q -ary converter. The Q -ary word in turn is passed through the decoder

which makes a hard decision as to what symbol was actually sent. The Q-ary to binary converter then recreates the best estimate of the data sequence [Ref. 7:p. 332].

The performance of the total system is a measure of the demodulator's performance plus any increase due to error correction ability of the particular coding scheme. The analysis of the demodulator is identical to the uncoded case except the symbol energy per coded M-ary word is

$$E_d = \frac{kKE_b}{n} . \quad (4.2)$$

When applied to a fast-frequency-hopping system the energy per hop becomes

$$E_h = \frac{E_d}{L} = \frac{kKE_b}{nL} . \quad (4.3)$$

These values replace the symbol energy value in (3.28) when the density for the self-normalizing receiver is found. Then the probability of Q-ary symbol error is found through (3.39). The analysis for the coder performance depends on the ratio of q to K .

If $q > K$, then q/K M-ary words are mapped to the Q-ary symbol. At the receiver, the Q-ary symbol will be in error if any of the q/K M-ary symbols are in error. Therefore, P_c (the Q-ary symbol error ratio after the M-ary to Q-ary mapping) is

$$P_c = 1 - (1 - P_d)^{q/K} , \quad (4.4)$$

where P_d is the M-ary symbol error from the demodulator and q/K is an integer as specified above. And if $K > q$, then $d = K/q$ coded Q-ary symbols are grouped to form one M-ary word for transmission. Using the fact that $M = Q^d$, then, of the M symbols consisting of d Q-ary symbols, $Q^{d-1} = M/Q$ of the M-ary symbols have the same Q-ary symbol in a given position. Therefore the probability of a Q-ary symbol error given that an M-ary symbol error occurs is

$$Pr(\text{symbol error} \mid \text{word error}) = \frac{M}{(M-1)} \left(1 - \frac{1}{Q} \right). \quad (4.5)$$

The average symbol error rate then becomes

$$P_c = \frac{M}{(M-1)} (1 - 2^{-q}) P_d. \quad (4.6)$$

This still requires that K/q be an integer. In the special case of the binary encoder ($q = 1$) this becomes the formula for the orthogonal M-ary to binary conversion

$$P_c = \frac{M/2}{(M-1)} P_d. \quad (4.7)$$

The decoder will then make hard symbol decisions based on the Q-ary symbol at its input. Equations (4.5), (4.6), and (4.7) will be used as required in the following sections for the specific codes under investigation.

A. REED-SOLOMON NON-BINARY BLOCK CODES

Reed-Solomon codes are a special case of Bose-Chaudhuri-Hocquenghem (BCH) codes from the Galois field $GF(q)$ and as (n,k) block codes exhibit the following characteristics [Ref. 7:p. 171]:

$$\begin{array}{ll} \text{Block length:} & n = q - 1, \\ \text{Number of parity bits:} & n - k = 2t, \\ \text{Minimum distance:} & d_{\min} = 2t + 1, \end{array}$$

where t is the maximum number of errors the code can correct and d_{\min} is the minimum distance between codewords. Specifically, $q = 2^m$ is used here because it is the simplest to implement in digital circuitry. The value of m can be any value depending only on the constraints of the system under design (available memory size, speed of operation, real-time versus non-real-time data, etc.). Then, choosing a code such that $Q > M$ ($q > K$), the Q -ary symbol error is given by (4.5) and the output from the decoder will have a corrected probability of symbol error of

$$\begin{aligned} P_q \approx & \frac{d}{n} \sum_{i=t+1}^d \binom{n}{i} P_c^i (1 - P_c)^{n-i} \\ & + \frac{1}{n} \sum_{i=d+1}^n i \binom{n}{i} P_c^i (1 - P_c)^{n-i}. \end{aligned} \quad (4.8)$$

The probability of bit error is then

$$P_b = \frac{Q/2}{Q-1} P_q \quad (4.9)$$

B. CONVOLUTIONAL CODES

The convolutional codes used here are binary codes ($q = 1$); therefore, (4.7) will be used where applicable in evaluating the performance of the convolution codes.

Use of the Viterbi decoding algorithm is assumed in all cases.

The constraint length for convolutional codes is defined to be [Ref. 7:p. 291],

$$n_A \triangleq n(m_s+1) , \quad (4.9)$$

where n is the number of encoder outputs and m_s is maximum number of memory stages in any single input section. A simpler definition is the maximum number of encoder outputs that can be affected by a single input data bit. The codes used here have constraint length 7 and are called best rate 1/2 and 1/3, meaning that they deliver the best performance of any other rate 1/2 or 1/3 convolutional codes from a Viterbi decoder as defined in [Ref. 15]. Analysis of the the Viterbi decoder performance is approximated through use a Chernoff bound. For the rate 1/2 codes, the information bit error rate is bounded by

$$P_b \leq \frac{1}{2}(36D^{10} + 211D^{12} + 1404D^{14} + 11633D^{16} + \dots) , \quad (4.11)$$

and the rate 1/3 codes by

$$P_b \leq \frac{1}{2} (D^{14} + 20D^{16} + 53D^{18} + 184D^{20} + \dots) , \quad (4.12)$$

where

$$D = 2\sqrt{P_c(1 - P_c)} \quad (4.13)$$

The higher order terms in (4.11) and (4.12) are neglected since P_c (the symbol error rate) is usually quite small.

V. DISCUSSION OF RESULTS

Probability of error analysis for both the uncoded and coded systems is based on worst-case partial-band jamming. The first computer runs were done for 15 values of η from 0.001 to 1.0. The worst-case values were subsequently selected from these 15 values for each value of E_b/N_j from zero to 40 dB. After plotting the curves of Figure 7 and 8, it was determined that the value of η which maximized the probability of error in a Rician-faded channel continuously increased as the bit energy-to-jamming noise density ratio (SNR_j) was decreased. This allowed the program to be modified to check two consecutive values of η and select the maximum. If the larger of the two values of η caused the greatest probability of error, the program compared the results of the second to the third and then the third to the fourth and so forth, continuing until $\eta = 1.0$. This increased the speed of calculations for all values of E_b/N_j by a factor of five, since the simulation no longer had to calculate 15 different outcomes for each value of E_b/N_j . Figure 7 for low SNR_T , however, implies that a jammer could obtain good results (reasonably high error ratios) if broadband jamming ($\eta = 1.0$) was employed at all times regardless of the power it expected to deliver to the receiver. The predicted probability of error for broadband jamming is only slightly better than for worst-case partial-band jamming. In fact, worst-case partial-band jamming and broadband jamming produce essentially the same probability of error at both high (30 to 40 dB) and low (0 to 10

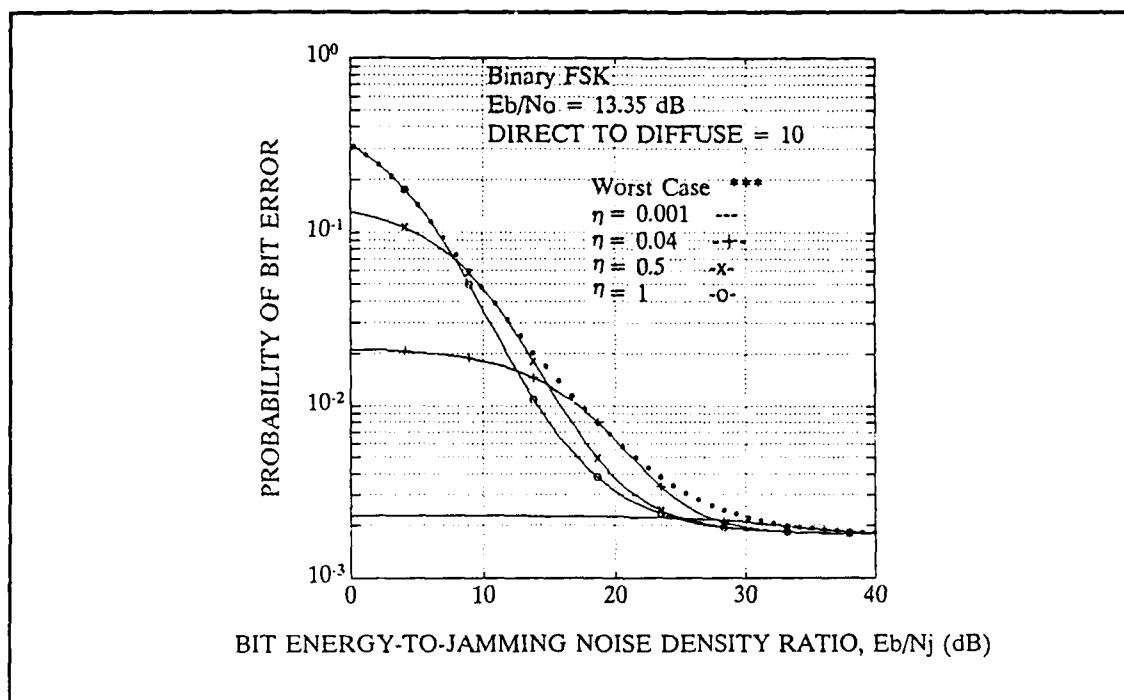


Figure 7. System Performance for various Partial-Band Jamming Ratios in a Rician fading channel with $E_b/N_o = 13.35$ dB.

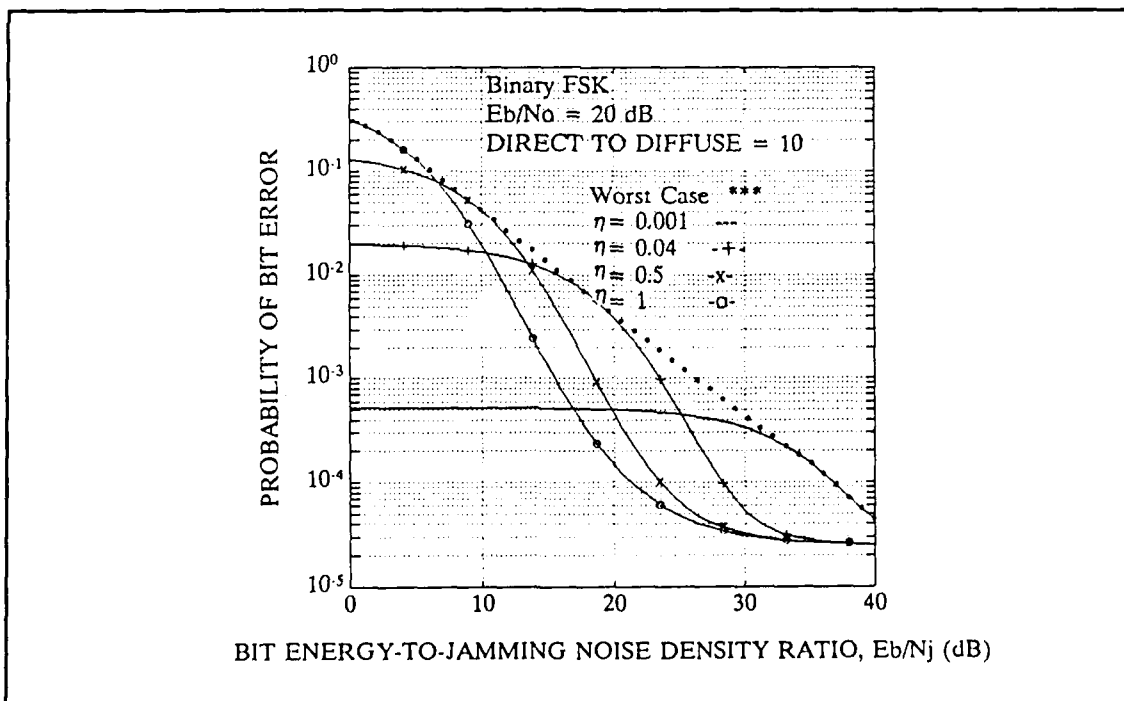


Figure 8. System Performance for various Partial-Band Jamming Ratios in a Rician fading channel with $E_b/N_o = 20$ dB.

dB) SNR_J ratios. There is only a slight difference in the range from 10 to 30 dB. This is not the situation when the system operates at higher SNR_T as witnessed in Figure 8. Although at both ends of the curve the results are the same, in the range of $E_b/N_J = 15$ to 35 dB, the jammer would obtain an appreciable increase in effectiveness by using an optimum jamming bandwidth.

In the case of Rayleigh fading, the worst-case jamming ratio η was found to be 1.0 at all levels of jamming power. This would make the jammer's job much simpler since it would not need to acquire any information about the receiver (location, received signal strength, etc.) to be effective against it. In the following sections, the importance of signal-to-thermal noise ratios and signal-to-jamming noise ratios are discussed along with the ability of fast-frequency-hopping diversity to overcome their effects.

A. UNCODED SYSTEM PERFORMANCE

The uncoded system performance versus signal-to-jamming noise ratio (SNR_J) for BFSK, $M = 2$, and $E_b/N_o = 20$ dB is shown in Figures 9 through 12 for direct-to-diffuse component fading ratios of 0.01, 1, 10, and 1000. These values represent deeply and moderately-faded Rayleigh channels, a Rician-faded channel, and a nonfading channel, respectively. Figures 13 and 14 show results for direct-to-diffuse ratios of 10 and 1000, respectively, with $E_b/N_o = 13.35$ dB. Additional graphs for $E_b/N_o = 13.35$ and 30 dB are enclosed in Appendix C. These figures demonstrate that fading can severely affect the performance of the self-normalization receiver, particularly for low to moderate signal-to-thermal noise ratios (SNR_T). They also

show that diversity can be very effective in overcoming the effects of partial-band jamming and the effect of fading channels associated with the multipath satellite signals. An interesting point is illustrated in Figures 12 and 13, the results for $E_b/N_o = 13.35$ in a Rayleigh-faded channel and a non-fading channel, respectively. As SNR_T increases, the best diversity level (the diversity case that delivers the lowest probability of error) increases from $L = 1$ to $L = 3$ in Figure 12, and then in Figure 13, at approximately 35 dB, it reverts to $L = 1$. This indicates that for low SNR_T ratios the best-case diversity level performance is only marginally better than $L = 1$

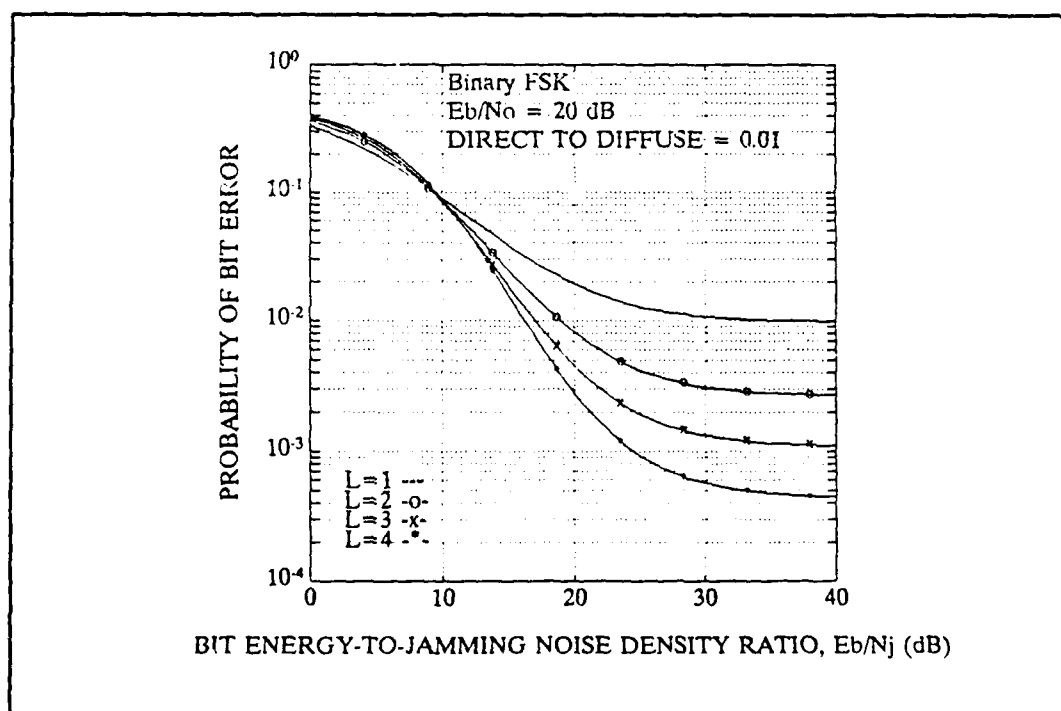


Figure 9. Uncoded System Performance for BFSK in deep-faded Rayleigh channel for $E_b/N_o = 20$ dB.

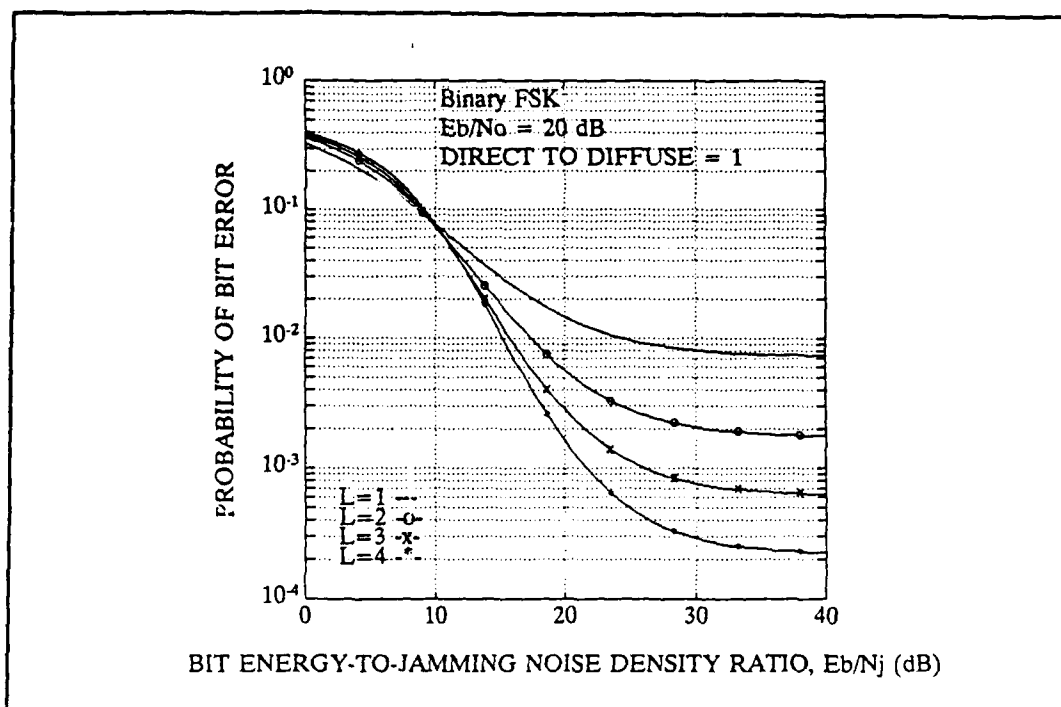


Figure 10. Uncoded System Performance for BFSK in a moderately-faded Rayleigh Channel with $E_b/N_0 = 20$ dB.

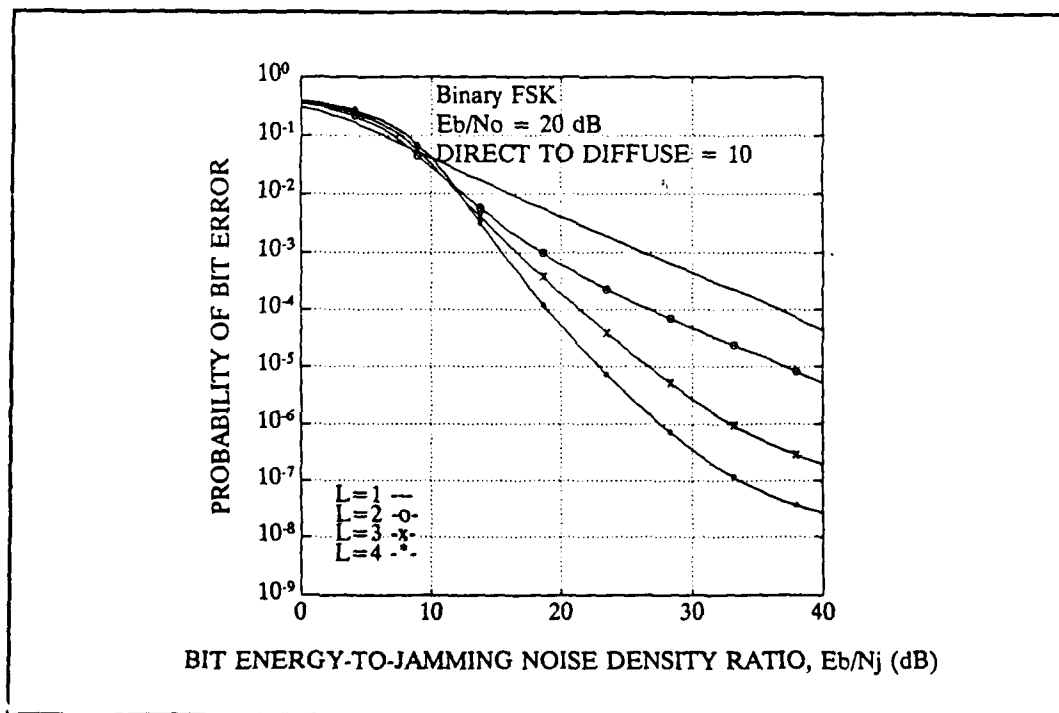


Figure 11. Uncoded System Performance for BFSK in a Rician-faded channel with $E_b/N_0 = 20$ dB.

in nonfading or Rician fading channels. In contrast, Rayleigh fading channels provide the best performance by operating at the greatest possible diversity level at all SNR_T ratios. The phenomenon of the optimum diversity level reverting to $L = 1$ in Figure 13 also occurs at higher SNR_T levels as the jamming power at the receiver goes to zero; however, the crossover points on the other figures is outside the scale of the figures. The cause is nonlinear combining losses that occur from not using the phase information of the received signal in the diversity combining process [Ref. 8].

Examples of the results for the Union bound developed in Chapter III for $M = 4$ and $M = 8$, MFSK with $E_b/N_o = 20$ dB are shown in Figures 15 through 18. Figures 15 and 17 show the results for Rayleigh fading and Figures 16 and 18 are for

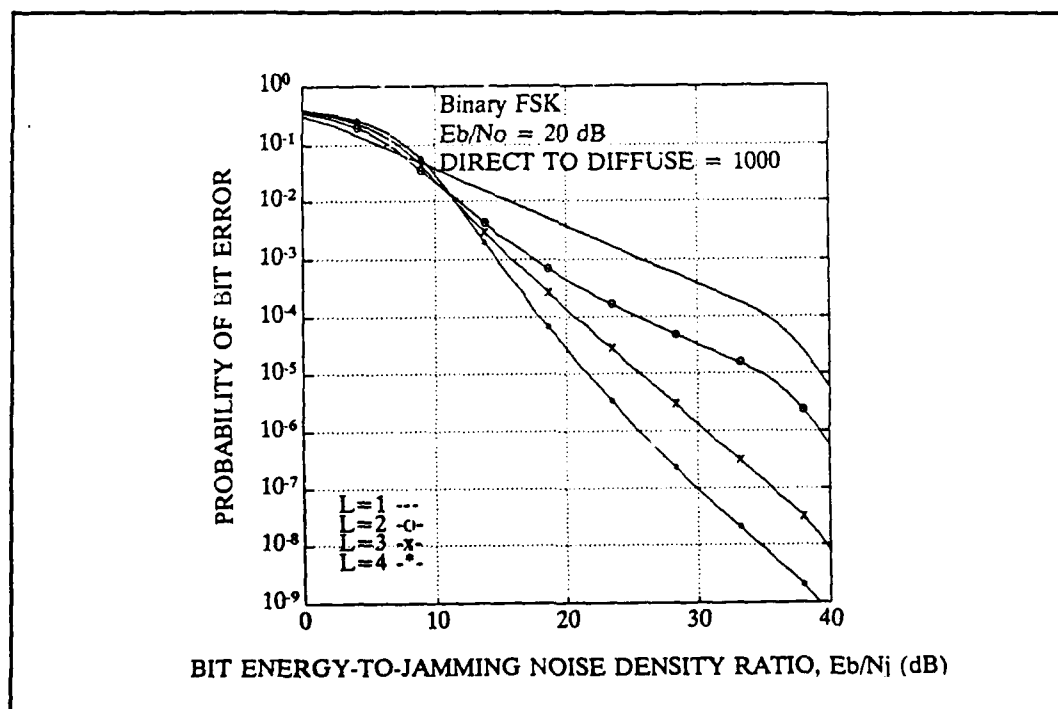


Figure 12. Uncoded System Performance for BFSK in a nonfaded Channel with $E_b/N_o = 20$ dB.

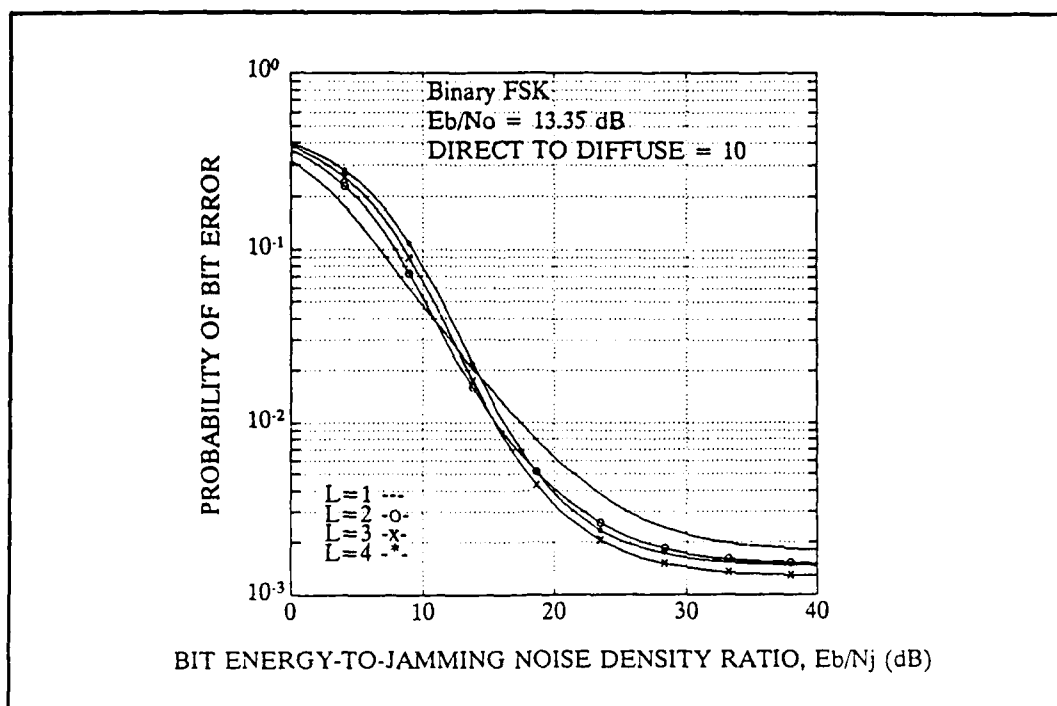


Figure 13. Uncoded System Performance for BFSK in a Rician-faded Channel with $E_b/N_0 = 13.35$ dB.

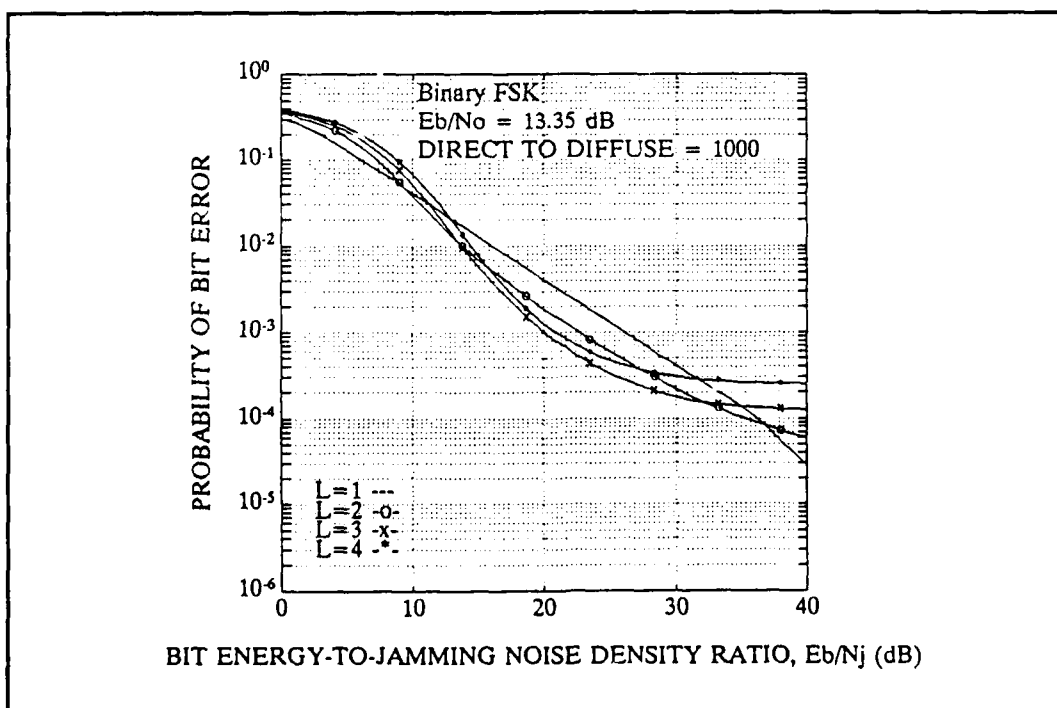


Figure 14. Uncoded System Performance for BFSK in a nonfading channel for $E_b/N_0 = 13.35$ dB.

Rician fading channels, respectively. The curves follow the same general form of the curves of the BFSK cases since they are based on the same calculation technique, with a different energy per hop and multiplicative factor. A better illustration of the effects of using MFSK, with increasing values of M , are shown in Figures 19 through 22. These graphs are a direct comparison for $M = 2$ to 32 ($k = 1$ to 5) with $E_b/N_o = 20$ dB and the four fading levels as used above. All four figures show that performance improves as k increases or consequently as M increases. The results for $M = 8, 16$, and 32 in Rayleigh fading (Figures 19 and 20) are almost identical over the entire range of SNR, while Figure 21, for the Rician fading channel, exhibits a general improvement in system performance as M increases. The non-fading channel

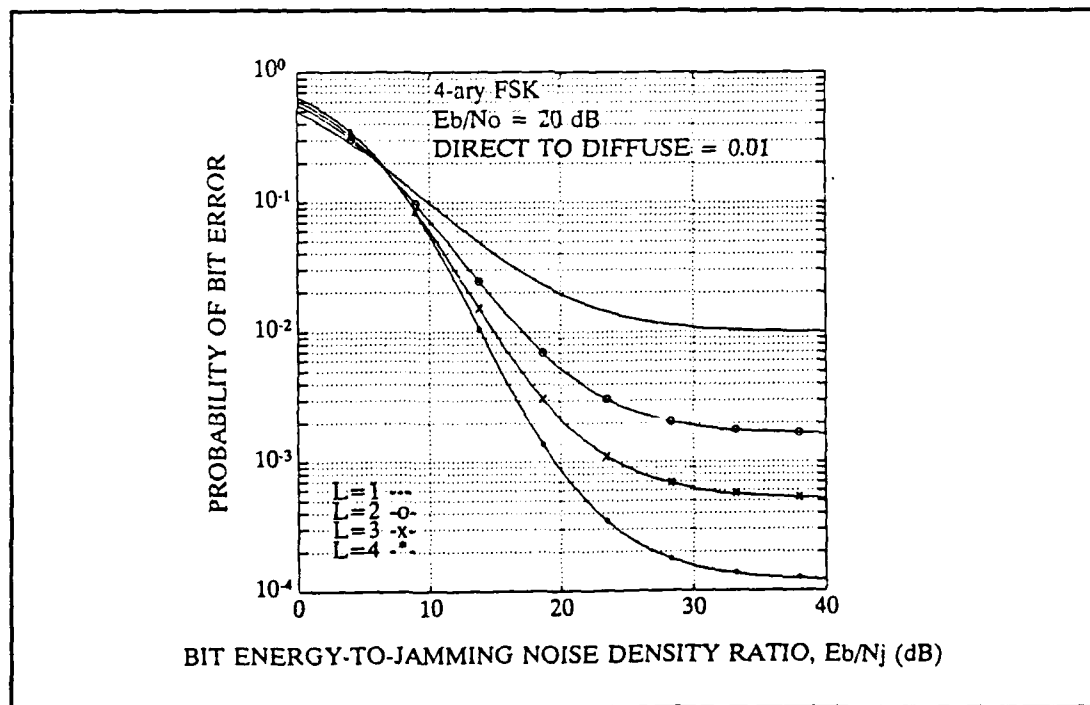


Figure 15. Uncoded Performance for 4-ary FSK in a Rayleigh-faded channel with $E_b/N_o = 20$ dB.

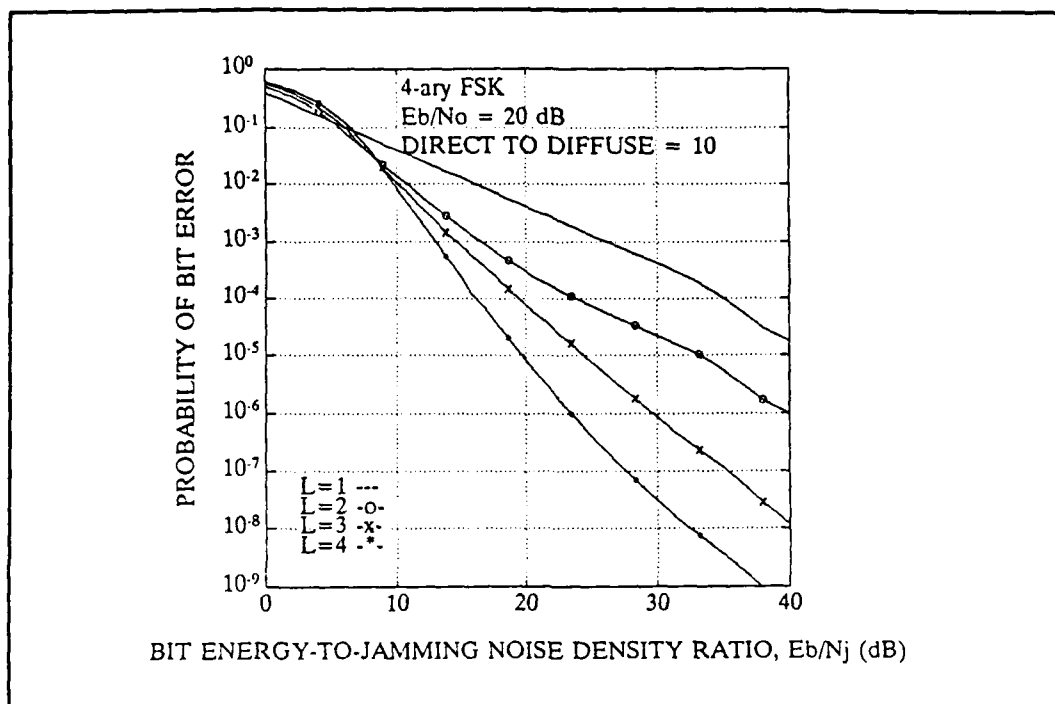


Figure 16. Uncoded Performance for 4-ary FSK in a Rician-faded channel with $E_b/N_o = 20$ dB.

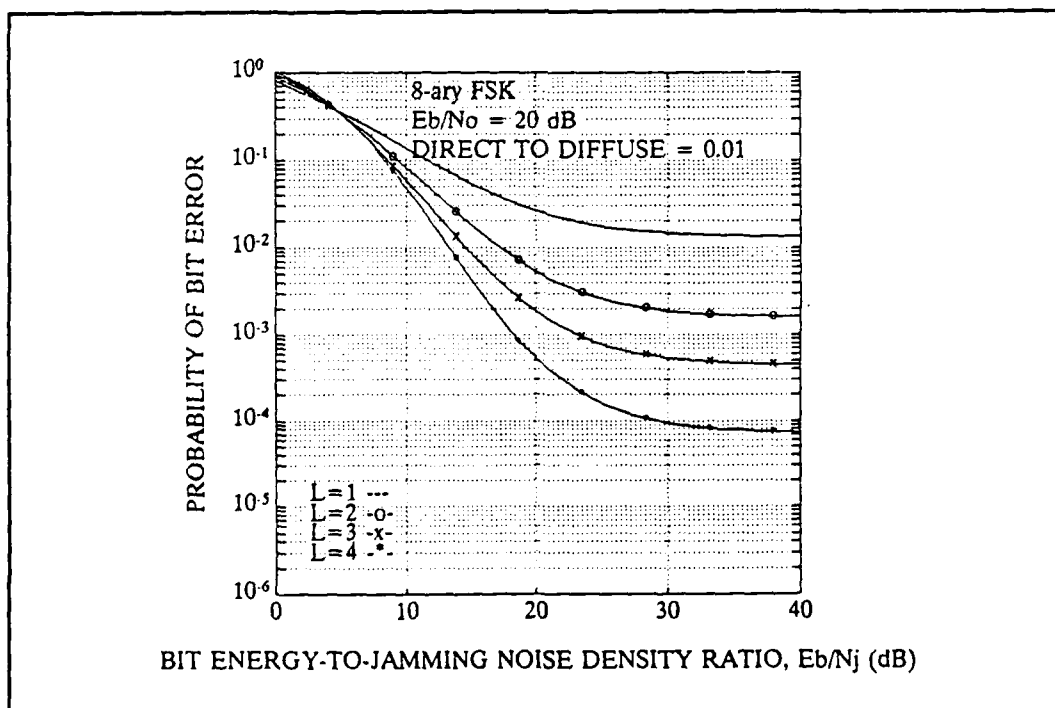


Figure 17. Uncoded Performance for 8-ary FSK in a deeply-faded Rayleigh channel with $E_b/N_o = 20$ dB.

in Figure 22 again shows little or no distinction between $M = 8, 16$, or 32 until the SNR_j ratio is approximately 32 dB. This may be due to the inaccuracy of the bound used to derive the results for $M > 2$, or it may be an accurate representation for the receiver in that very little improvement in system performance is achieved for values of $M > 8$, with the former being the most likely cause. As a comparison, the results for a noise-normalization receiver (the samples from the quadratic detector are divided by an estimate of the ambient noise from a separate channel outside of the bandwidth of the M signal frequencies) is shown in Figures 23 and 24 [Ref. 15]. The self-normalization receiver can be viewed as a practical implementation of the noise-normalization receiver since it essentially obtains an estimate of the noise power directly from the M detectors of the demodulator. Therefore, the performance of the two receiver designs should be similar. Comparing Figures 19 and 21 with Figures 23 and 24, it is evident that the noise-normalization receiver continues to improve as M increases, while the bound for the self-normalization receiver shows little or no improvement beyond $M = 8$. This is evidence that the bound may not be as accurate as desired; however, it does indicate that the self-normalization receiver may provide even better performance with higher values of M , contrary to the results of Figures 19 and 21.

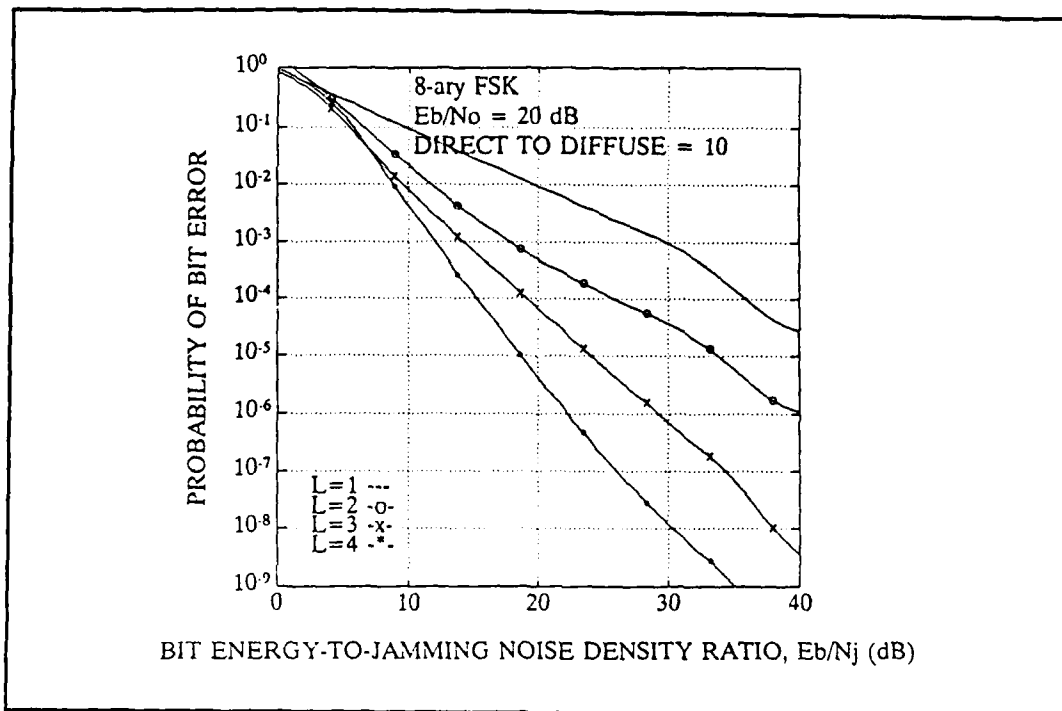


Figure 18. Uncoded Performance for 8-ary FSK in a Rician-faded channel with $E_b/N_o = 20$ dB.

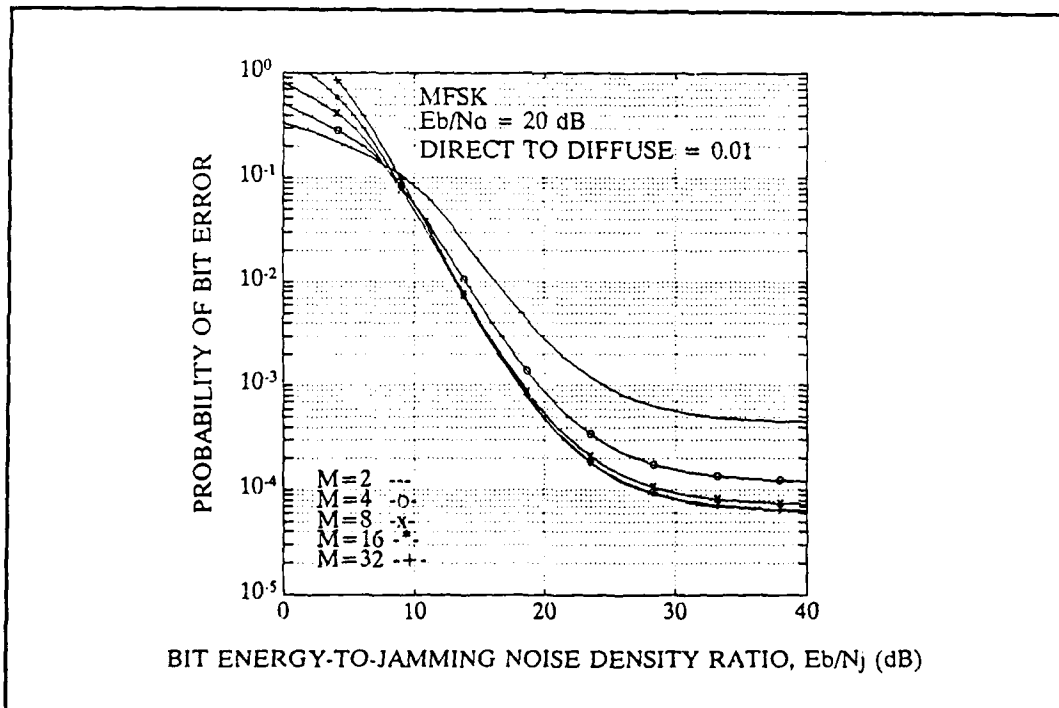


Figure 19. Uncoded Performance for MFSK, $M = 2$ to 32, in a deeply-faded Rayleigh channel with $E_b/N_o = 20$ dB.

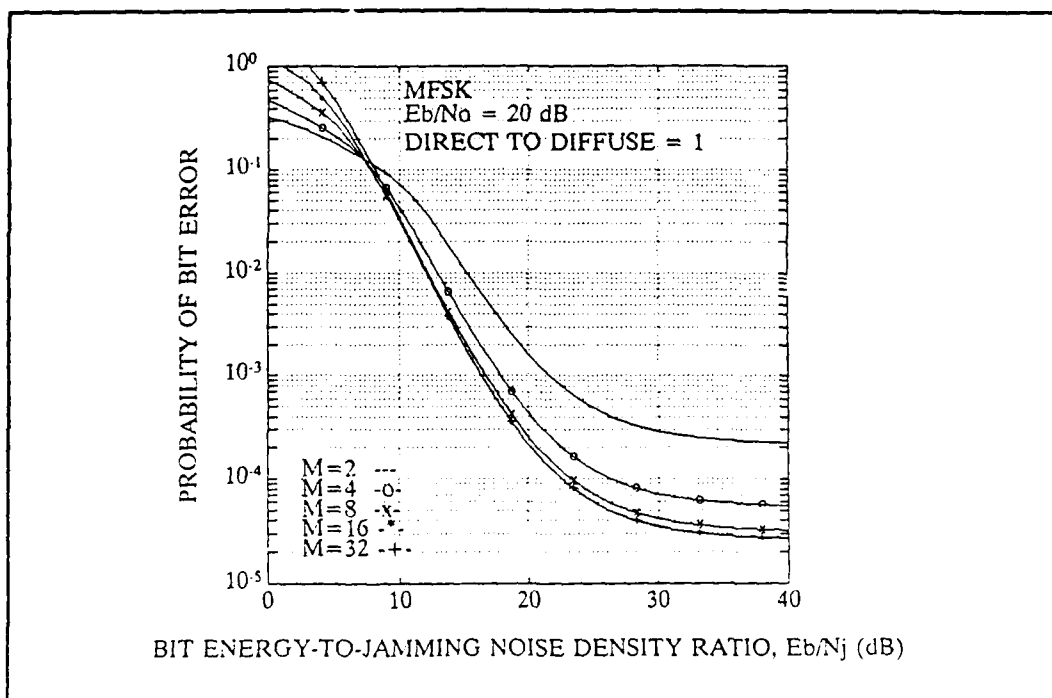


Figure 20. Uncoded Performance for MFSK, $M = 2$ to 32, in a moderately faded Rayleigh channel with $E_b/N_o = 20$ dB.

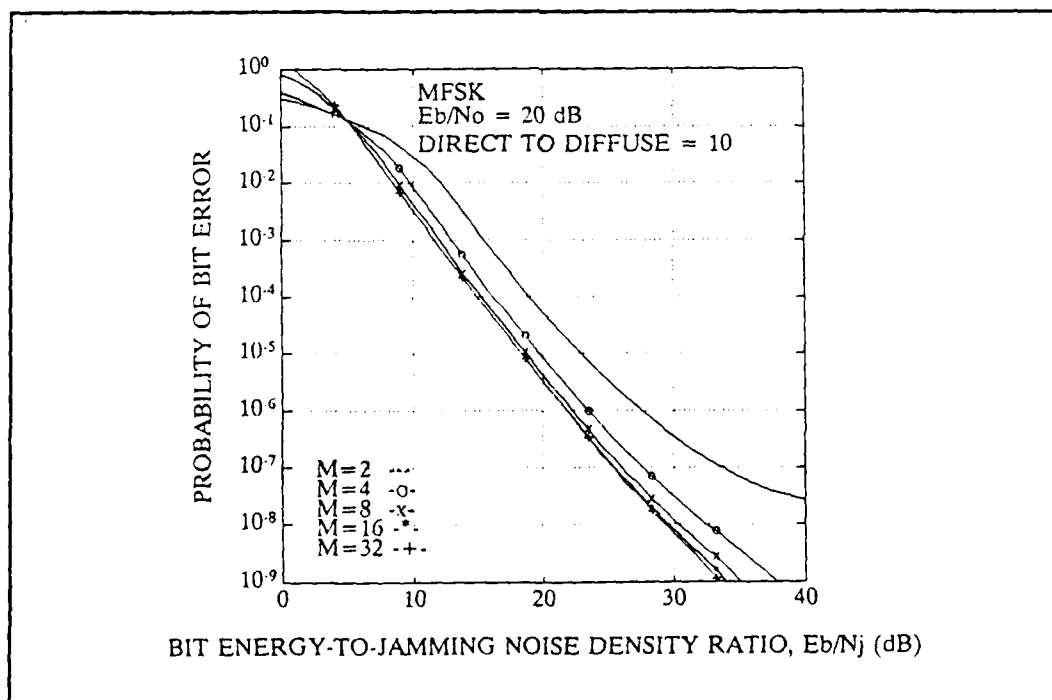


Figure 21. Uncoded Performance for MFSK, $M = 2$ to 32, in a Rician-faded channel with $E_b/N_o = 20$ dB.

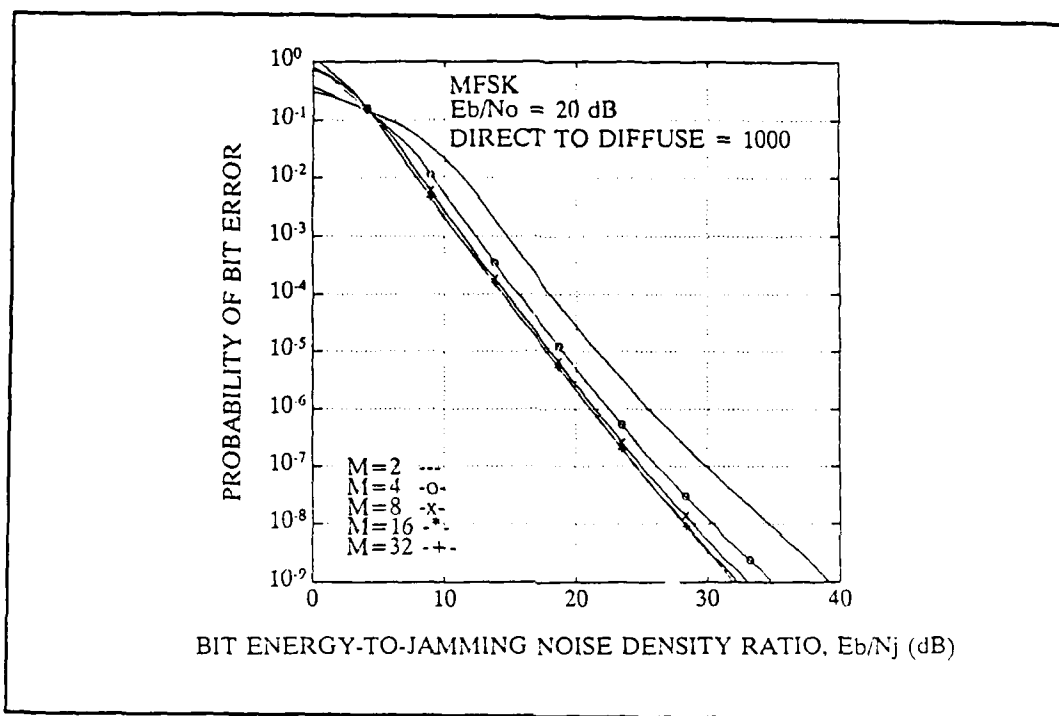


Figure 22. Uncoded Performance for MFSK, $M = 2$ to 32, in a non-faded channel with $E_b/N_0 = 20 \text{ dB}$.

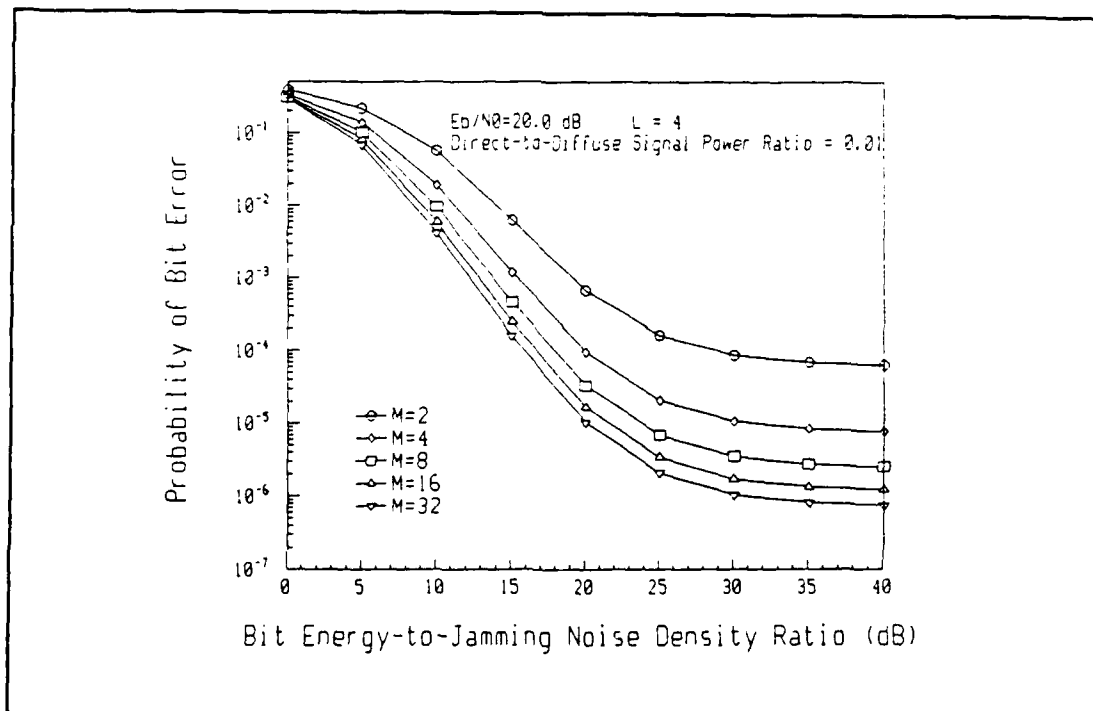


Figure 23. Uncoded Performance for a Noise-normalization Receiver, for $M = 2$ to 32, in Rayleigh-faded channel, with $E_b/N_0 = 20 \text{ dB}$.

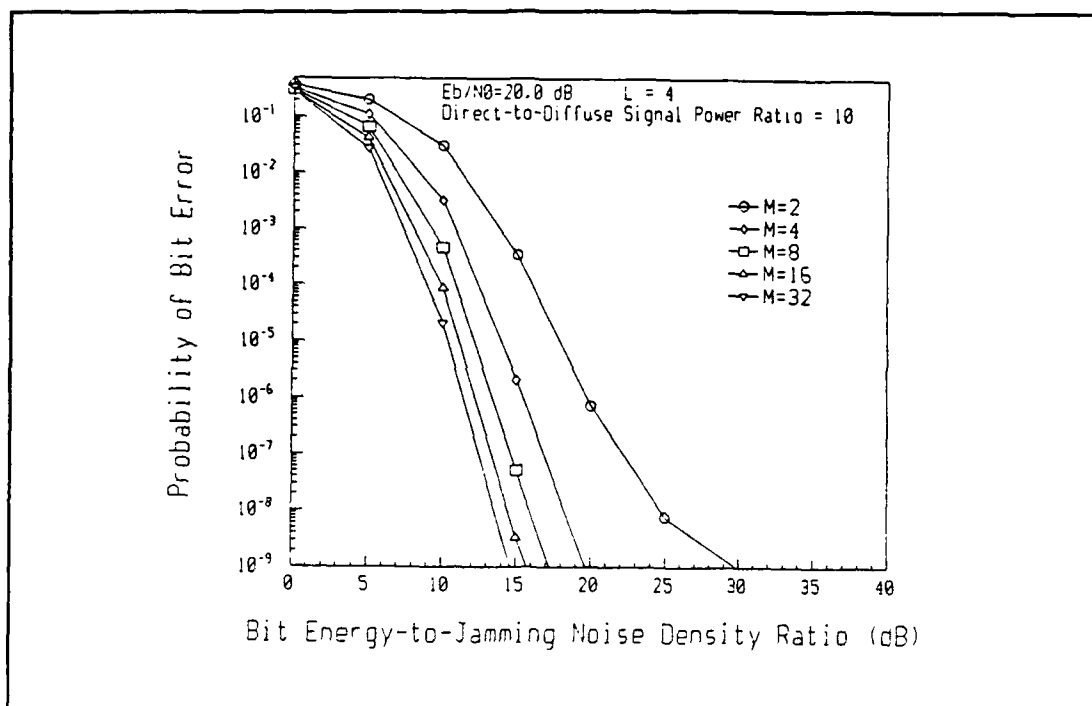


Figure 24. Uncoded Performance for a Noise-normalization Receiver, for $M = 2$ to 32, in a Rician-faded channel, with $E_b/N_0 = 20$ dB.

B. CODED SYSTEM PERFORMANCE

The coding results in all cases showed an appreciable improvement in system performance as was expected. Figures 25 through 28 show results for (7,3) and (15,5) Reed-Solomon codes on BFSK signals in Rayleigh and Rician fading channels with $E_b/N_0 = 20$ dB. These codes are able to correct two and 5 errors, respectively. The ratio of n to k was chosen in all cases to yield code rates similar to those of the rate $1/2$ and $1/3$ convolution codes described in Chapter IV. This was a matter of convenience to simplify comparing performance of the two types of codes. Also, q was adjusted to provide a q/K ratio of two in most of the simulation runs. The only deviation from that ratio was for $K=1$ (BFSK). The ratio was changed here since a

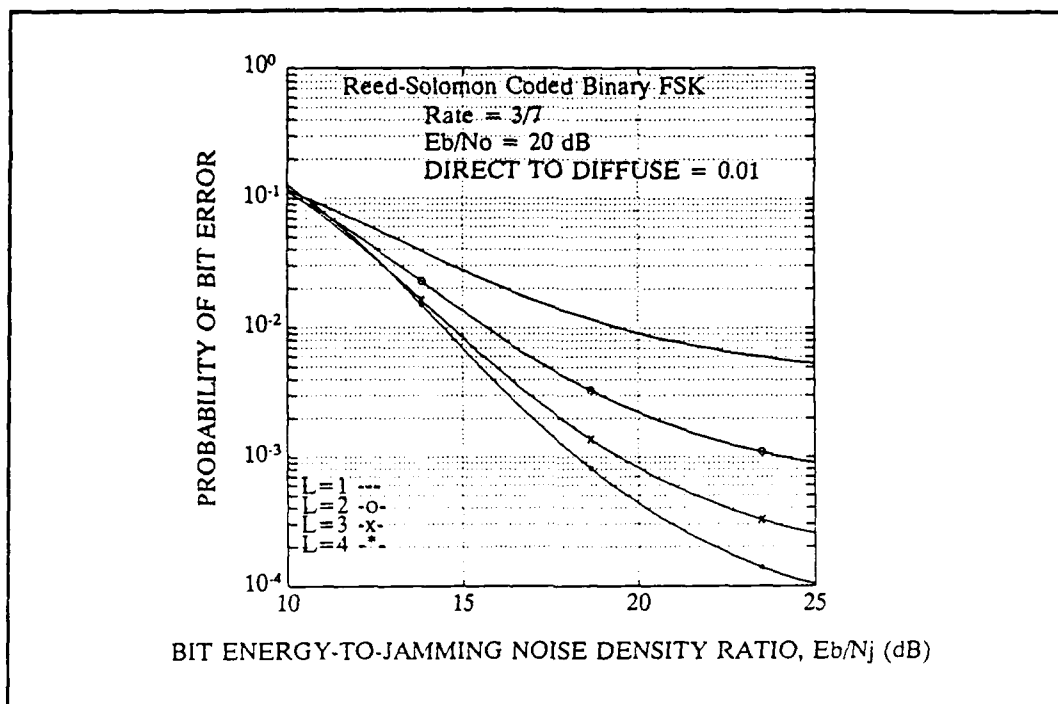


Figure 25. Reed-Solomon (7,3) Coded Performance for BFSK in a Rayleigh faded channel with $E_b/N_0 = 20$ dB.

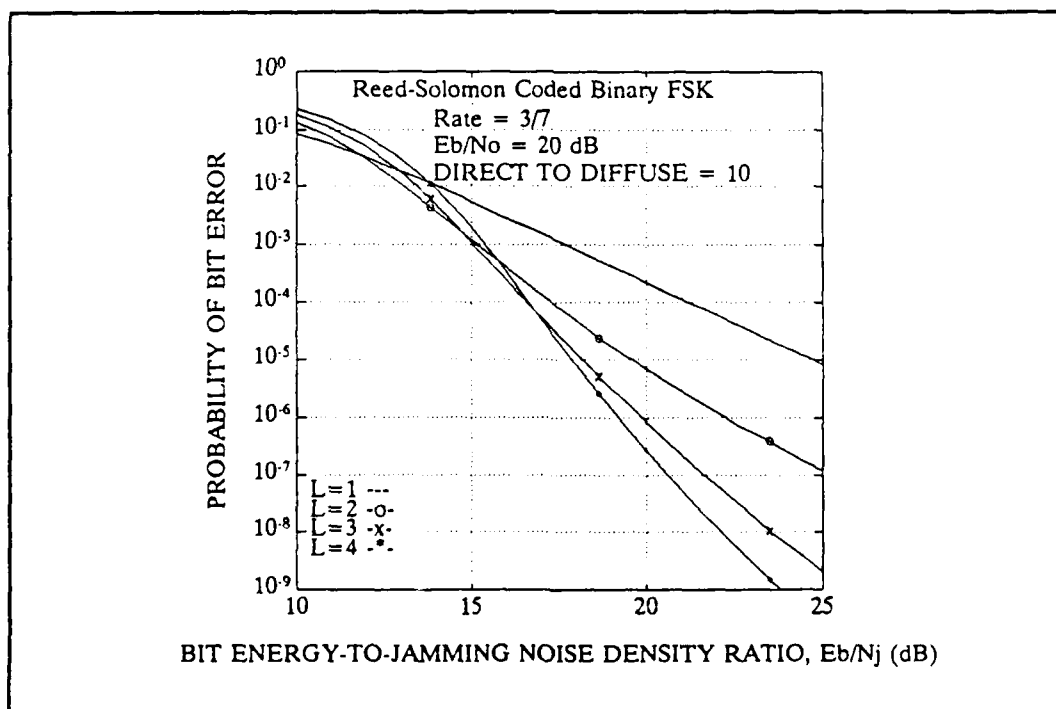


Figure 26. Reed-Solomon (7,3) Coded Performance for BFSK in a Rician faded channel with $E_b/N_0 = 20$ dB.

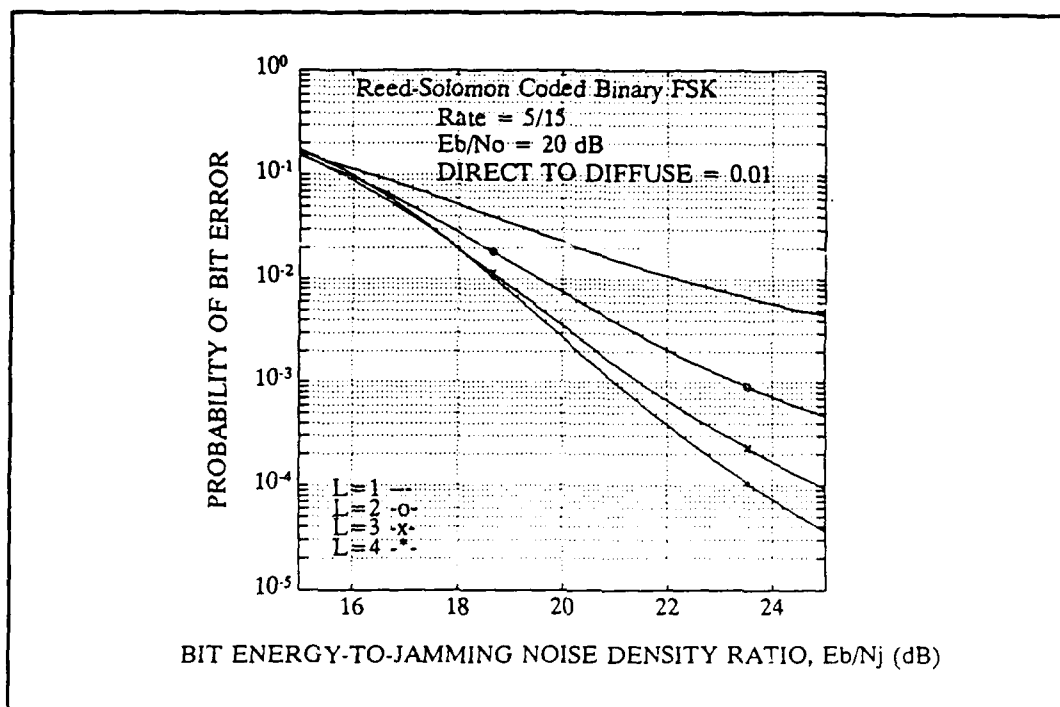


Figure 27. Reed-Solomon (15,5) Coded Performance for BFSK in a Rayleigh faded channel with $E_b/N_o = 20$ dB.

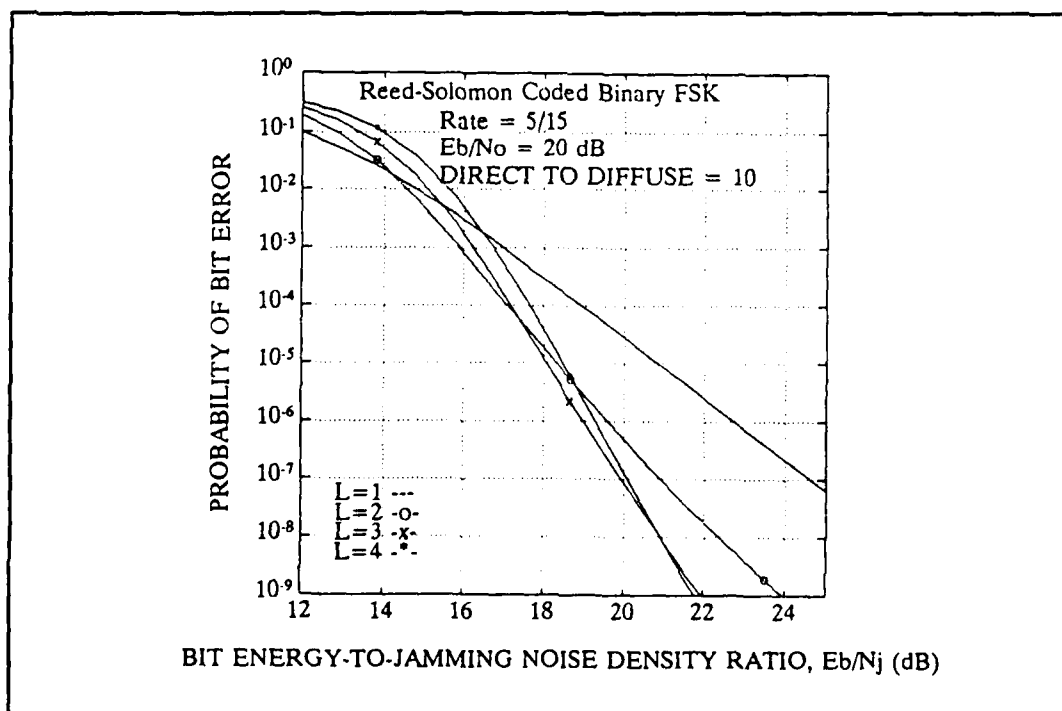


Figure 28. Reed-Solomon (15,5) Coded Performance for BFSK in a Rician faded channel with $E_b/N_o = 20$ dB.

(3,1) code is nothing more than a repeat majority count code and provides little more than the diversity of the frequency-hopping carrier. Therefore, the BFSK results are given for (7,3), (15,7), and (15,5) Reed-Solomon codes which correspond to $q=3$ for the first code and $q=4$ for the latter two codes.

Comparison of the performance of the Reed-Solomon codes above with the uncoded performance of Figures 9 and 11 shows that the (7,3) Reed-Solomon code provides a coding gain of approximately 6 dB at an error ratio of $P_b = 10^{-3}$ in a Rayleigh-faded channel and 5 dB at $P_b = 10^{-5}$ in the Rician-faded channel. The (15,5) Reed-Solomon code provides 3 dB and 5 dB at the same error ratios. These gains are based on the optimum diversity level. The optimum level being the level that provides the lowest probability of error for a specific value of SNR_T .

The rate 1/2 and 1/3 convolutional codes in Figures 29 through 32 show that convolutional codes provide superior performance to Reed-Solomon codes for BFSK. The rate 1/2 code provides coding gains of 9 dB at $P_b = 10^{-3}$ in the Rayleigh channel and 8 dB at $P_b = 10^{-5}$ in the Rician-faded channel. The rate 1/3 code provides a coding gain of 8 dB in the calculation for the Rayleigh channel and 8.5 dB gain in the Rician-faded channel at the reference points for probability of errors indicated above. The comparison is better illustrated in Figures 33 and 34, which show the results of all four coding schemes for $L=2$ (solid lines) and $L=3$ (dashed lines) in Rayleigh and Rician channels. Notice here that the (7,3) Reed-Solomon code was replaced with a (15,7) Reed-Solomon code in the comparison to keep the ratio of q to K the same in both coding schemes, and thereby provide a direct relationship of

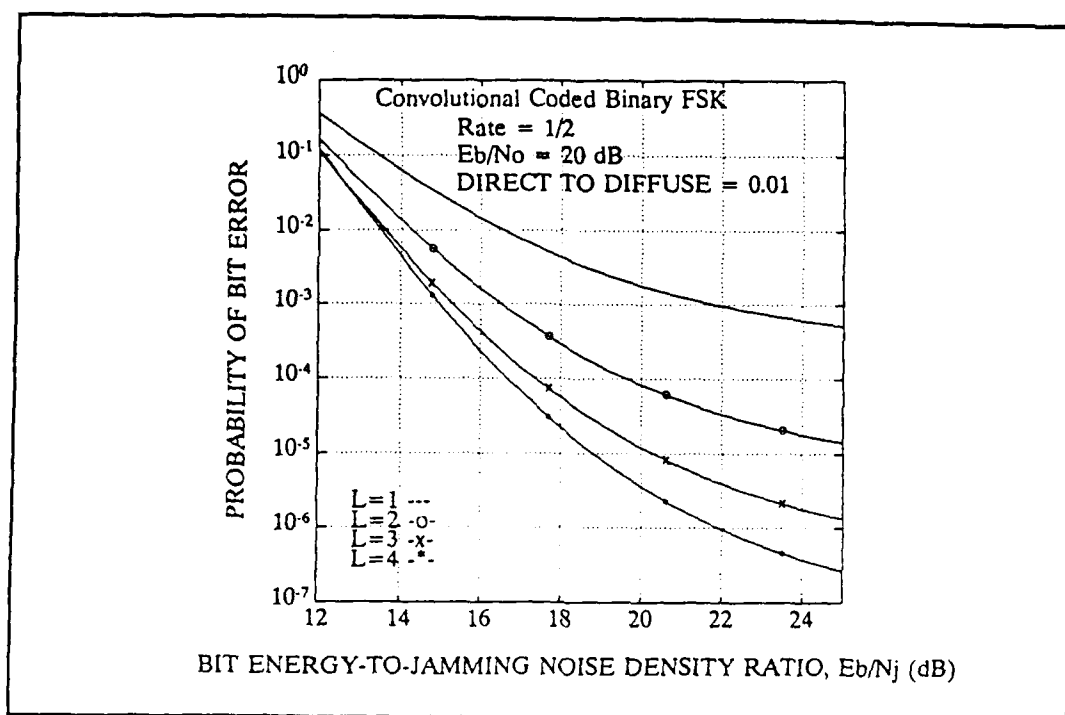


Figure 29. Rate 1/2 Convolutional Coded BFSK in a Rayleigh-faded channel with $E_b/N_o = 20$ dB.

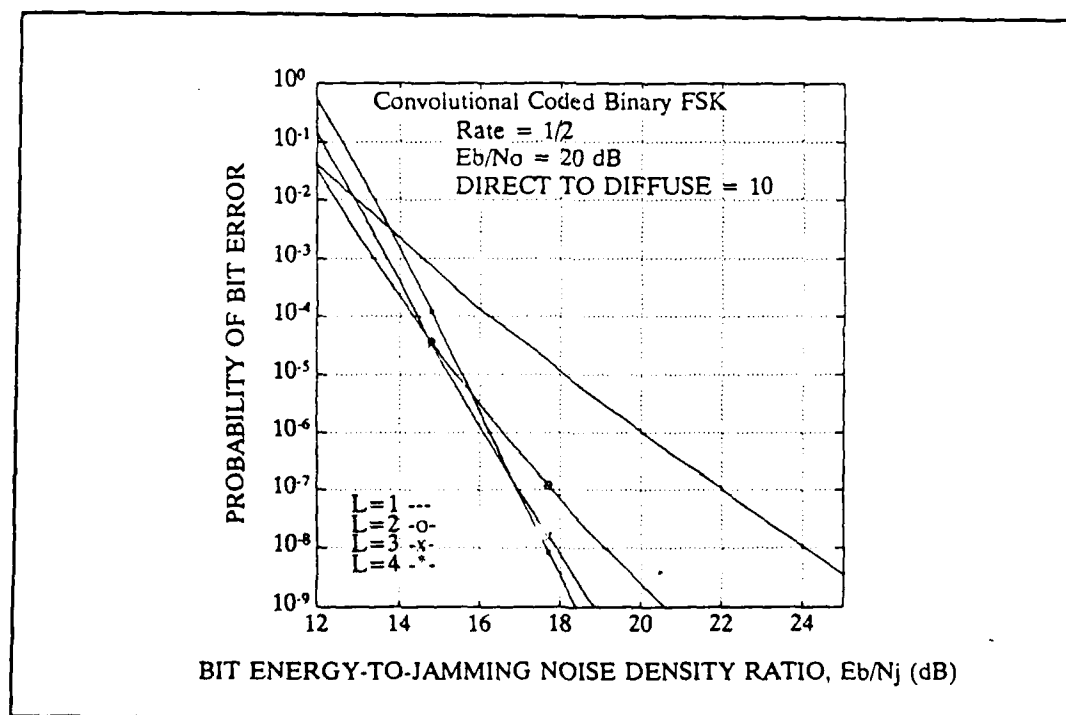


Figure 30. Rate 1/2 Convolutional Coded BFSK in a Rician-faded channel with $E_b/N_o = 20$ dB.

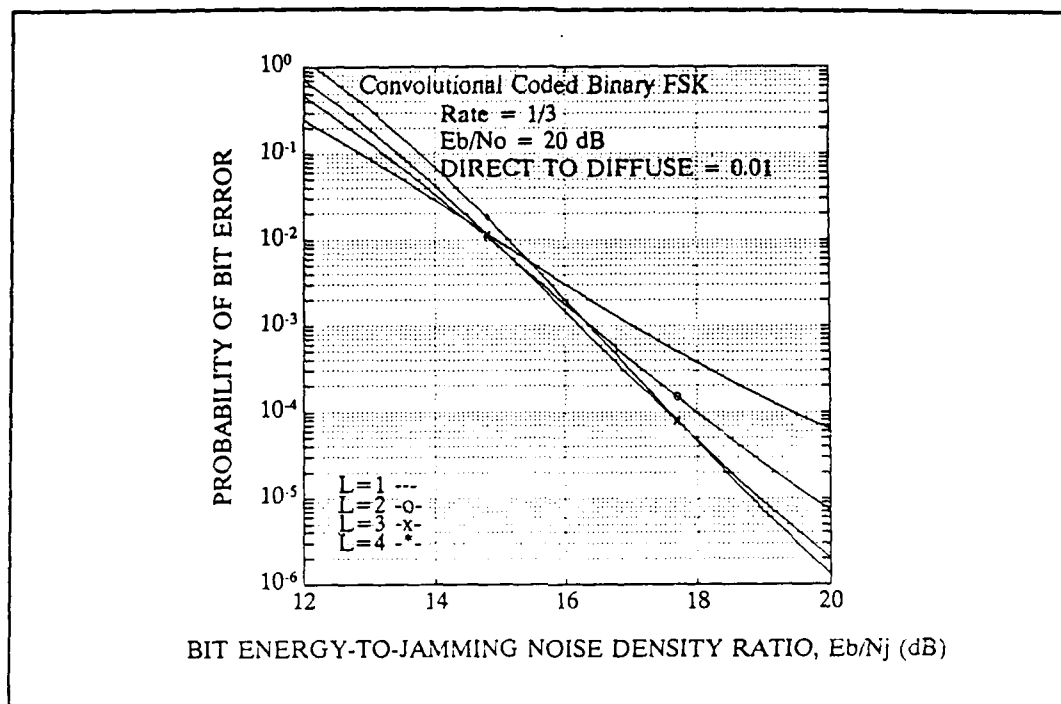


Figure 31. Rate 1/3 Convolutional Coded BFSK in a Rayleigh-faded channel with $E_b/N_o = 20$ dB.

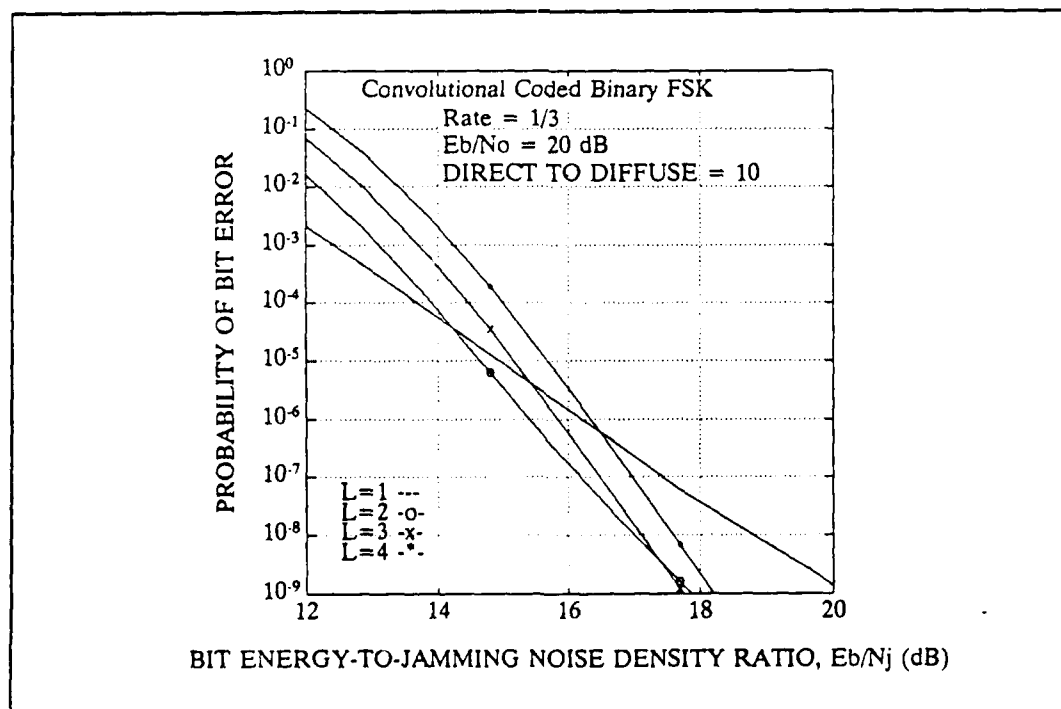


Figure 32. Rate 1/3 Convolutional Coded BFSK in a Rician-faded channel with $E_b/N_o = 20$ dB.

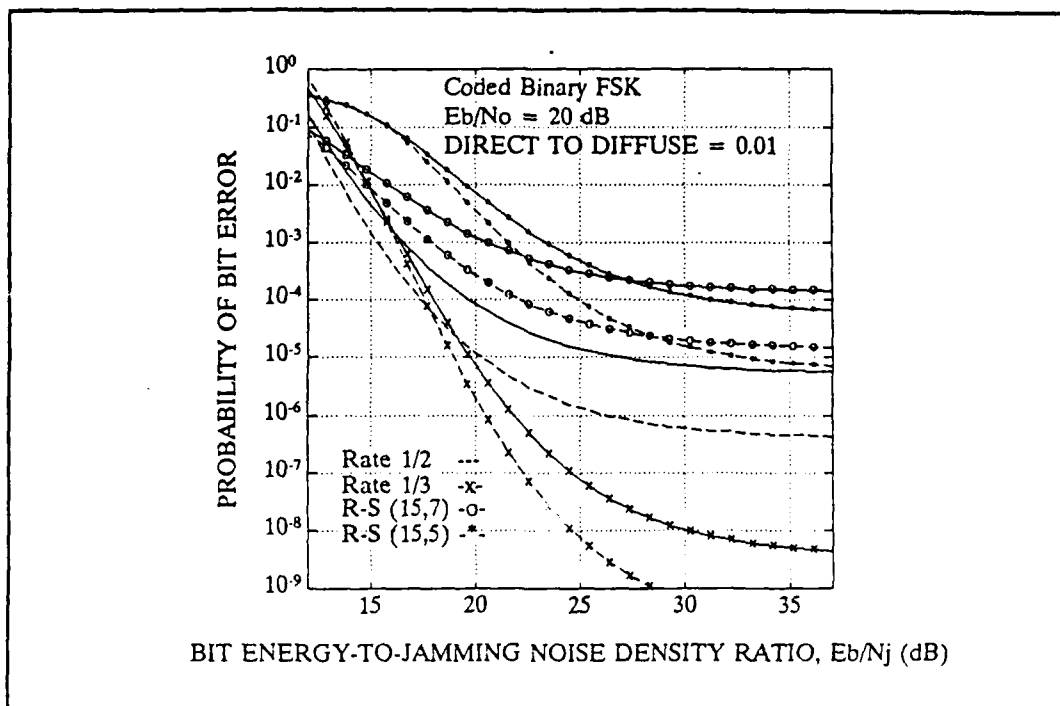


Figure 33. Coded Performance for BFSK, $L=2$ (solid) and $L=3$ (dashed) in a Rayleigh channel with $E_b/N_o = 20$ dB.

system performance to number of symbol errors that can be corrected. The maximum number of correctable bit errors are 4 and 5, respectively, for the two codes shown. The power of the Reed-Solomon block codes is further illustrated by Figures 35 through 38, where the block length is increased from 15 to 63 for 4-ary MFSK (meaning that the constraint specified previously that $q/K = 2$ is increased to $q/K = 3$). These figures show the difference in system performance between Reed-Solomon and convolutional codes narrowing for both Rayleigh- and Rician-channel models as the block length increases from 15 in BFSK to 63 in the 4-ary FSK system. In Figure 36 the (15,5) Reed-Solomon code performance surpasses that of the (15,7) at $E_b/N_j = 14$ dB for $L=2$ and at 16.5 dB for $L=3$. This figure also shows the rate

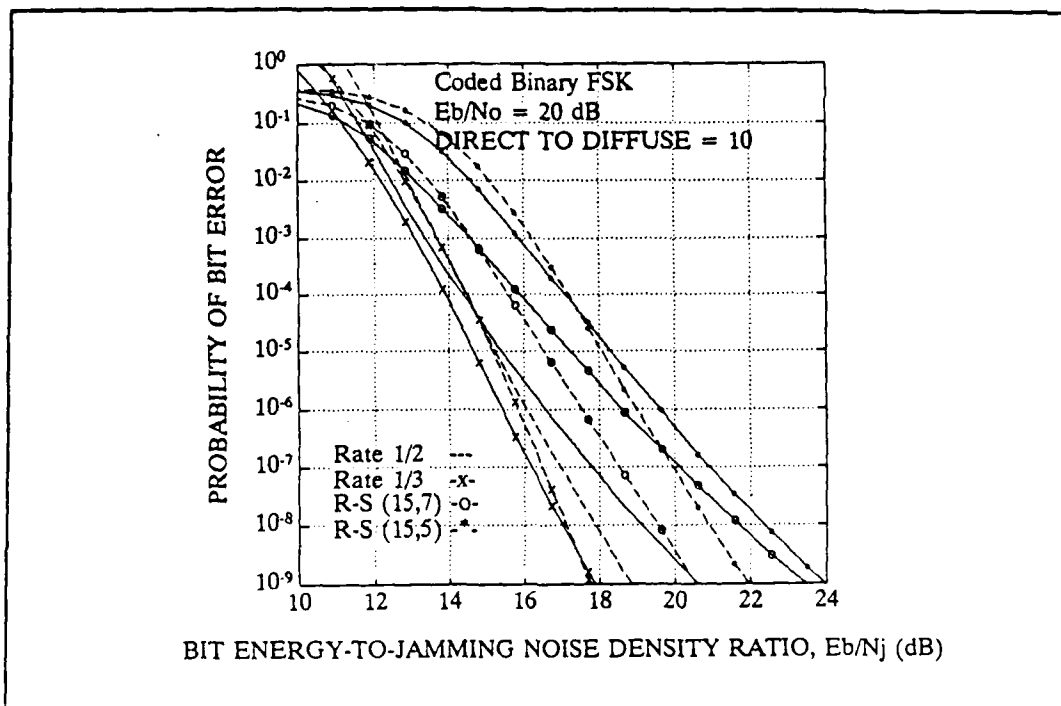


Figure 34. Coded Performance for BFSK, $L=2$ (solid) and $L=3$ (dashed), in a Rician channel with $E_b/N_o = 20$ dB.

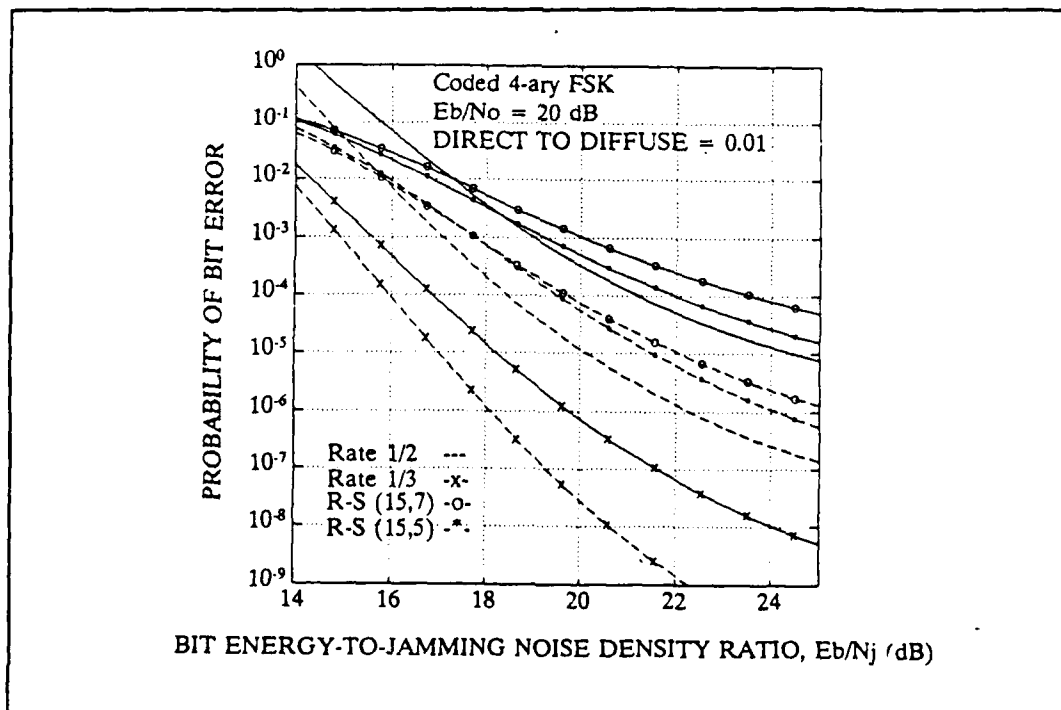


Figure 35. Coded Performance for 4-ary FSK, for $L=2$ (solid) and $L=3$ (dashed), in a Rayleigh-faded channel with $E_b/N_o = 20$ dB.

1/3 convolutional code is still superior to all the codes with respect to best performance. In Figures 37 and 38 the block length of the Reed-Solomon code has been increased to 63 resulting in (63,31) and (63,21) codes to maintain rates close to 1/2 and 1/3 for comparison. Notice that, where the results of Figures 35 and 36 show the rate 1/2 and 1/3 convolutional codes superior for jamming power ratios down to 12 dB, the Reed-Solomon codes become superior at 19 dB for $L = 2$ and 16.5 dB for $L = 3$ in Rayleigh fading (Figure 37) and at 12 dB and 12.5 dB in Rician fading (Figure 38). In theory, the block length can be increased to any value without changing the overall code rate. Thereby producing further improvement in system performance, so that the Reed-Solomon block codes should eventually out perform

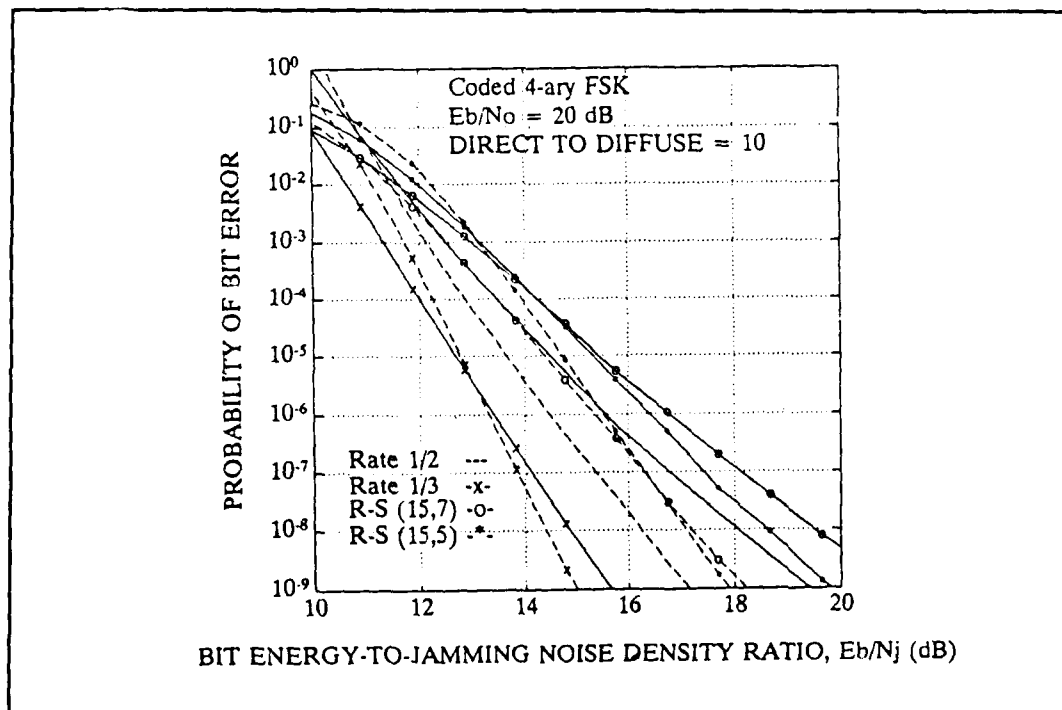


Figure 36. Coded Performance for 4-ary FSK, $L=2$ (solid) and $L=3$ (dashed), in a Rician channel with $E_b/N_0 = 20$ dB.

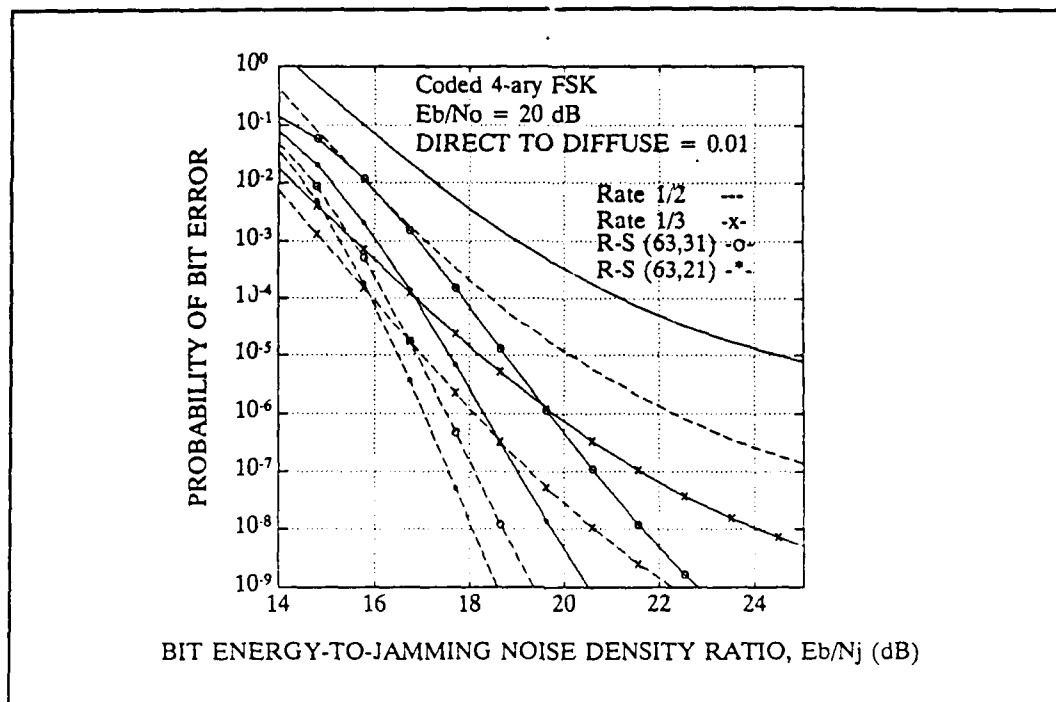


Figure 37. Coded Performance for 4-ary FSK, $L=2$ (solid) and $L=3$ (dashed), in a Rayleigh channel with $E_b/N_o = 20$ dB.

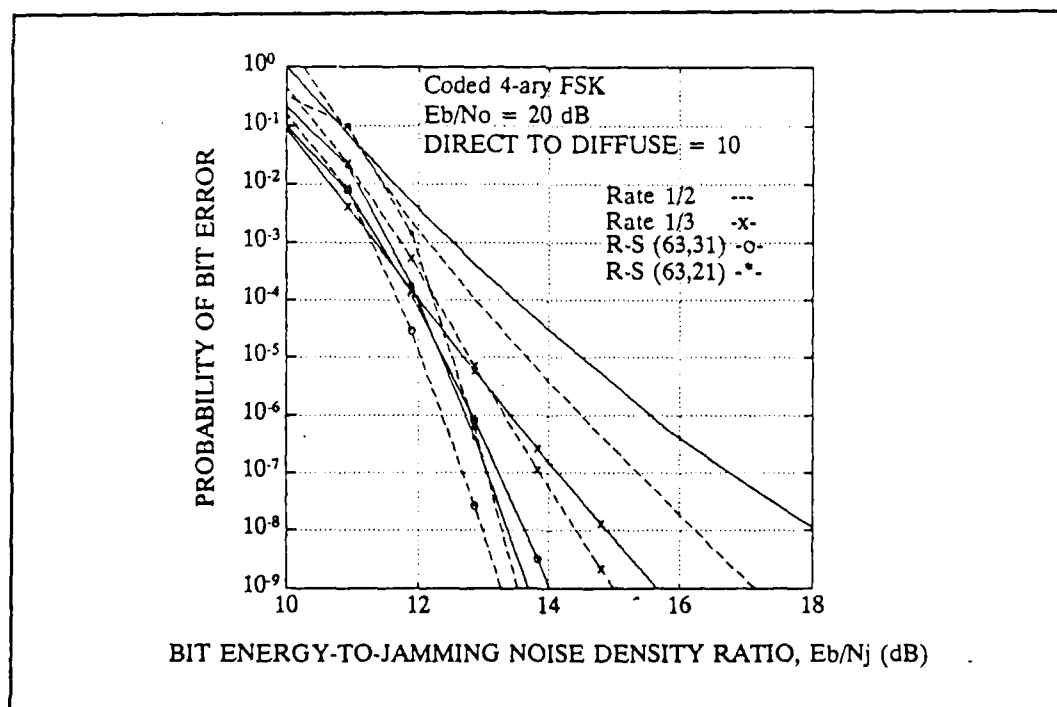


Figure 38. Coded Performance for 4-ary FSK, for $L=2$ (solid) and $L=3$ (dashed), in a Rician-faded channel with $E_b/N_o = 20$ dB.

the convolutional codes regardless of the jamming power ratio. The performance increases further still by using $M = 8$, as shown in Figures 39 and 40, where $q/K = 2$ is used again. Here the Reed-Solomon codes have surpassed the performance of the convolutional codes without increasing the block length over the previous value. The analysis for a (511,255) Reed-Solomon ($q/K = 3$) was attempted for $M = 8$, but the small values of probability of error caused a numerical underflow in the computer calculation of (4.8). The main drawback of the approach of increasing block length to obtain an acceptable performance standard is that the large block size requires larger and larger memory circuits to form the codewords for transmission. This inherently prevents the transmission of real-time data because of the codeword formulation time.

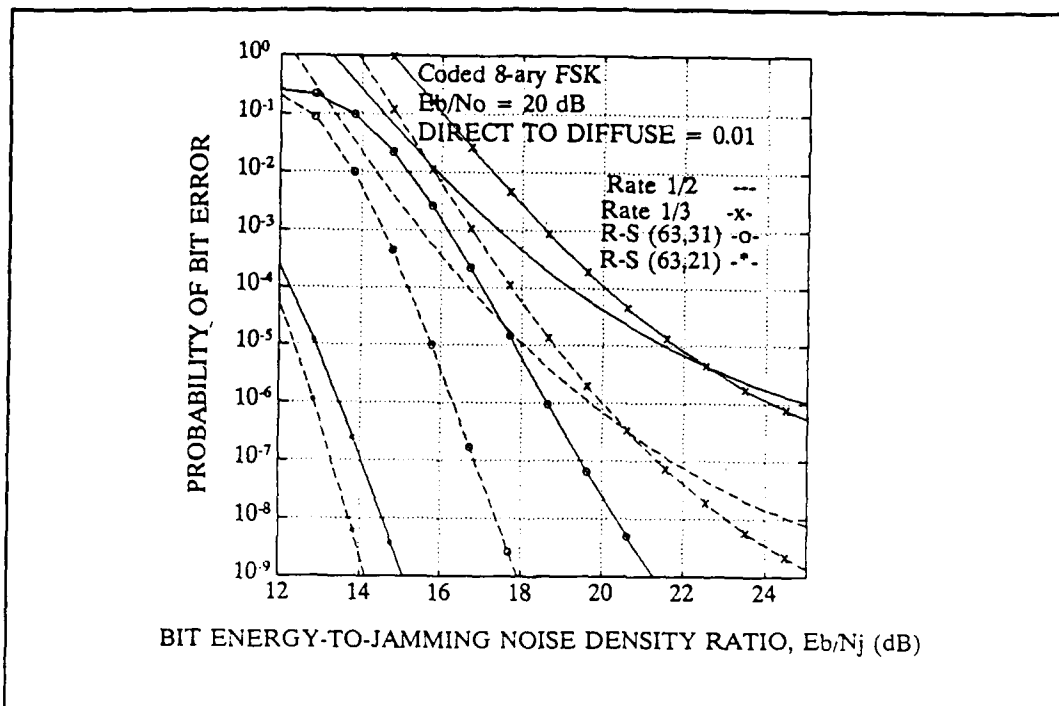


Figure 39. Coded Performance for 8-ary FSK, for $L=2$ (solid) and $L=3$ (dashed), in a Rayleigh-faded channel with $E_b/N_o = 20$ dB.

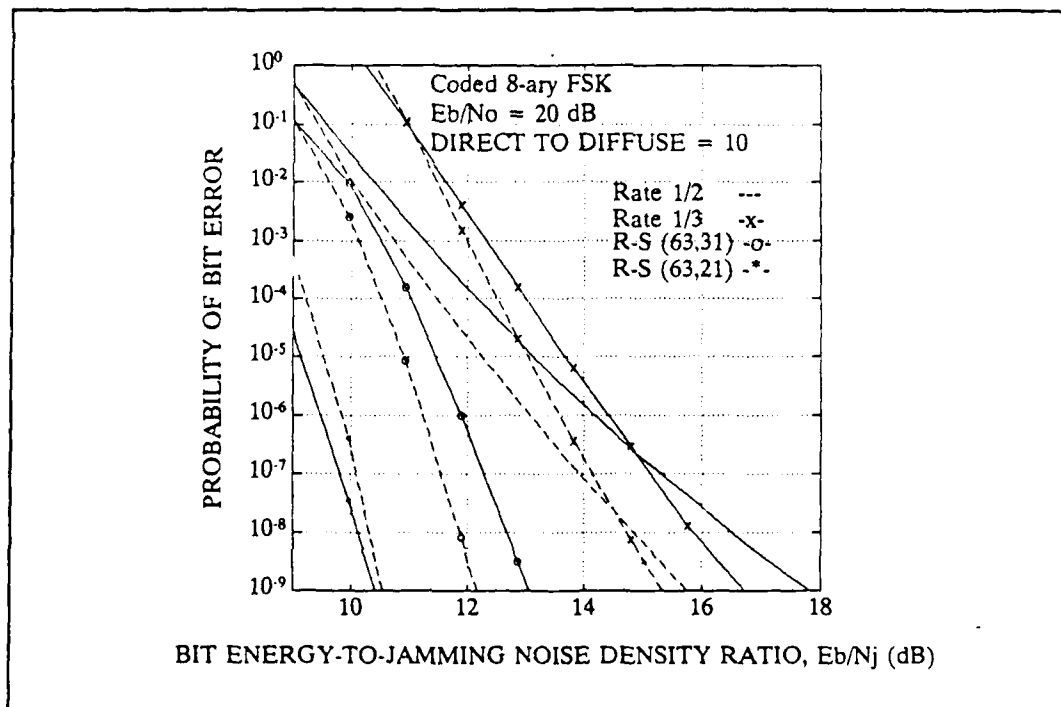


Figure 40. Coded Performance for 8-ary FSK, for $L=2$ (solid) and $L=3$ (dashed), in a Rician-faded channel with $E_b/N_o = 20$ dB.

VI. CONCLUSIONS AND RECOMMENDATIONS

A. CONCLUSIONS

Theoretical results for the self-normalizing quadratic detector have been presented for both the uncoded and error correction coded performance in Rayleigh- and Rician-faded channels. The effects of fading were detrimental for either fading model, but it was found that fast-frequency-hopping in general could provide a means to overcome, at least partially, those effects as well as the effects of worst-case partial-band jamming. This was especially true for the Rayleigh-fading model, as higher levels of diversity always provided improved performance. However, the Rician channel for low values of SNR_T and without jamming present perform best for slow-frequency hopping ($L = 1$).

Incorporation of FEC coding always improved the performance of the system in either Rayleigh- or Rician-faded channels. The improvement in bit-error ratios is seen to be exponential in nature, i.e., as uncoded performance improves, the coded performance improves exponentially faster for the same signal-to-total-noise ratio. In particular, the research investigated Reed-Solomon (n,k) block codes and constraint length 7, best rate 1/2 and 1/3 convolutional codes. In cases of low SNR_T , the rate 1/3 convolutional codes proved superior in performance to all other coding schemes, provided the block length of the Reed-Solomon codes was kept within reasonable limits. If the system were for data transmissions only, the Reed-Solomon

codes with large block lengths would be preferred over the convolutional codes since they would not only provide equal, if not better, performance, but also are well suited to correcting burst errors as described in Chapter II.

B. RECOMMENDATIONS

Theoretically, the self-normalization receiver performs well in fading channels with partial-band noise jamming. To verify the results presented here, a hardware system should be built and tested to obtain actual data for performance comparisons. The coding schemes presented have been used in numerous real-world systems, so, although the results for a tested system would be of interest, they are already well documented and need no further analysis on the basic codes. However, the benefits of the Reed-Solomon codes for burst error correction capabilities were not addressed here and should be pursued in the future. Additionally, the use of concatenated coding schemes and the advantages provided by interleaving the bit stream between hops would both be practical and provide significant improvement in system performance. Therefore, the benefits of these two schemes should also be addressed by further investigation and studies as well.

Since the LASAT system will be used for voice and data simultaneously, the effects of mixing voice and data packets should be investigated and the protocols necessary to perform the mixing need to be developed. Additionally, research should be done to determine the effects of increasing the block length of the Reed-Solomon codes on throughput of the system for both voice and data packets, including the effect of round-trip transmission delay to the satellite.

APPENDIX A - Derivation of Equation (3.14)

The unconditional probability density function X_{1k} is found by integrating the conditional probability density function over the range of the conditioning variable.

The conditioning variable is the amplitude value a_k and the integral is

$$\begin{aligned}
 f_{x_{1k}}(x_{1k}) &= \int_0^{\infty} f_{x_{1k}|a_k}(x_{1k}|a_k) f_{A_k}(a_k) da_k \\
 &= \int_0^{\infty} \left[\frac{a_k}{2\sigma_k^2\sigma^2} \right] \exp\left[-\frac{x_{1k} + 2Sa_k^2}{2\sigma_k^2}\right] \exp\left[-\frac{a_k^2 + \alpha_k^2}{2\sigma^2}\right] \times \\
 &\quad I_0\left(\frac{\sqrt{2Sx_{1k}}a_k}{\sigma_k^2}\right) I_0\left(\frac{\alpha_k a_k}{\sigma^2}\right) da_k, \tag{A.1}
 \end{aligned}$$

where $f_{x_{1k}|A_k}(x_{1k}|a_k)$ and $f_{A_k}(a_k)$ are given by (3.10) and (3.12) respectively. The

solution of the integral is found using the following equality [Ref. 17:p. 314]

$$\int_0^{\infty} t e^{-p^2 t^2} J_\nu(at) J_\nu(bt) dt = \frac{1}{2p^2} e^{-(a^2 + b^2)/4p^2} I_\nu\left(\frac{ab}{2p^2}\right), \tag{A.2}$$

where $J_\nu(x)$ is the ν th order Bessel function of the first kind. Using the relationship

$I_0(x) = J_0(ix)$ and the following substitutions

$$t = a_k, \quad v = 0,$$

$$p^2 = \left(\frac{\sigma^2 + 2S\sigma_k^2}{2\sigma_k^2 \sigma^2} \right), \quad (\text{A.3})$$

$$a = j \frac{\sqrt{2Sx_{1k}}}{\sigma_k^2}, \quad b = j \frac{\alpha_k}{\sigma^2},$$

the result is,

$$\begin{aligned} f_{x_{1k}}(x_{1k}) &= \frac{1}{2\sigma_k^2 \sigma^2} \exp \left[-\frac{1}{2} \left(\frac{x_{1k}}{\sigma_k^2} + \frac{\alpha_k^2}{\sigma^2} \right) \right] \frac{\sigma_k^2 \sigma^2}{\sigma_k^2 + 2S\sigma^2} \\ &\times \exp \left[\frac{\frac{2Sx_{1k}}{\sigma_k^4} + \frac{\alpha_k^2}{\sigma^4}}{2 \left(\frac{\sigma_k^2 + 2S\sigma^2}{\sigma_k^2 \sigma^2} \right)} \right] I_0 \left(\frac{\frac{\sqrt{2Sx_{1k}} \alpha_k}{\sigma_k^2 \sigma^2}}{\frac{\sigma_k^2 + 2S\sigma^2}{\sigma_k^2 \sigma^2}} \right). \end{aligned} \quad (\text{A.4})$$

Rearranging the terms yields

$$\begin{aligned}
f_{x_{1k}}(x_{1k}) &= \frac{1}{2(\sigma_k^2 + 2S\sigma^2)} \\
&\times \exp \left[-\frac{1}{2} \left[\frac{x_{1k}}{\sigma_k^2} \left(1 - \frac{2S\sigma^2}{(\sigma_k^2 + 2S\sigma^2)} \right) + \frac{\alpha_k^2}{\sigma^2} \left(1 - \frac{\sigma_k^2}{(\sigma_k^2 + 2S\sigma^2)} \right) \right] \right] \\
&\times I_0 \left(\frac{\sqrt{2Sx_{1k}} \alpha_k}{\sigma_k^2 + 2S\sigma^2} \right). \tag{A.5}
\end{aligned}$$

This can be rearranged again to yield

$$f_{x_{1k}}(x_{1k}) = \frac{1}{2(\sigma_k^2 + 2S\sigma^2)} \exp \left[-\frac{1}{2} \left(\frac{x_{1k} + 2S\alpha_k^2}{\sigma_k^2 + 2S\sigma^2} \right) \right] I_0 \left(\frac{\sqrt{2Sx_{1k}} \alpha_k}{\sigma_k^2 + \sigma^2} \right), \tag{A.6}$$

which is (3.14).

APPENDIX B - Derivation of Equation (3.28)

The unconditional probability density function for Z_{1k} is found by integrating the conditional density over the range of the auxiliary variable ζ_k . This integral is

$$f_{Z_{1k}}(z_{1k}) = \int_0^{\infty} f_{Z_{1k}|\zeta_k}(z_{1k}|\zeta_k) d\zeta_k. \quad (B.1)$$

This becomes

$$\begin{aligned} f_{Z_{1k}}(z_{1k}) &= \frac{1}{(1 + \beta_k)} \left(\frac{1}{2\sigma_k^2} \right)^M \exp \left[-\frac{\rho_k}{1 + \beta_k} \right] (1 - z_{1k})^{M-2} \frac{1}{(M-2)!} \\ &\times \int_0^{\infty} \zeta_k^{M-1} \exp \left[-\zeta_k \left(\frac{1 + \beta_k(1 - z_{1k})}{2\sigma_k^2(1 + \beta_k)} \right) \right] \\ &\times I_0 \left(\frac{2 \sqrt{\frac{z_{1k} \rho_k}{\sigma_k^2} \frac{1}{2} \sqrt{\zeta_k}}}{1 + \beta_k} \right) d\zeta_k. \end{aligned} \quad (B.2)$$

The solution of the integral is found using the following identity [Ref. 18:p. 720].

$$\int_0^{\infty} x^{n + \frac{\nu}{2}} e^{-ax} J_{\nu}(2\beta\sqrt{x}) dx = n! \beta^{\nu} e^{-\frac{\beta^2}{a}} a^{-n-\nu-1} L_n^{\nu} \left(\frac{\beta^2}{a} \right), \quad (B.3)$$

where $L_n^{\nu}(x)$ is the generalized LaGuerre polynomial

$$L_n^v(x) = \sum_{m=0}^n (-1)^m \binom{n+v}{n-m} \frac{(x)^m}{m!} . \quad (\text{B.4})$$

Then using the relationship, $I_o(x) = J_o(jx)$, and the following substitutions

$$v = 0, \quad n = m - 1, \quad (\text{B.5})$$

$$a = \frac{1 + \beta_k(1-z_{1k})}{2\sigma_k^2(1 + \beta_k)}, \quad b = j \frac{\sqrt{\frac{z_{1k} \rho_k}{2\sigma_k^2}}}{1 + \beta_k},$$

the density becomes

$$f_{Z_{1k}}(z_{1k}) = \frac{M-1}{(1+\beta_k)} (1 - z_{1k})^{M-2} \left[\frac{(1 + \beta_k)}{(1 + \beta_k(1 - z_{1k}))} \right]^M$$

$$\times \exp \left[-\frac{\rho_k (1 - z_{1k})}{1 + \beta_k(1 - z_{1k})} \right]$$

$$\times \sum_{m=0}^{M-1} \binom{M-1}{M-1-m} \frac{1}{m!} \left[\frac{z_{1k} \rho_k}{(1 + \beta_k)(1 + \beta_k(1 - z_{1k}))} \right]^m . \quad (\text{B.6})$$

This is the unconditional density function for Z_{1k} given in (3.25).

APPENDIX C - Additional Illustrations

This Appendix contains additional figures that illustrate various cases of signal-to-thermal-noise ratios and direct-to-diffuse ratios for fading channels. These are intended to provide the reader with supplemental information to the cases discussed in Chapter V. The specific information about each case is contained on the graphs and in the graph titles.

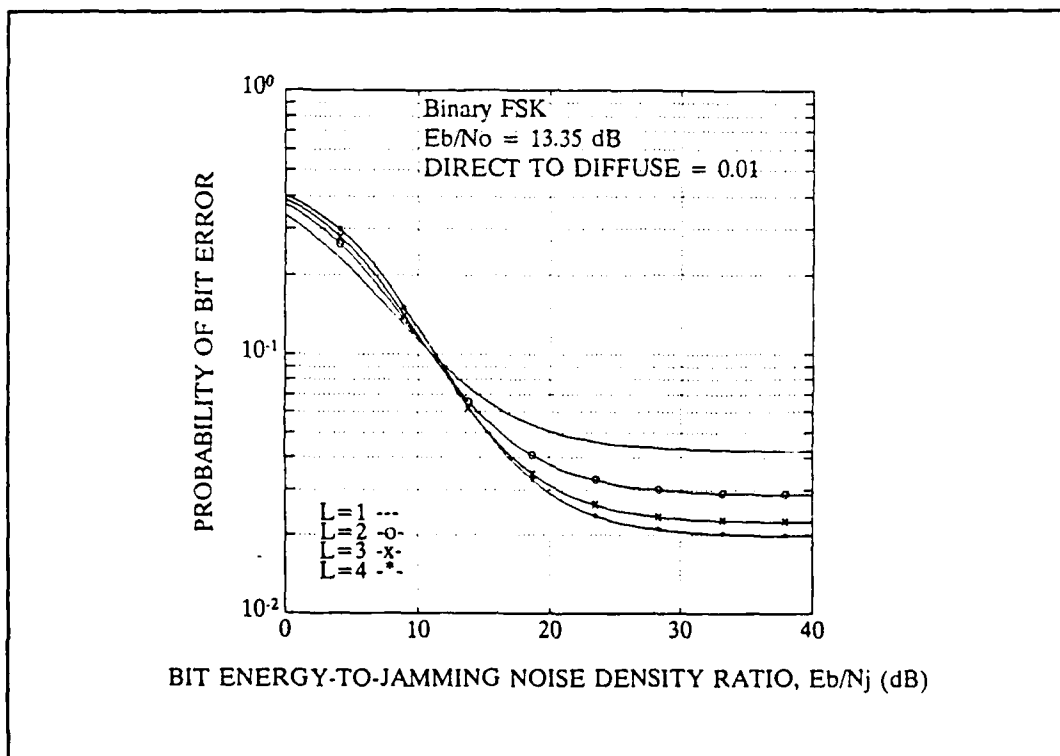


Figure C.1 Uncoded Performance for BFSK in a deeply-faded Rayleigh channel with $E_b/N_o = 13.35$ dB.

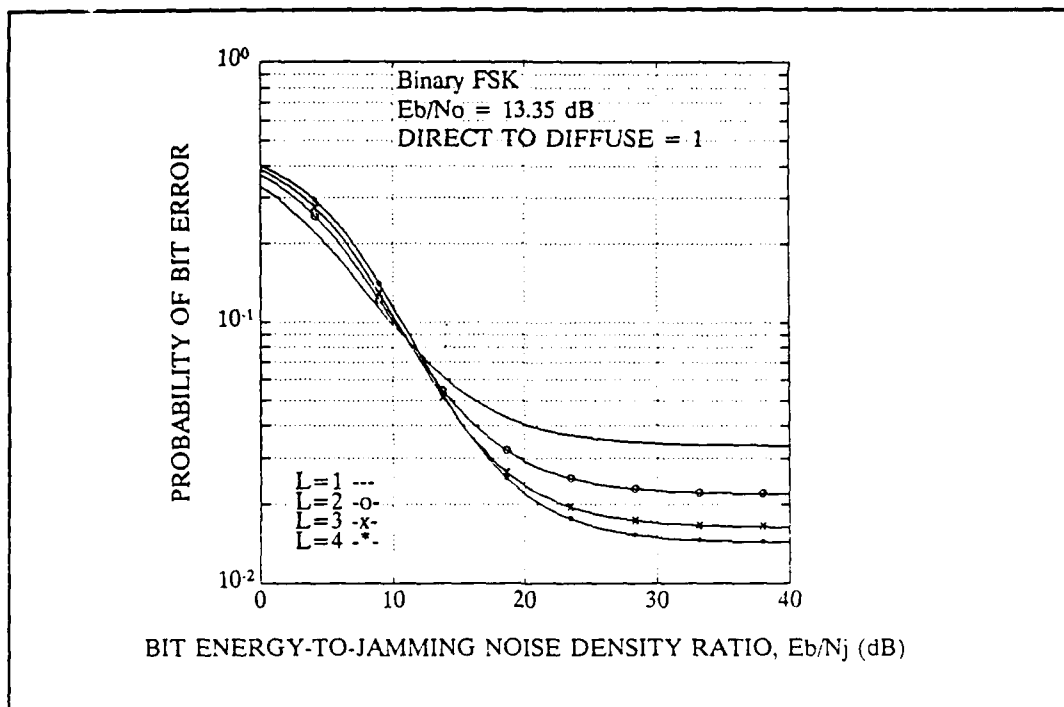


Figure C.2 Uncoded Performance for BFSK in a moderately-faded Rayleigh channel with $E_b/N_o = 13.35$ dB.

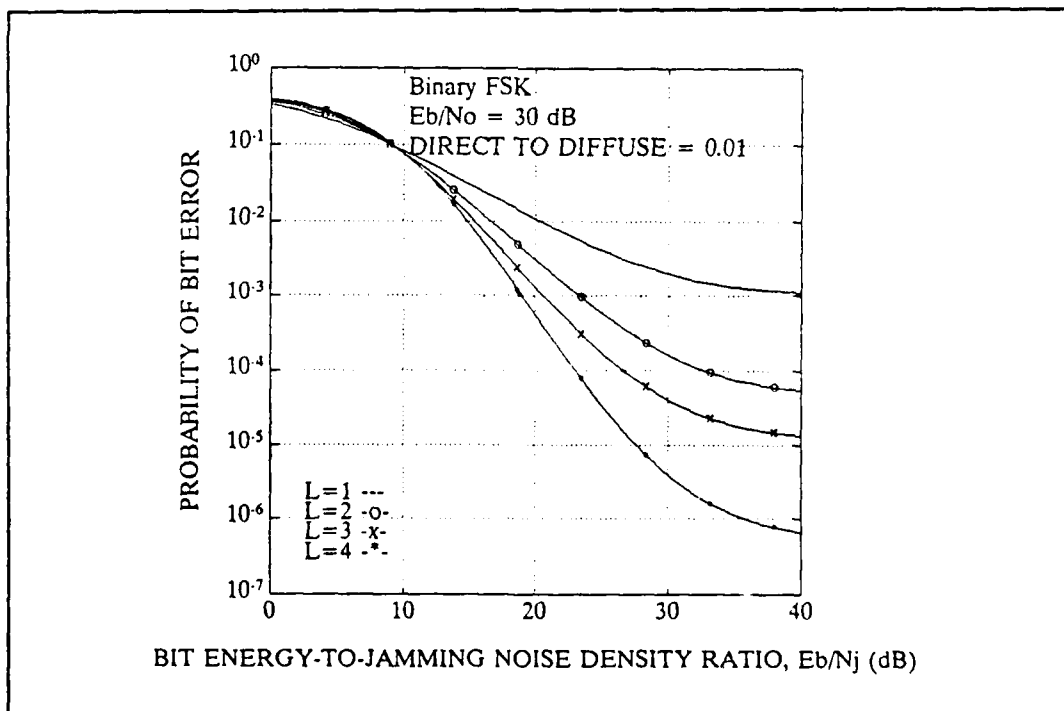


Figure C.3 Uncoded Performance for BFSK in a deeply faded Rayleigh channel with $E_b/N_o = 30$ dB.

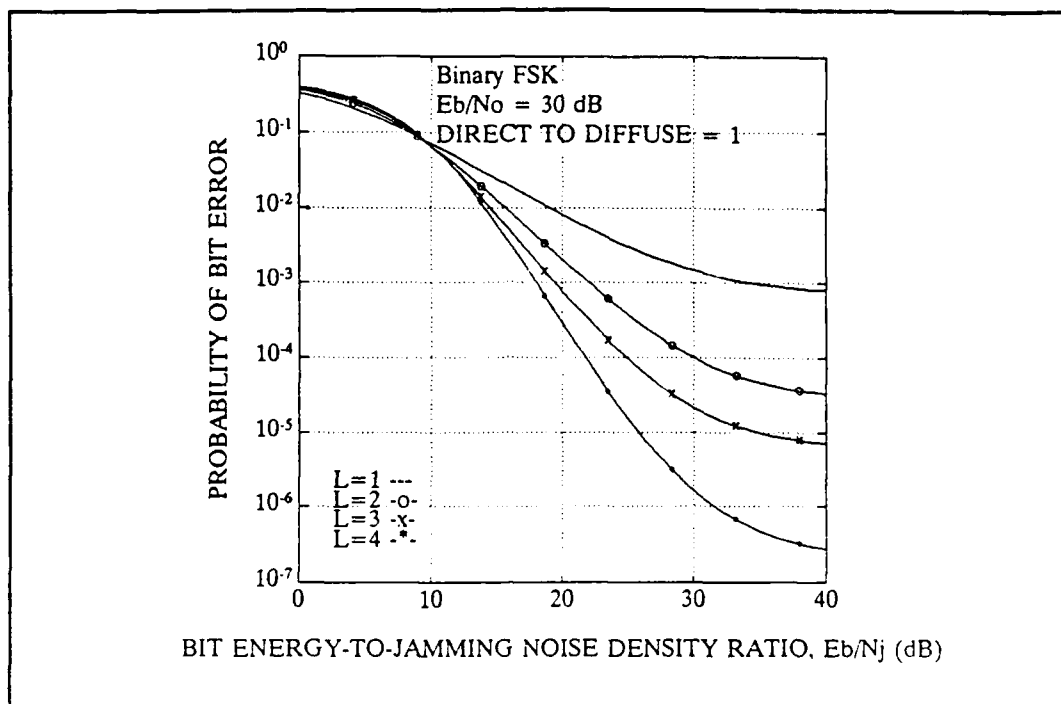


Figure C.4 Uncoded Performance for BFSK in a moderately-faded Rayleigh channel with $E_b/N_o = 30$ dB.

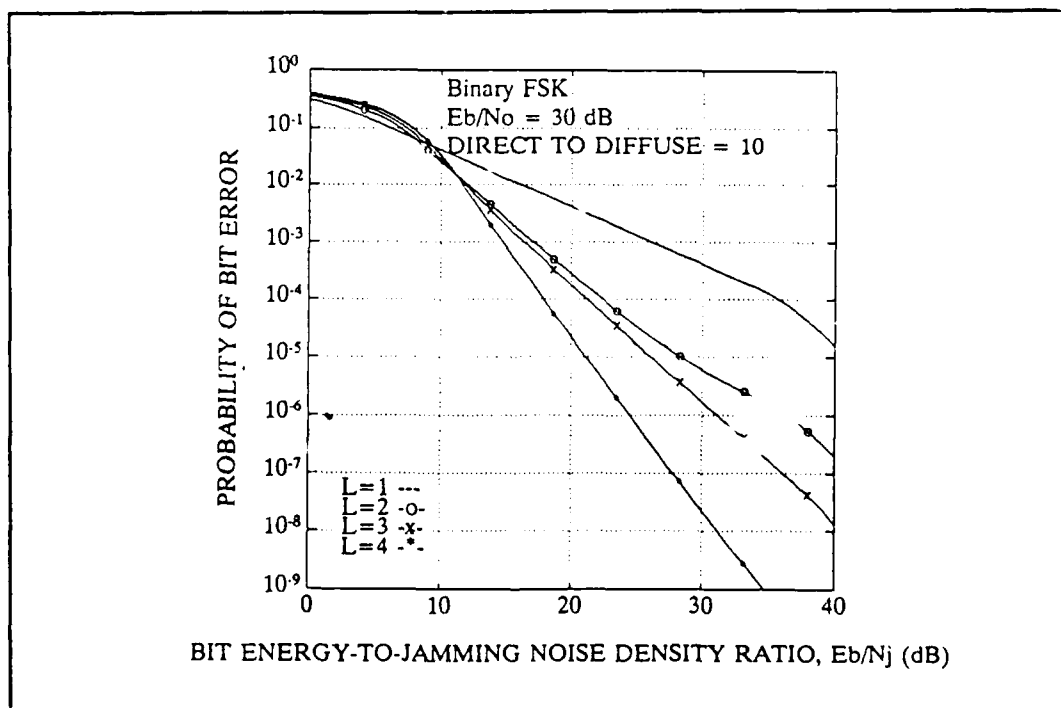


Figure C.5 Uncoded Performance for BFSK in a Rician-faded channel with $E_b/N_o = 30$ dB.

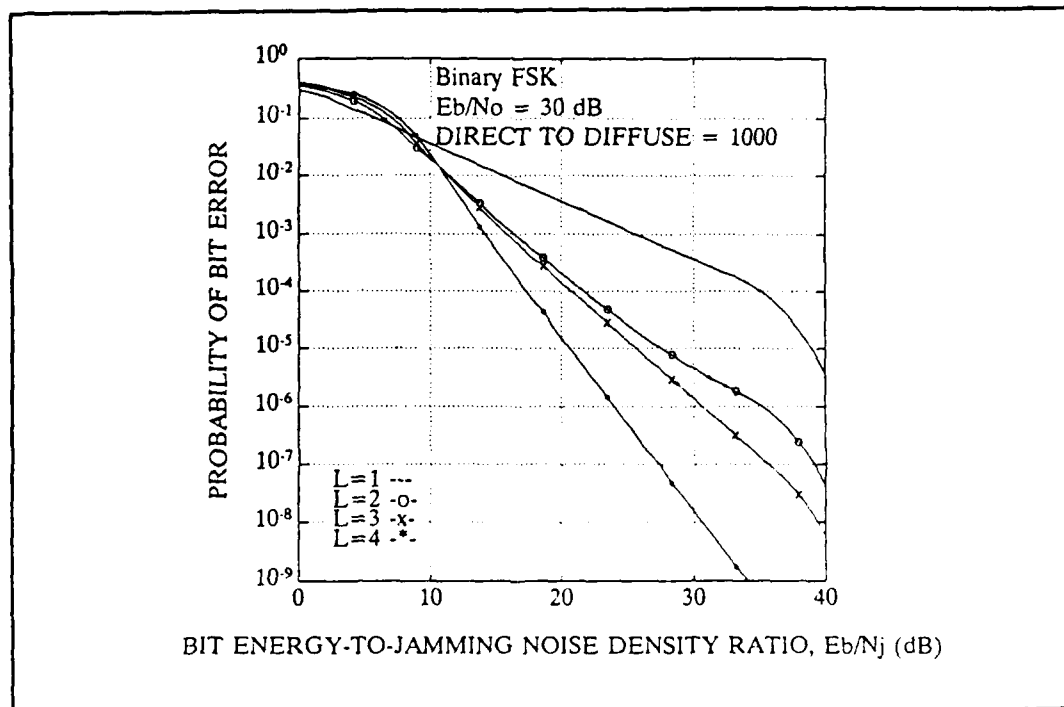


Figure C.6 Uncoded Performance for BFSK in a non-faded channel with $E_b/N_o = 30$ dB.

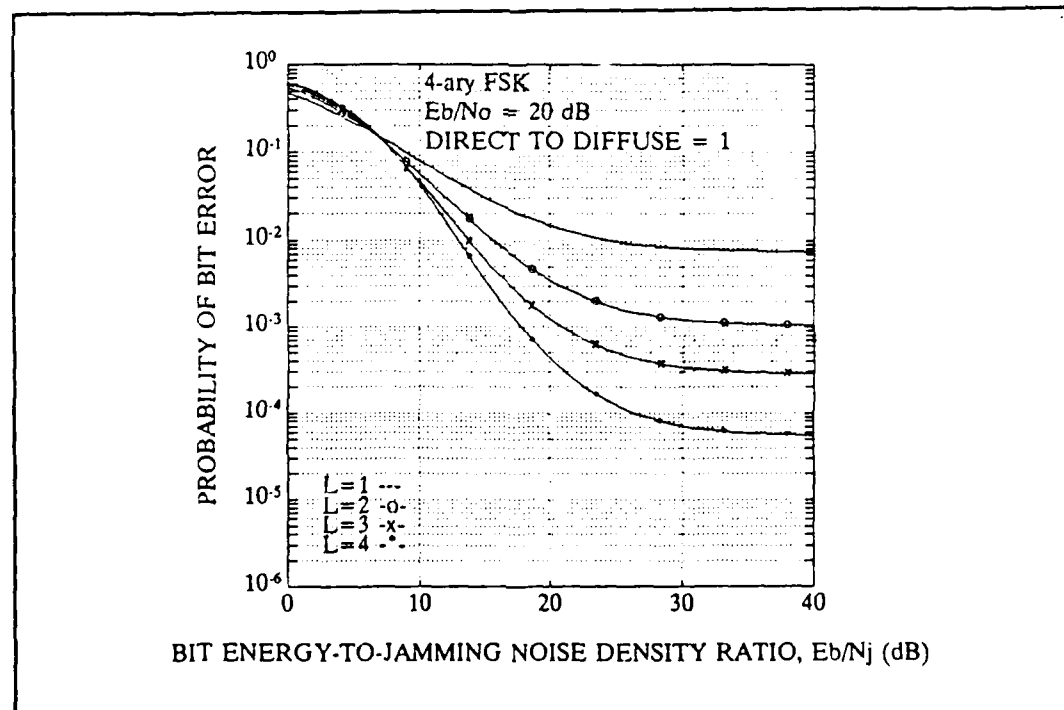


Figure C.7 Uncoded Performance for MFSK, $M=4$, in a moderately-faded Rayleigh channel with $E_b/N_o = 20$ dB.

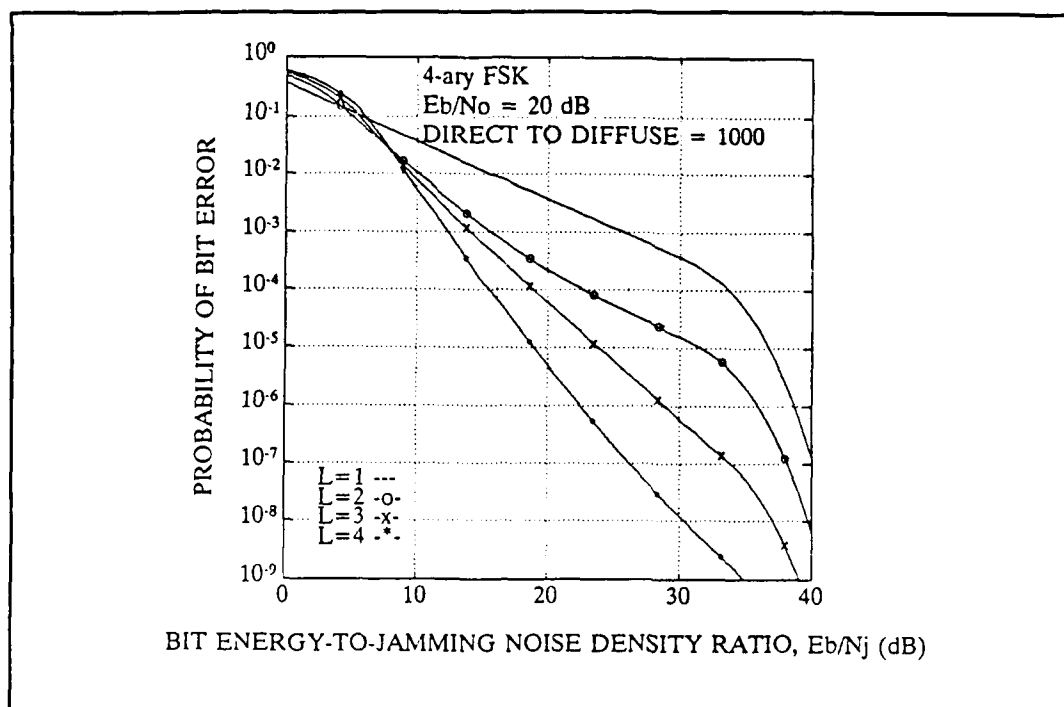


Figure C.8 Uncoded Performance for MFSK, $M=4$, in a non-faded Rayleigh channel with $E_b/N_o = 20$ dB.

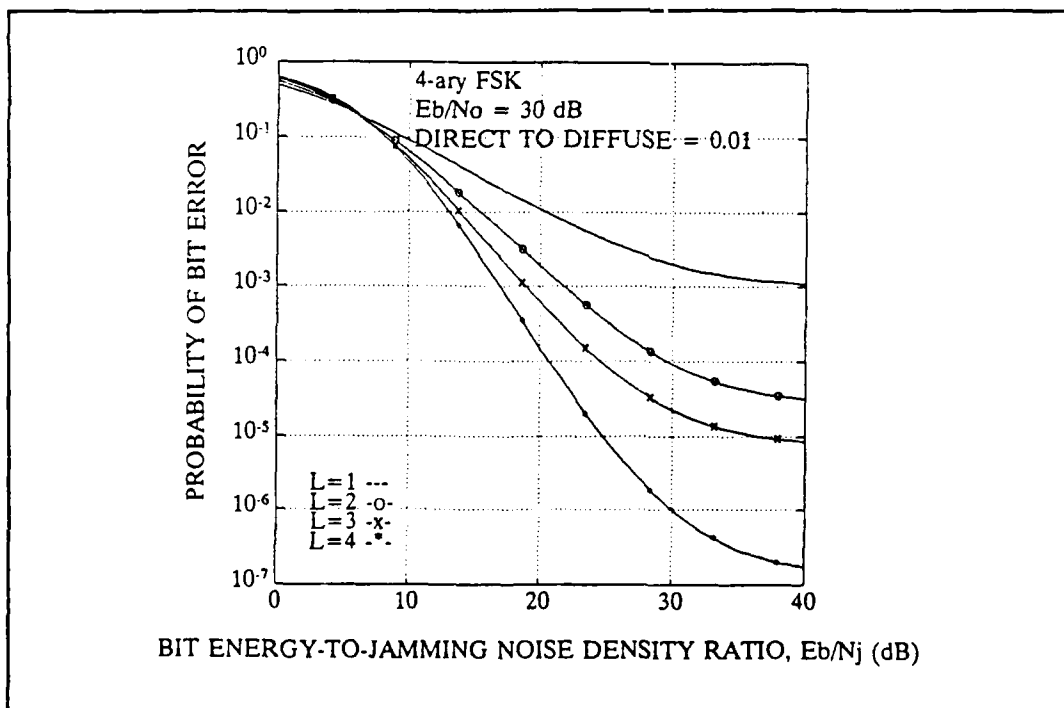


Figure C.9 Uncoded Performance for MFSK, $M=4$, in a deeply-faded Rayleigh channel with $E_b/N_o = 30$ dB.

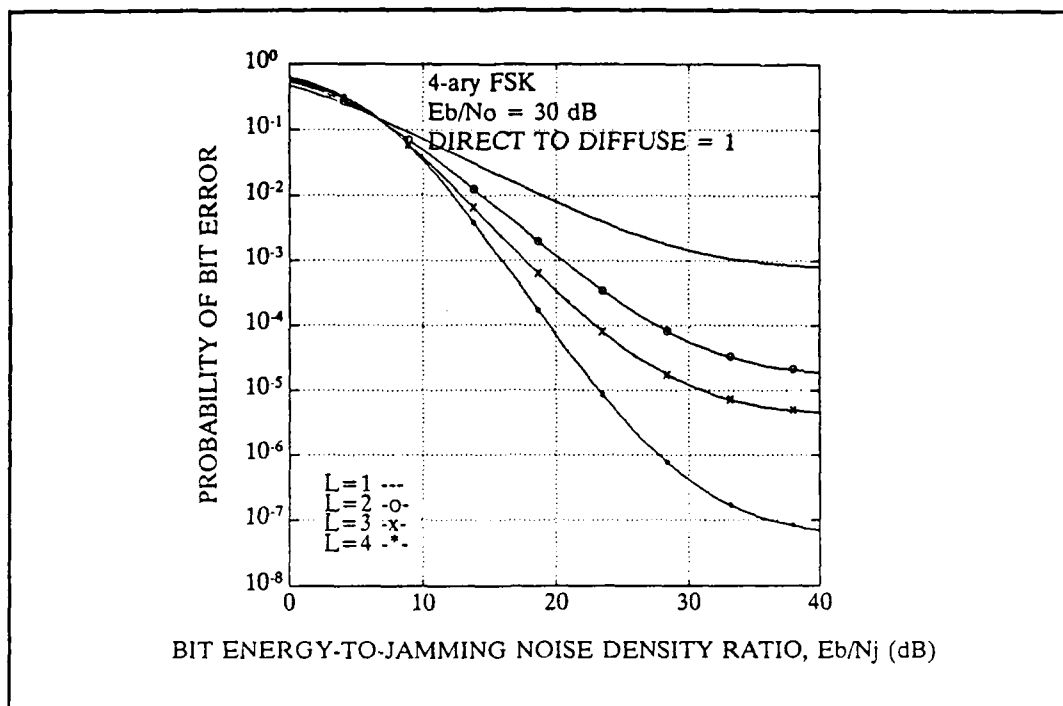


Figure C.10 Uncoded Performance for MFSK, $M=4$, in a moderately-faded Rayleigh channel with $E_b/N_o = 30$ dB.

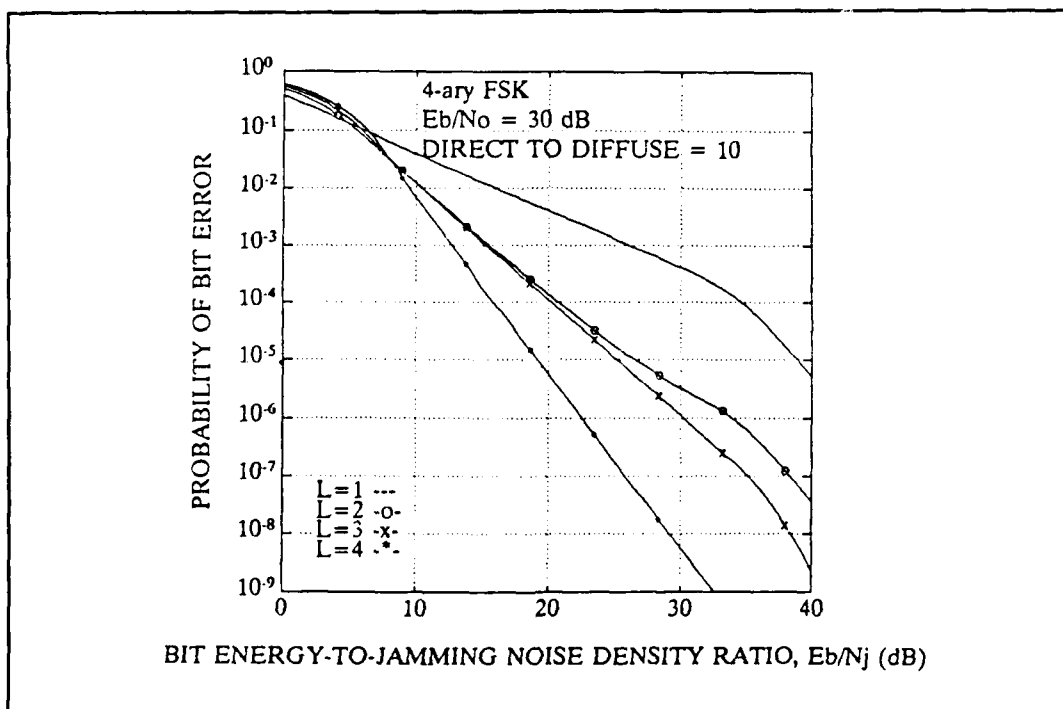


Figure C.11 Uncoded Performance for MFSK, $M=4$, in a Rician-faded channel with $E_b/N_o = 30$ dB.

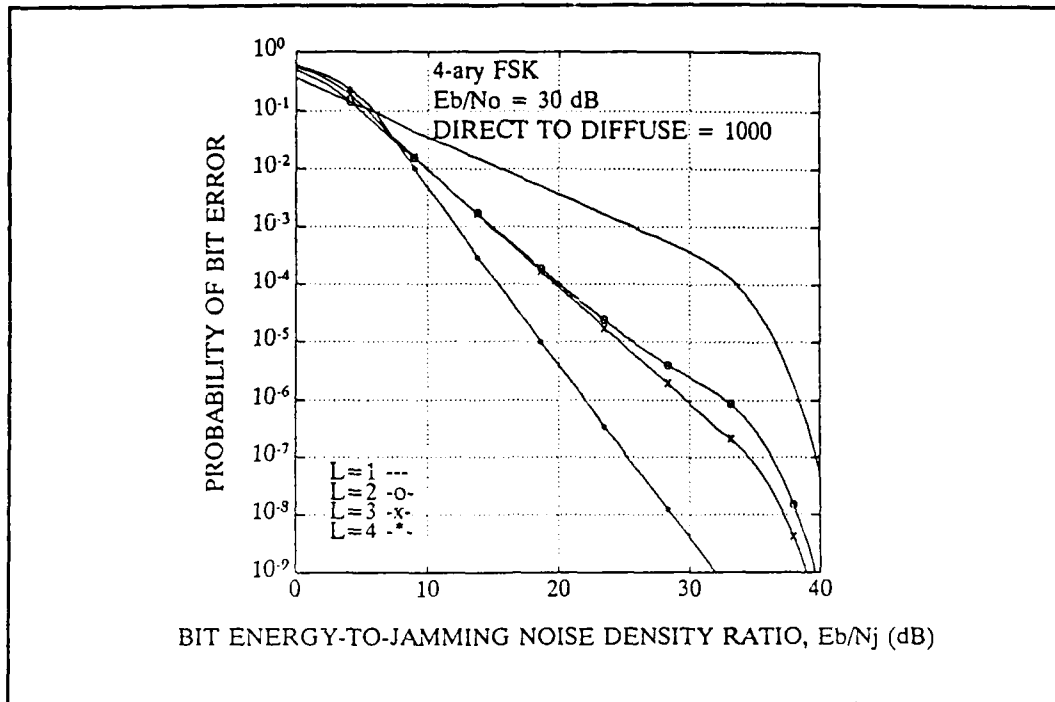


Figure C.12 Uncoded Performance for MFSK, $M=4$, in a non-faded channel with $E_b/N_o = 30$ dB.

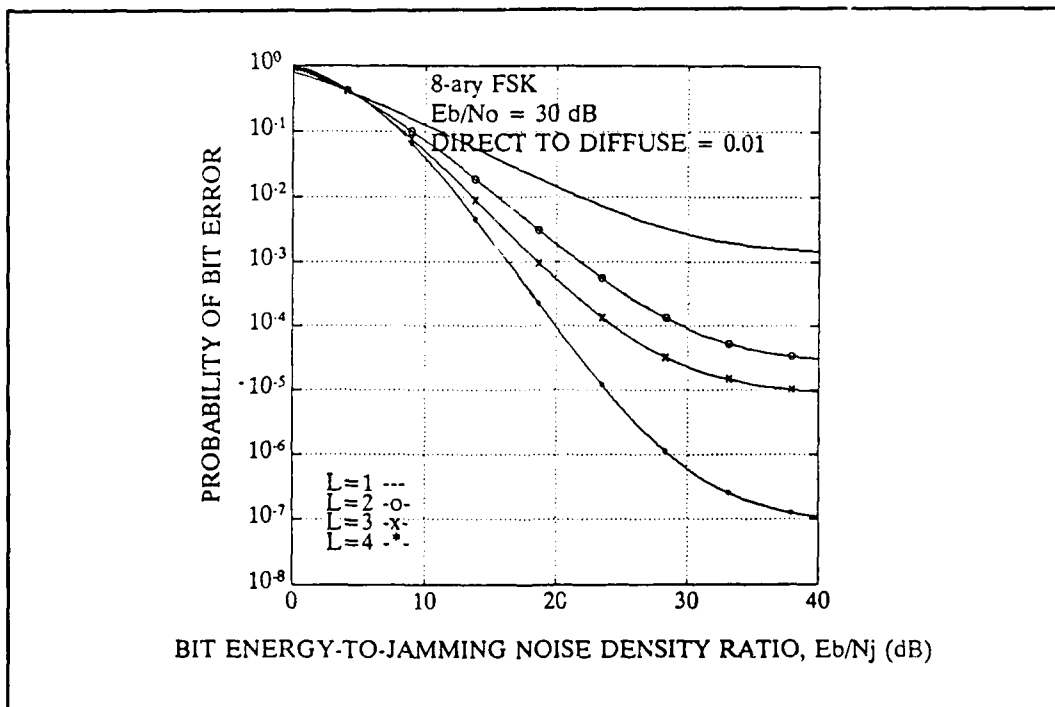


Figure C.13 Uncoded Performance for MFSK, $M=8$, in a Rayleigh-faded channel with $E_b/N_o = 30$ dB.

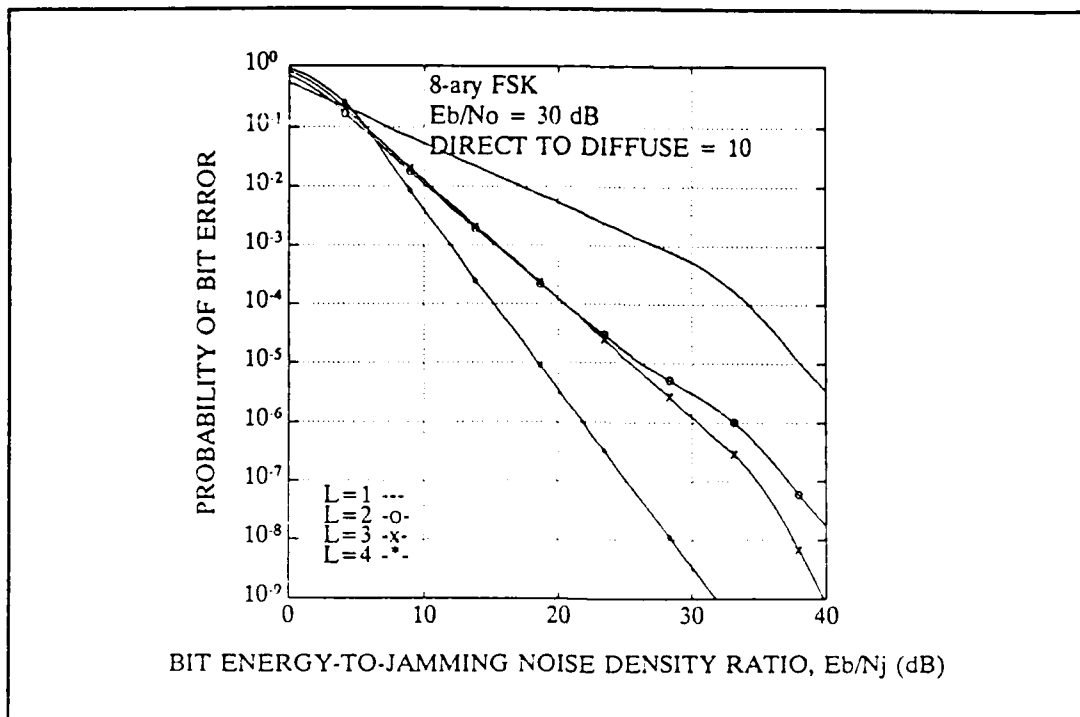


Figure C.14 Uncoded Performance for MFSK, $M=8$, in a Rician-faded channel with $E_b/N_o = 30$ dB.

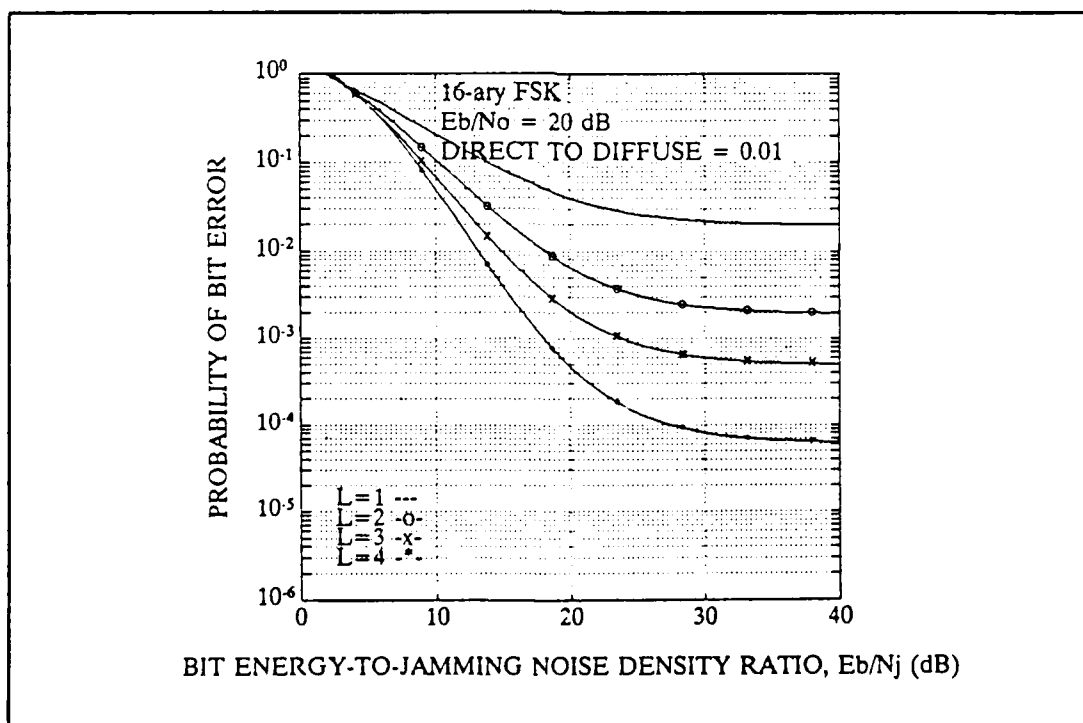


Figure C.15 Uncoded Performance for MFSK, $M=16$, in a Rayleigh-channel with $E_b/N_o = 20$ dB.

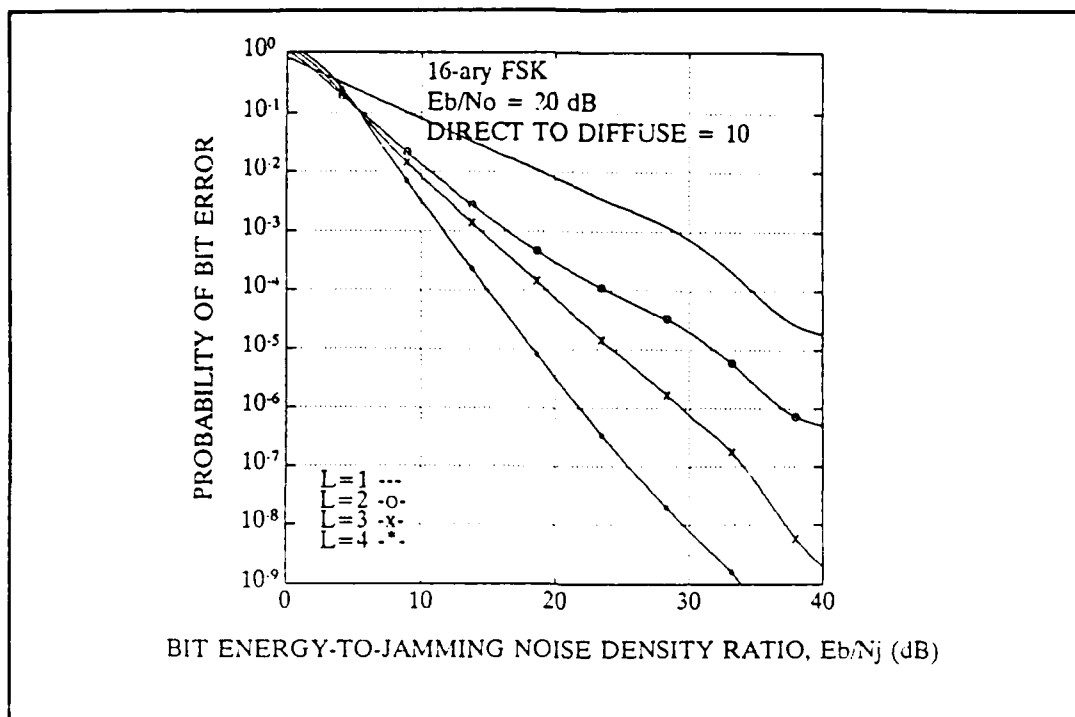


Figure C.16 Uncoded Performance for MFSK, $M=16$, in a Rician-faded channel with $E_b/N_o = 20$ dB.

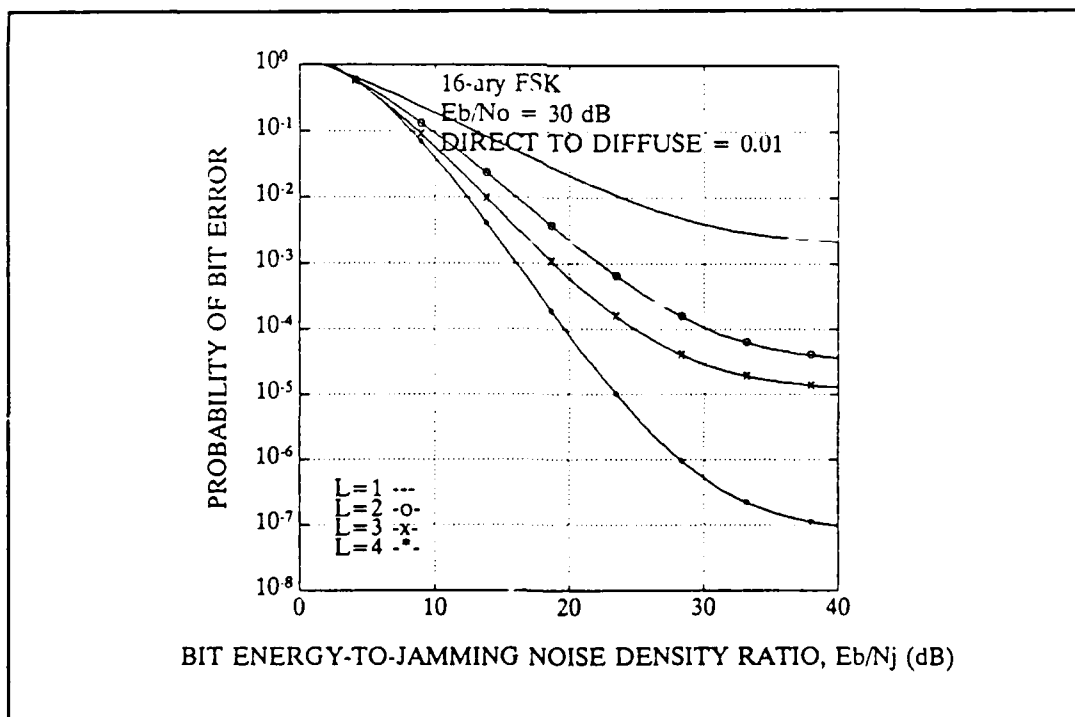


Figure C.17 Uncoded Performance for MFSK, $M=16$, in a Rayleigh-faded channel with $E_b/N_o = 30$ dB.

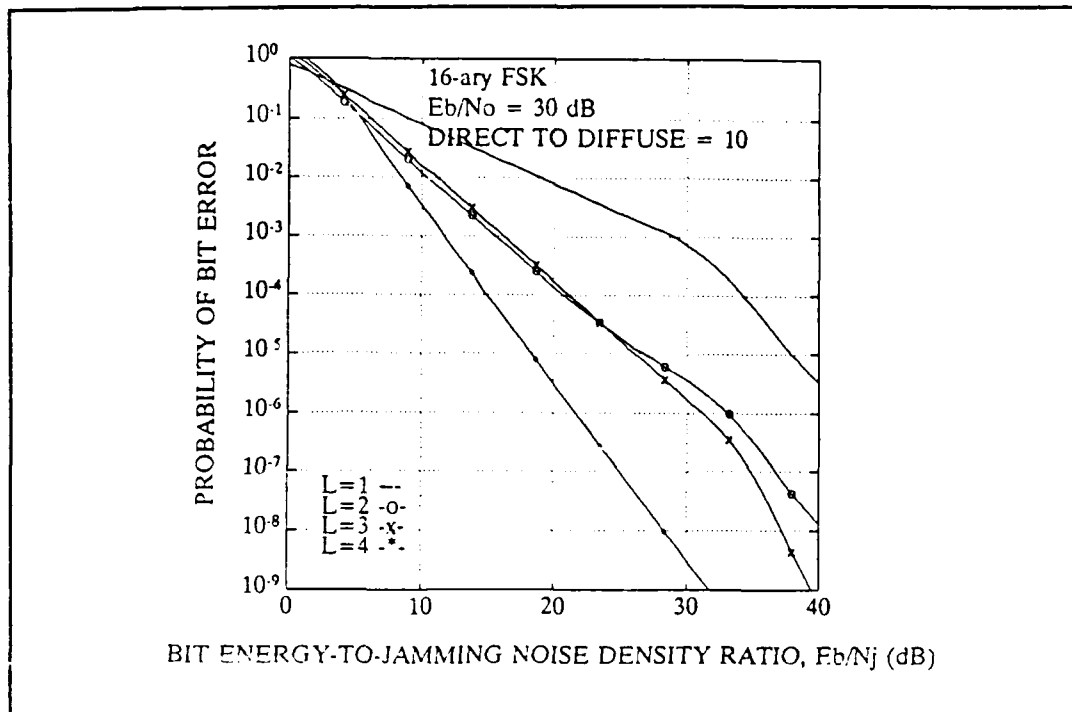


Figure C.18 Uncoded Performance for MFSK, $M=16$, in a Rician-faded channel with $E_b/N_o = 30$ dB.

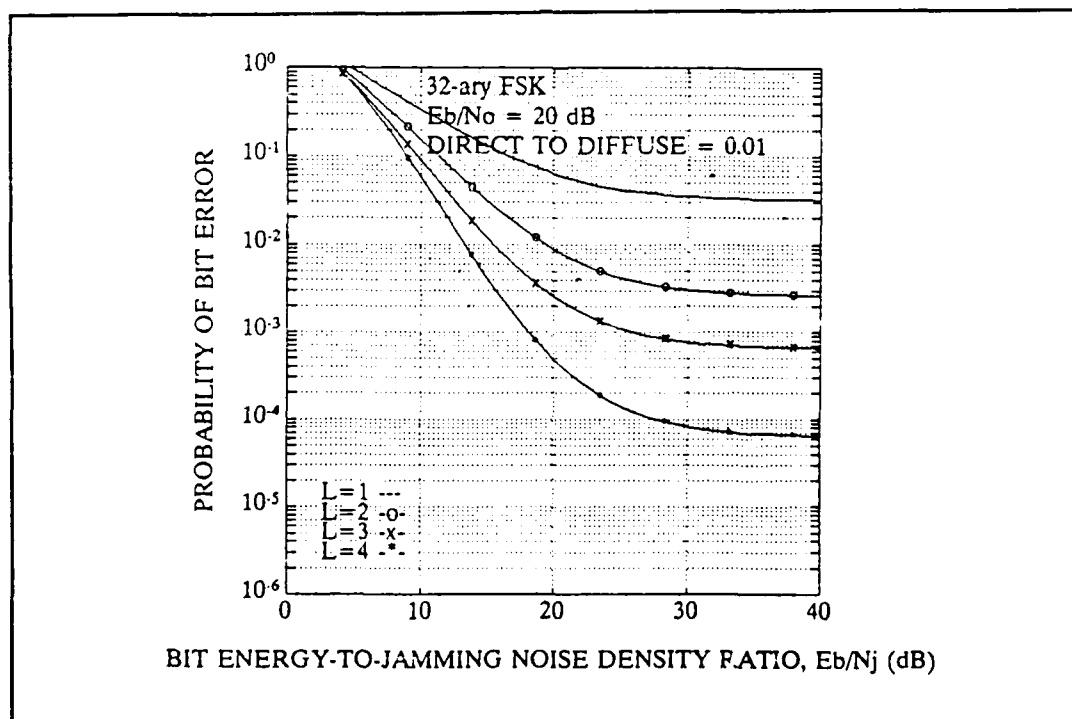


Figure C.19 Uncoded Performance for MFSK, $M=32$, in a Rayleigh-faded channel with $E_b/N_o = 20$ dB.

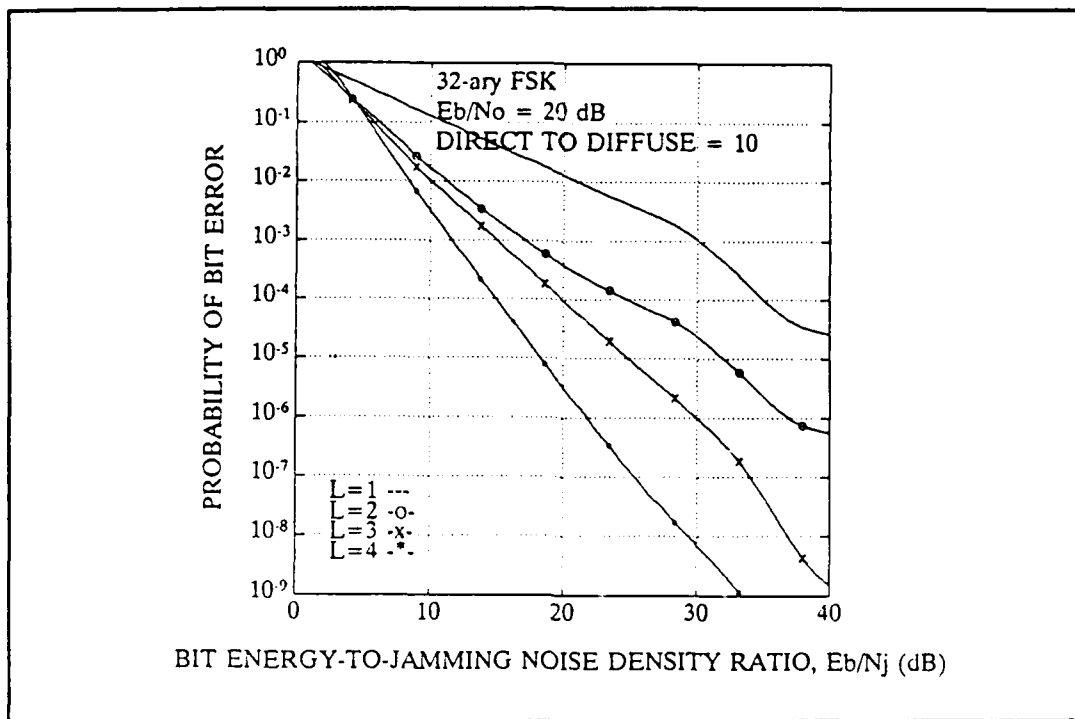


Figure C.20 Uncoded Performance for MFSK, $M=32$, in a Rician-faded channel with $E_b/N_o = 20$ dB.

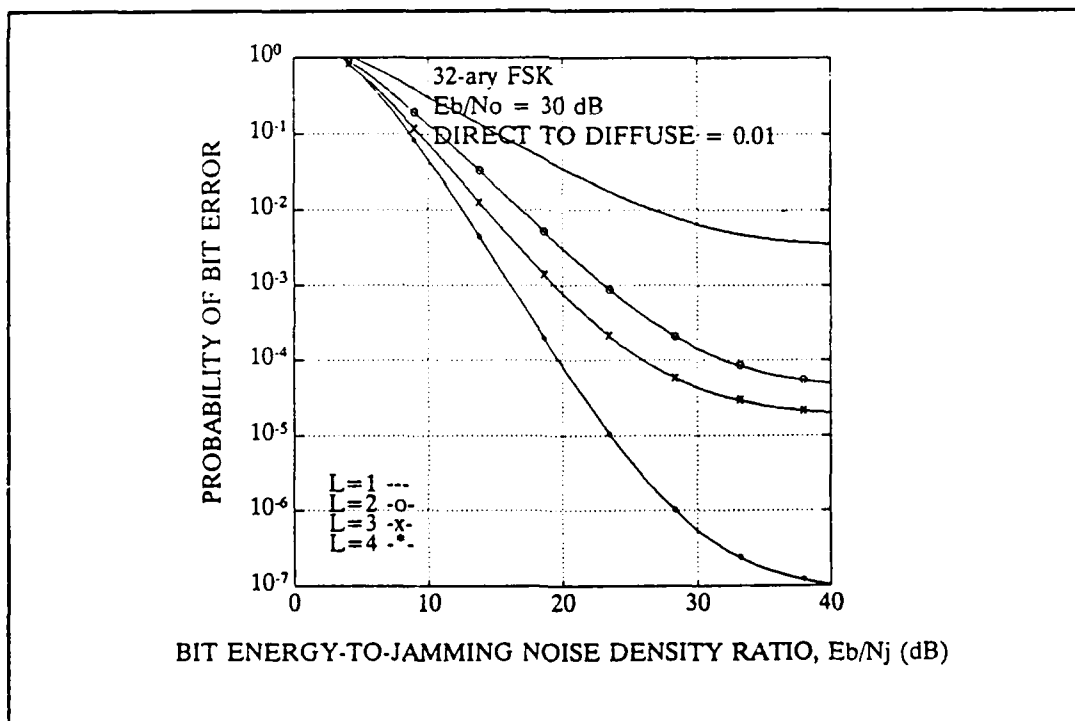


Figure C.21 Uncoded Performance for MFSK, $M=32$, in a Rayleigh-faded channel with $E_b/N_o = 30$ dB.

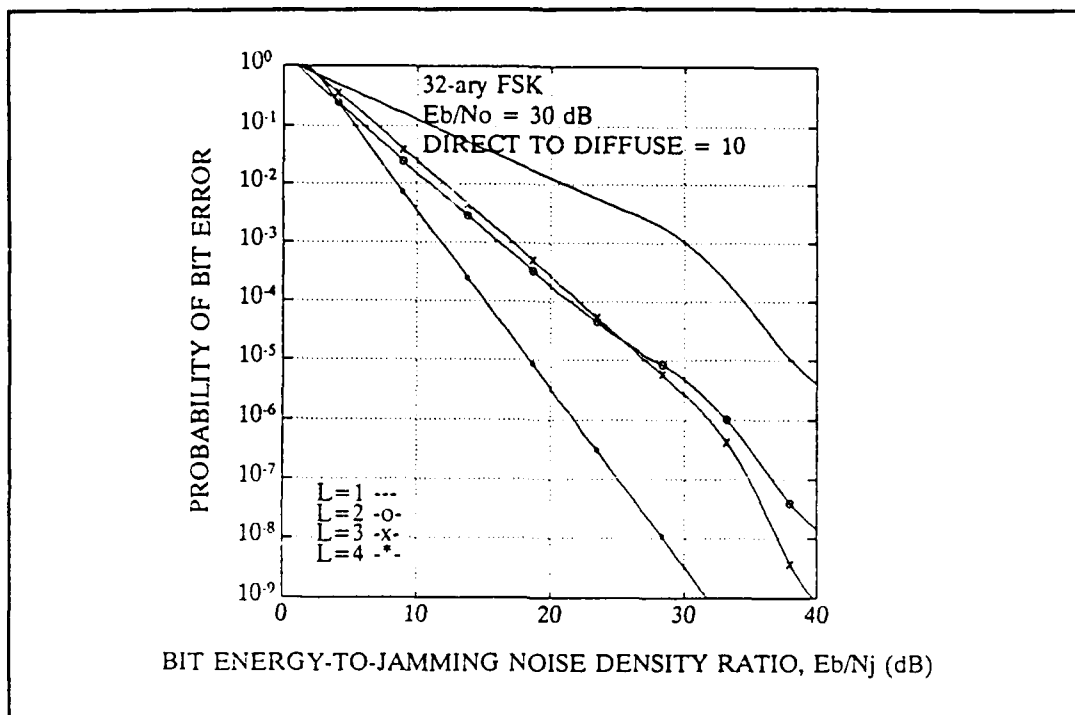


Figure C.22 Uncoded Performance for MFSK, $M=32$, in a Rician-faded channel with $E_b/N_o = 30$ dB.

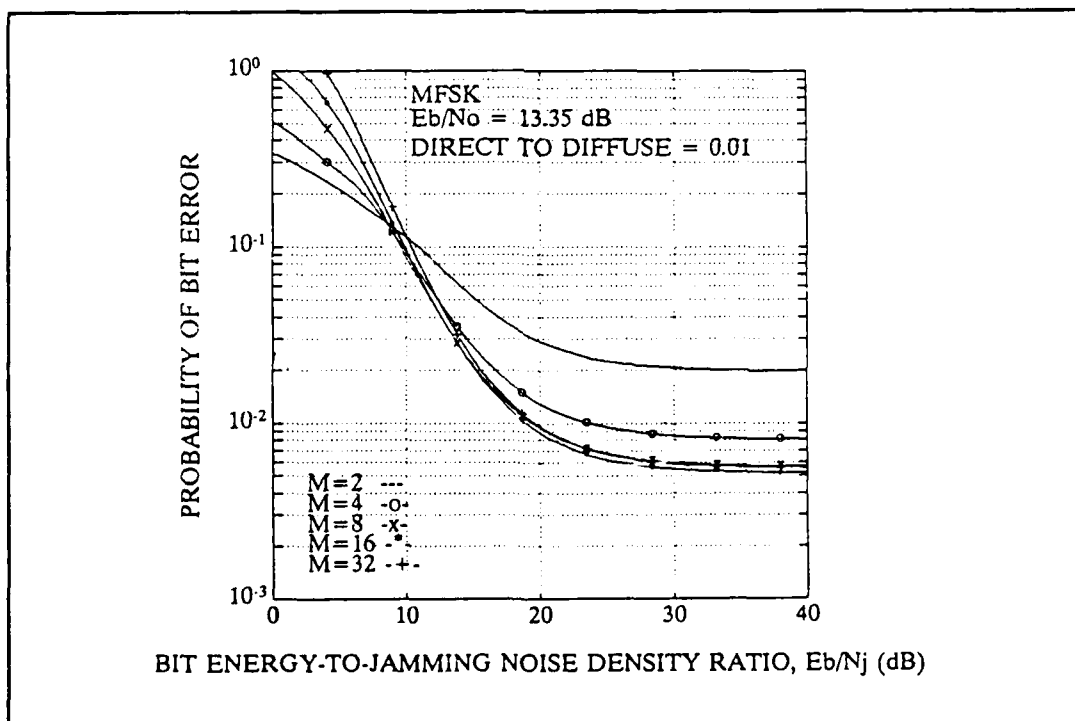


Figure C.23 Uncoded Performance for MFSK, $M= 2$ to 32, in a deeply-faded Rayleigh channel with $E_b/N_o = 13.35$ dB.

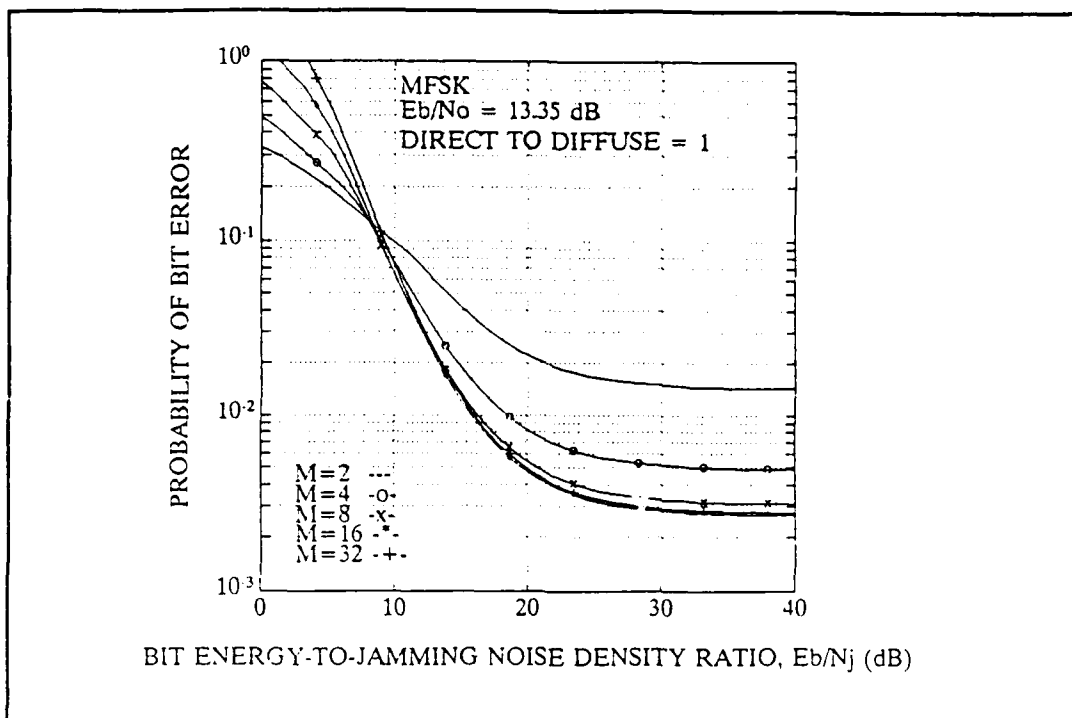


Figure C.24 Uncoded Performance for MFSK, $M=2$ to 32, in a moderately faded Rayleigh channel with $E_b/N_o = 13.35$ dB.

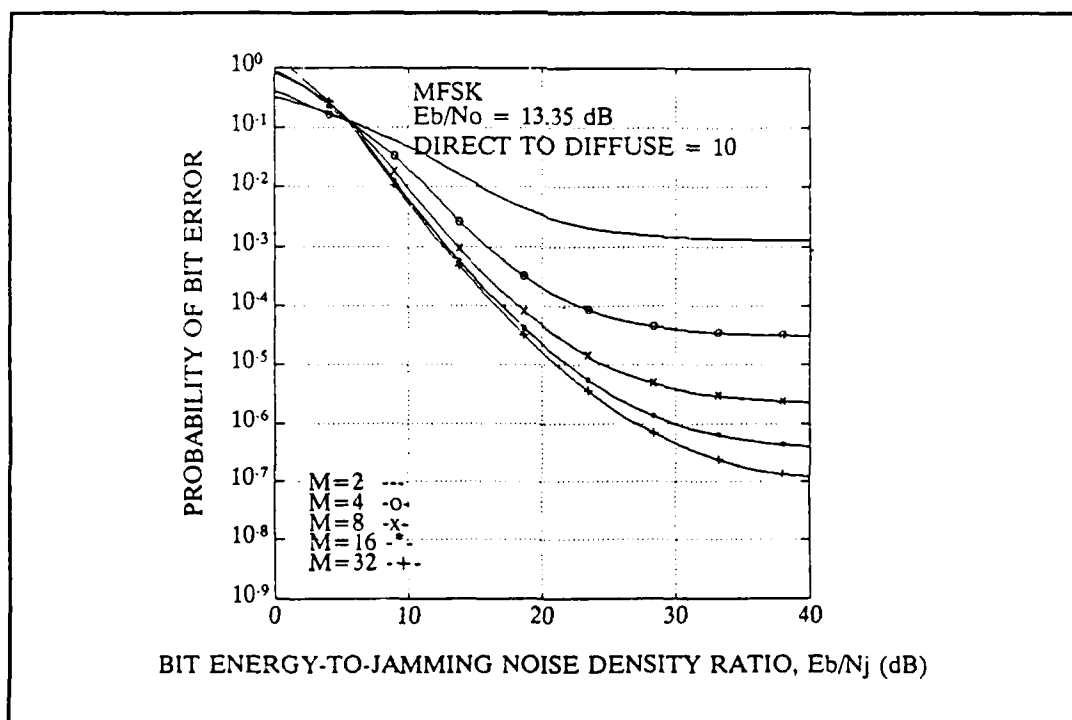


Figure C.25 Uncoded Performance for MFSK, $M=2$ to 32, in a Rician-faded channel with $E_b/N_o = 13.35$ dB.

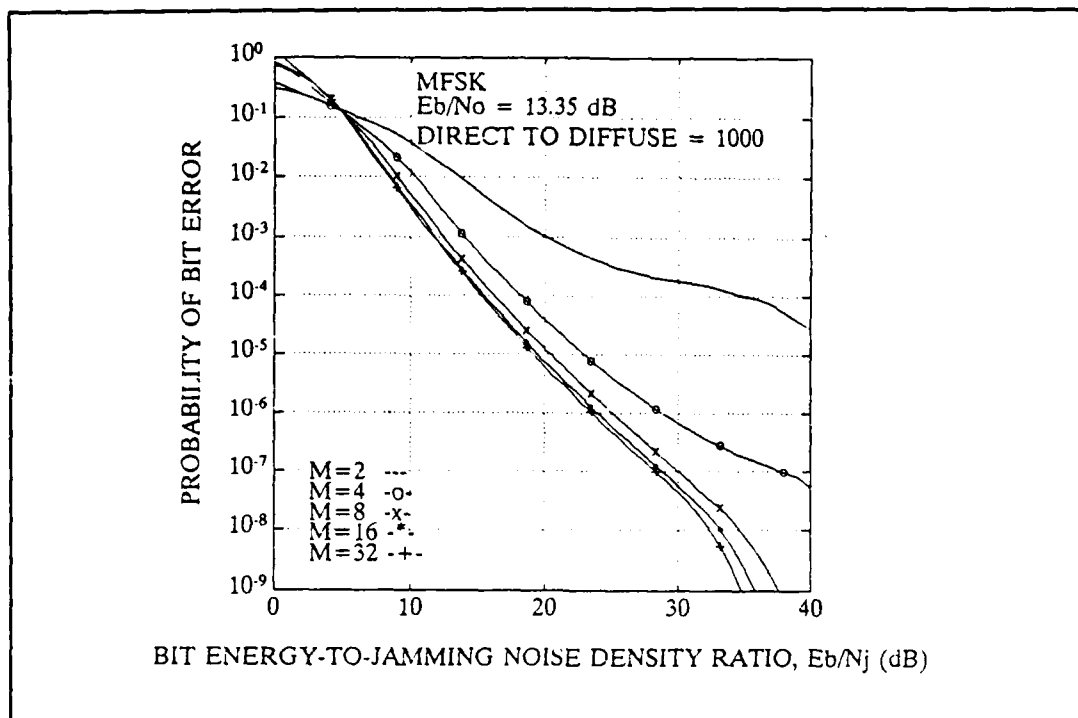


Figure C.26 Uncoded Performance for MFSK, $M=2$ to 32, in a non-faded channel with $E_b/N_o = 13.35$ dB.

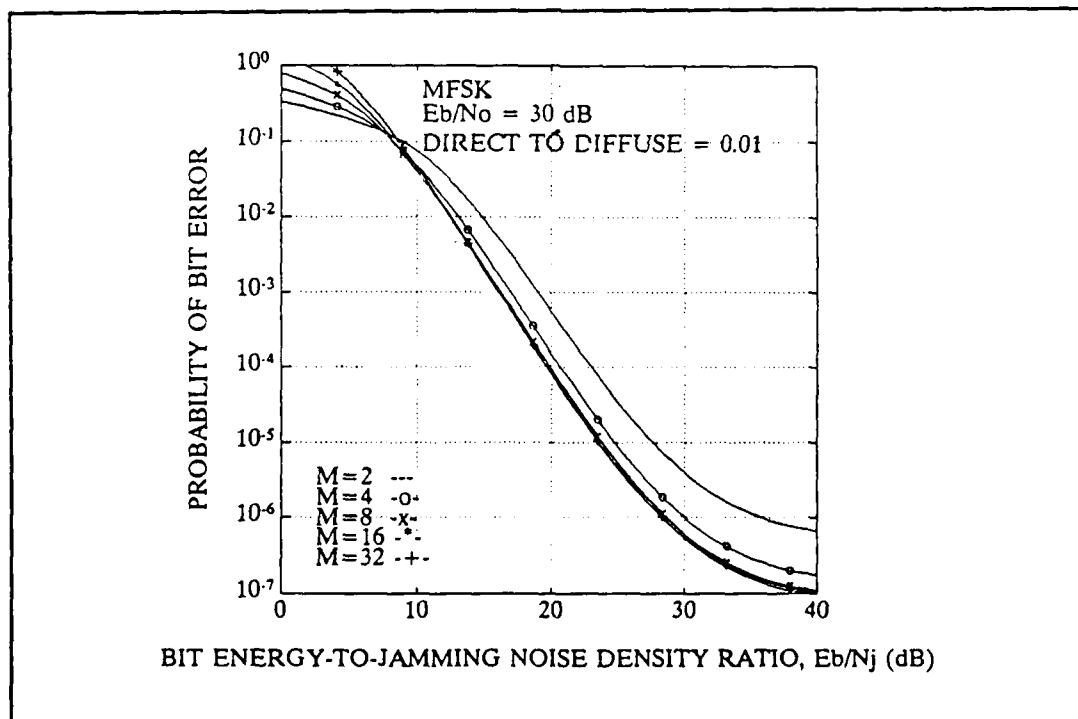


Figure C.27 Uncoded Performance for MFSK, $M=2$ to 32, in a deeply-faded Rayleigh channel with $E_b/N_o = 30$ dB.

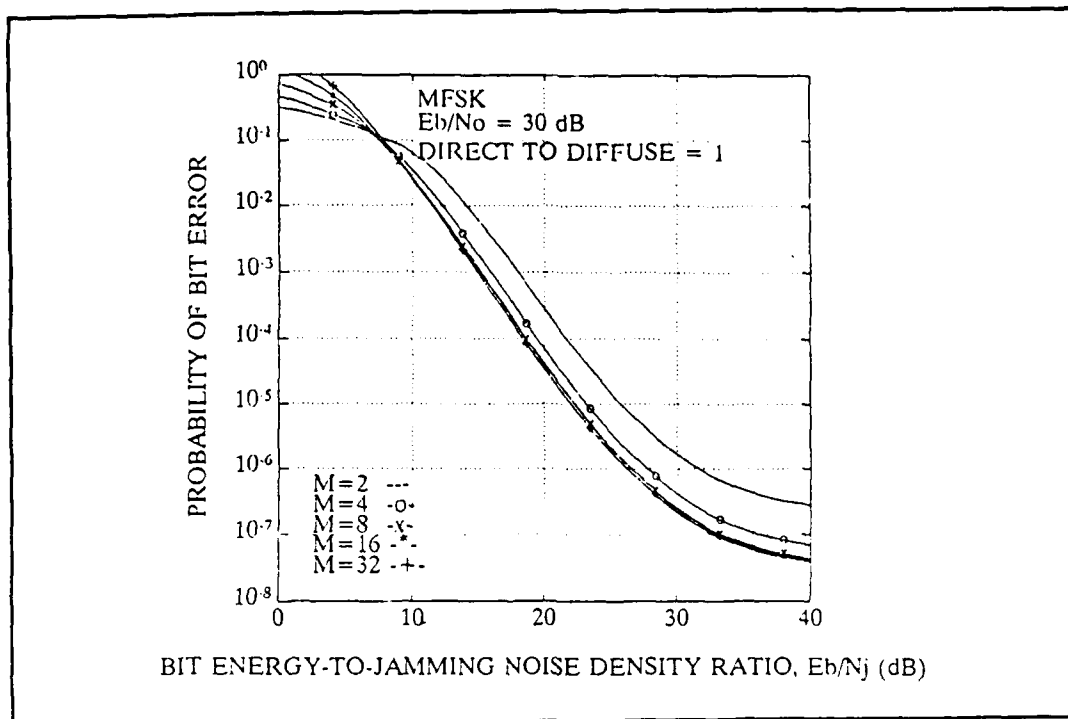


Figure C.28 Uncoded Performance for MFSK, $M=2$ to 32, in a moderately faded Rayleigh channel with $E_b/N_o = 30$ dB.

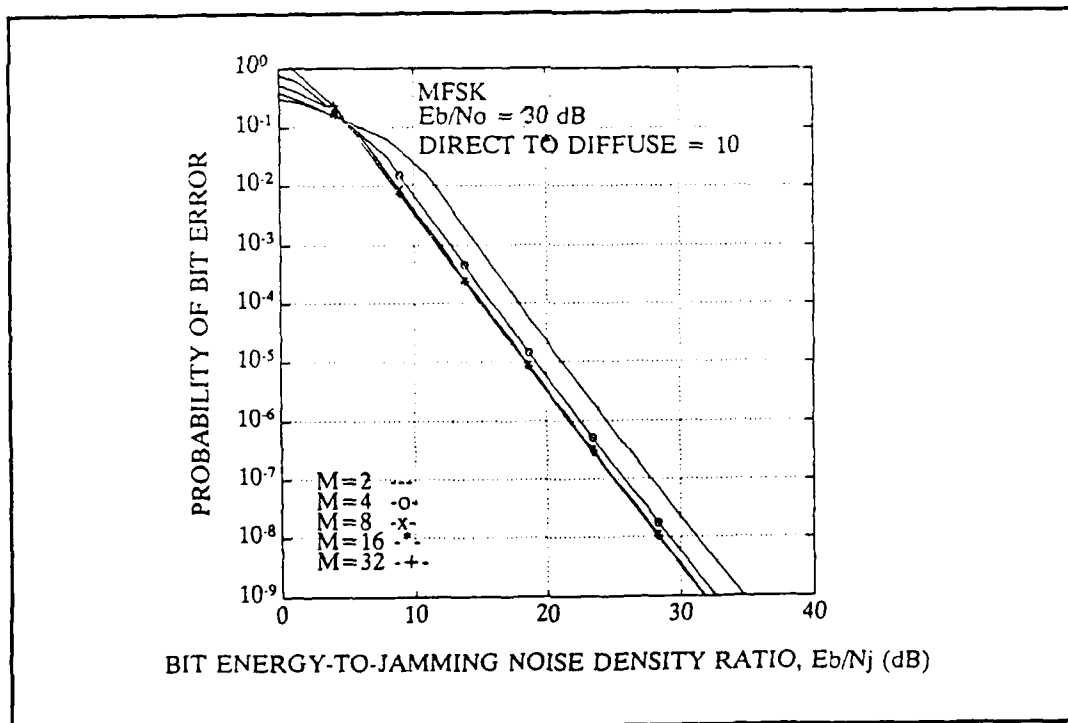


Figure C.29 Uncoded Performance for MFSK, $M=2$ to 32 in a Rician-faded channel with $E_b/N_o = 30$ dB.

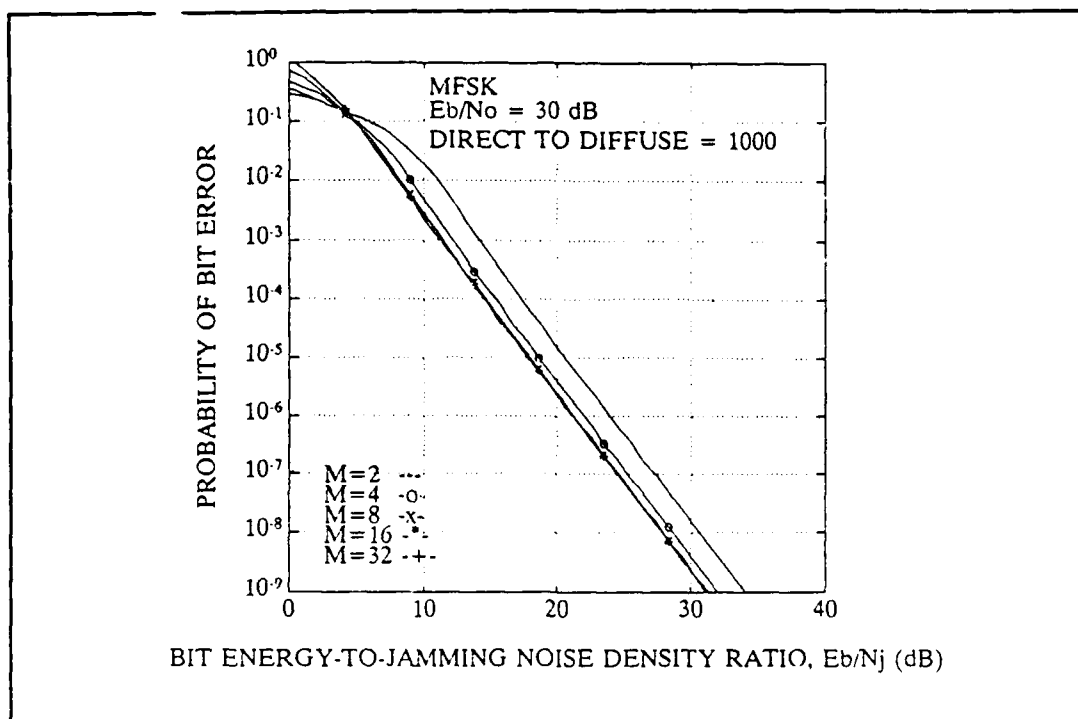


Figure C.30 Uncoded Performance for MFSK, $M=2$ to 32, in a non-faded channel with $E_b/N_o = 30$ dB.

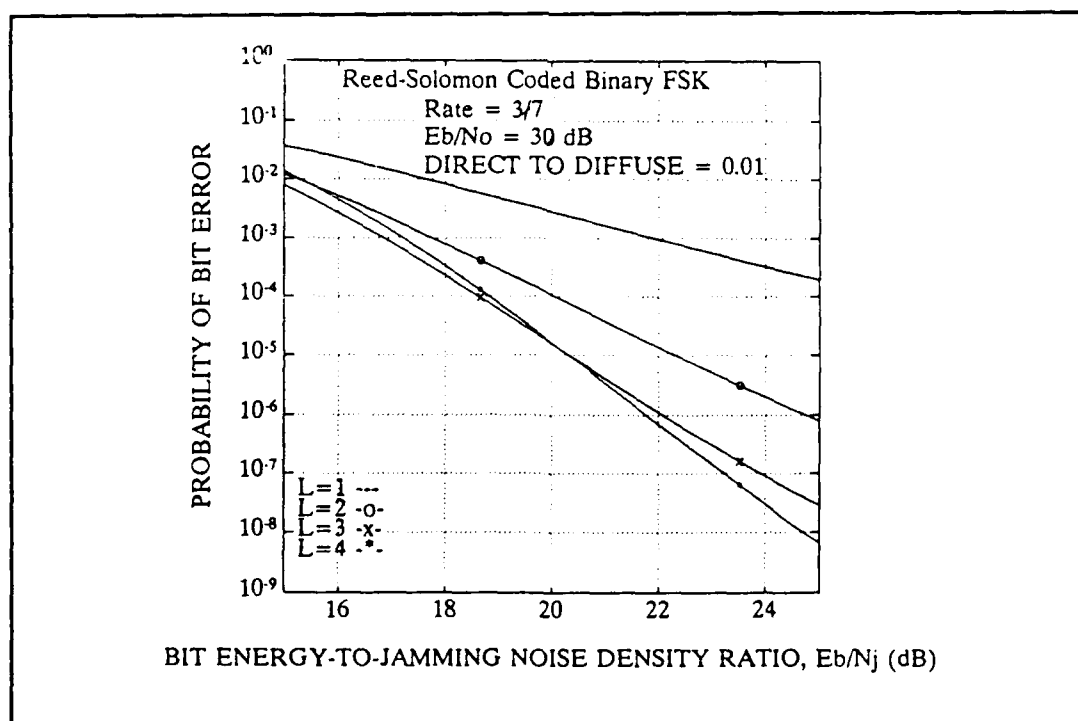


Figure C.31 Reed-Solomon (7,3) Coded Performance for BFSK in a deeply faded Rayleigh channel with $E_b/N_o = 30$ dB.

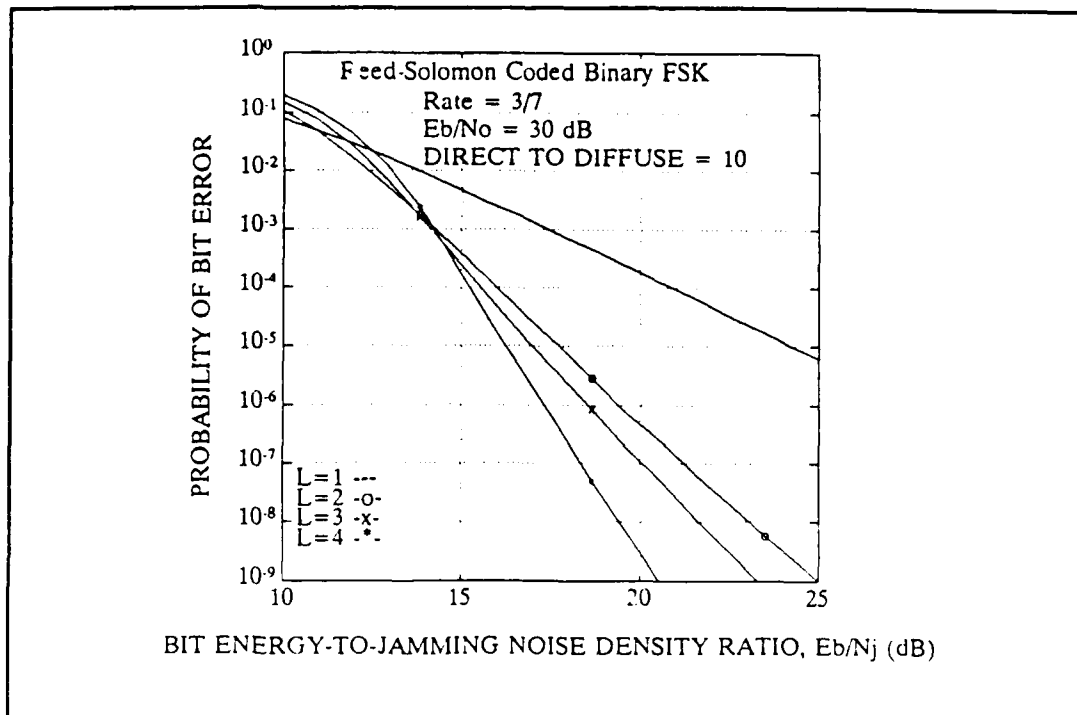


Figure C.32 Reed-Solomon (7,3) Coded Performance for BFSK in a Rician channel with $E_b/N_o = 30$ dB.

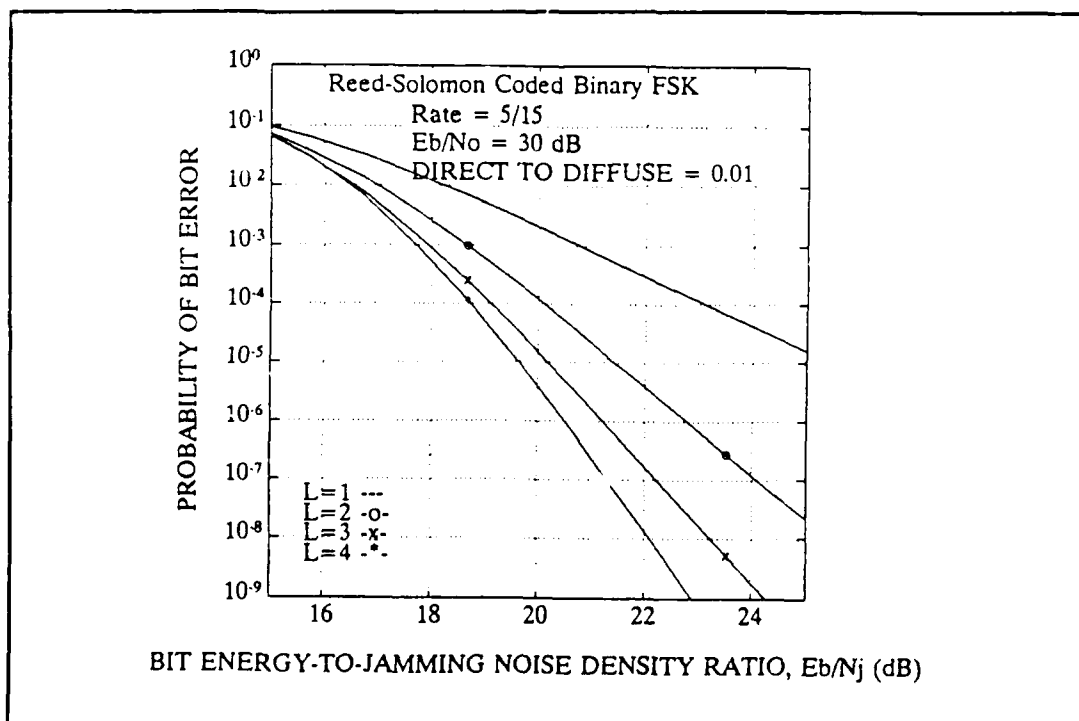


Figure C.33 Reed-Solomon (15,5) Coded Performance for BFSK in a deeply faded Rayleigh channel with $E_b/N_o = 30$ dB.

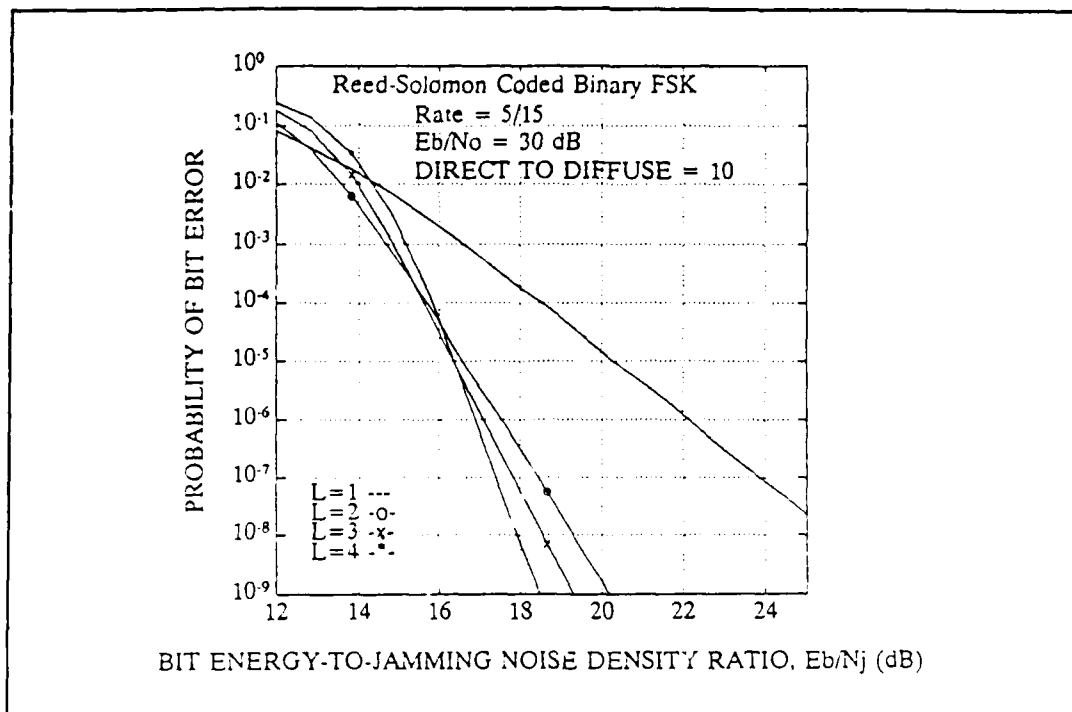


Figure C.34 Reed-Solomon (15,5) Coded Performance for BFSK in a Rician channel with $E_b/N_o = 30$ dB.

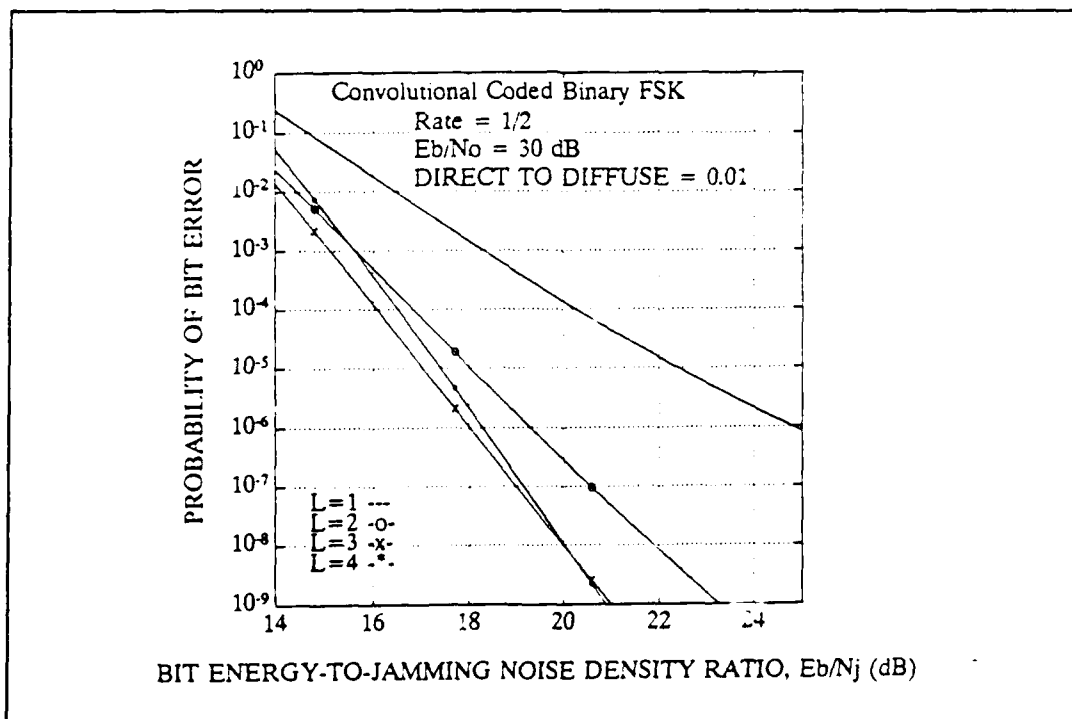


Figure C.35 Convolutional Code Rate 1/2 Performance for BFSK in a deeply faded Rayleigh channel with $E_b/N_o = 30$ dB.

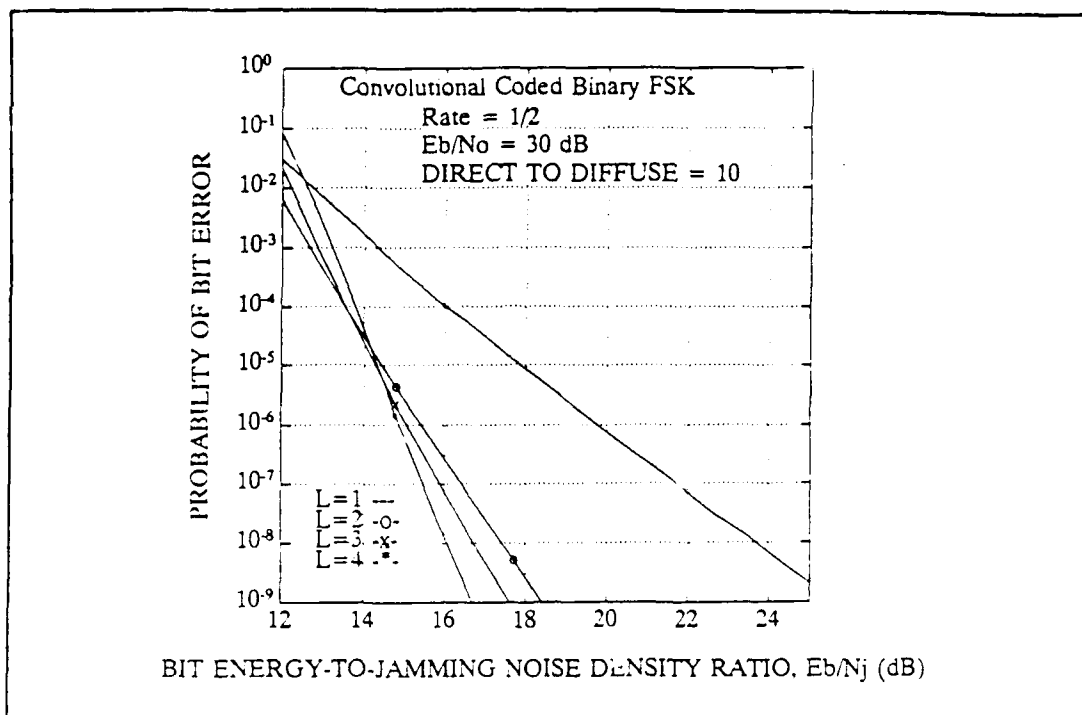


Figure C.36 Convolutional Code Rate 1/2 Performance for BFSK in a Rician channel with $E_b/N_0 = 30$ dB.

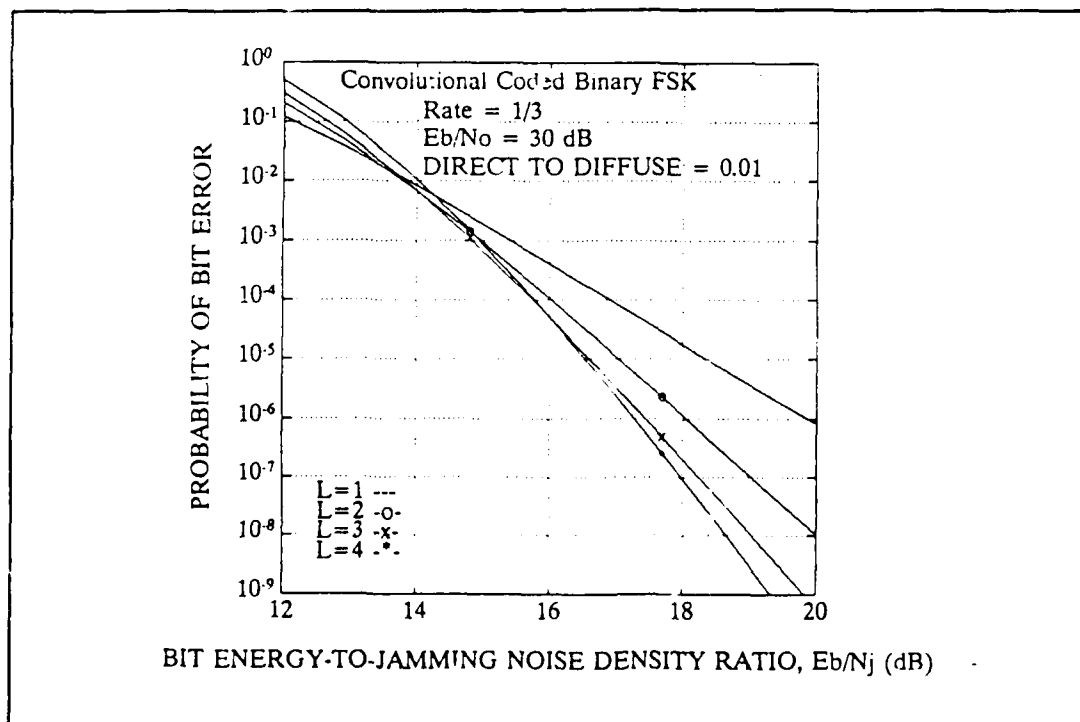


Figure C.37 Convolutional Code Rate 1/3 Performance for BFSK in a deeply faded Rayleigh channel with $E_b/N_0 = 30$ dB.

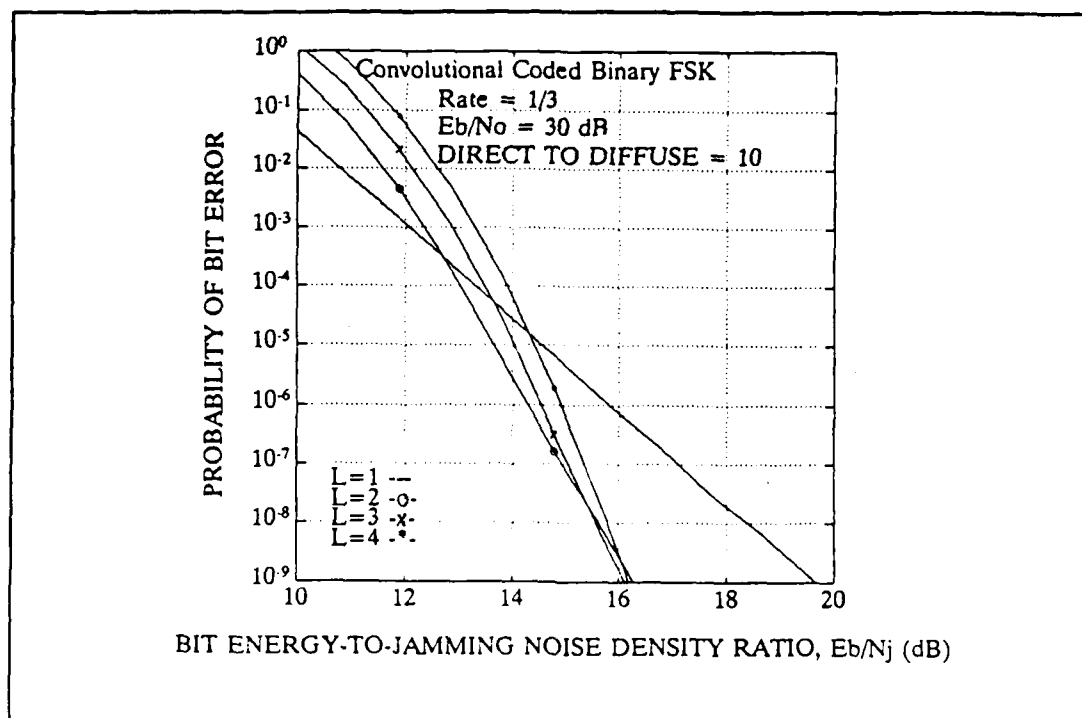


Figure C.38 Convolutional Code Rate 1/3 Performance for BFSK in a Rician channel with $E_b/N_o = 30$ dB.

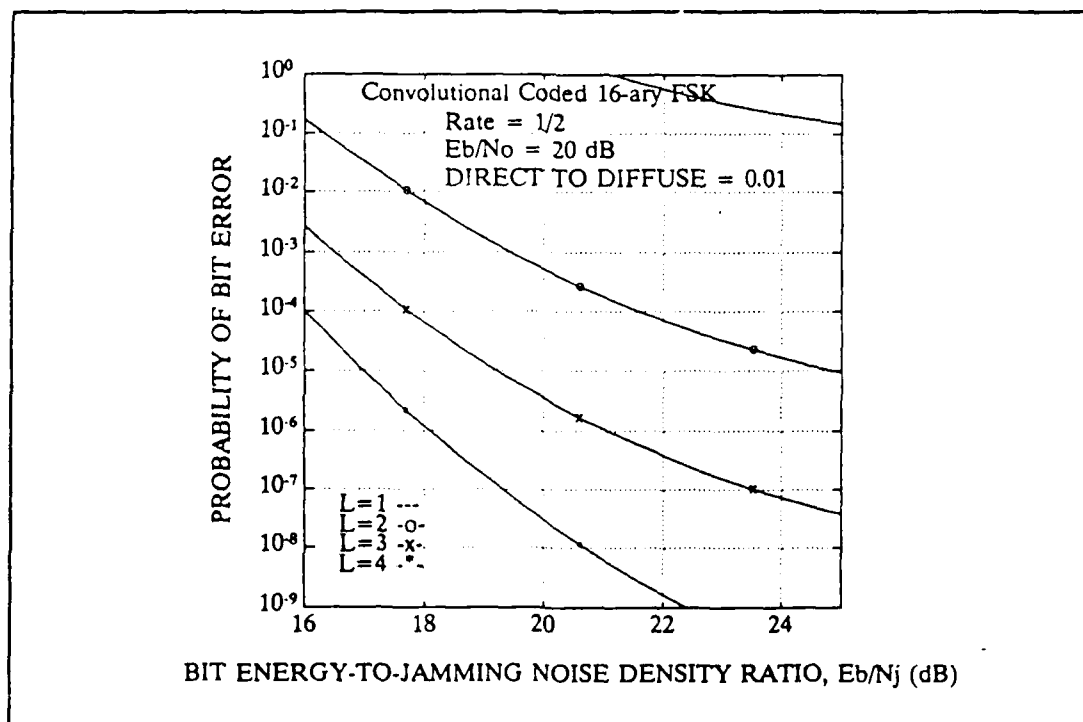


Figure C.39 Convolutional Code Rate 1/2 Performance for 16-ary FSK in a deeply-faded Rayleigh channel with $E_b/N_o = 20$ dB.

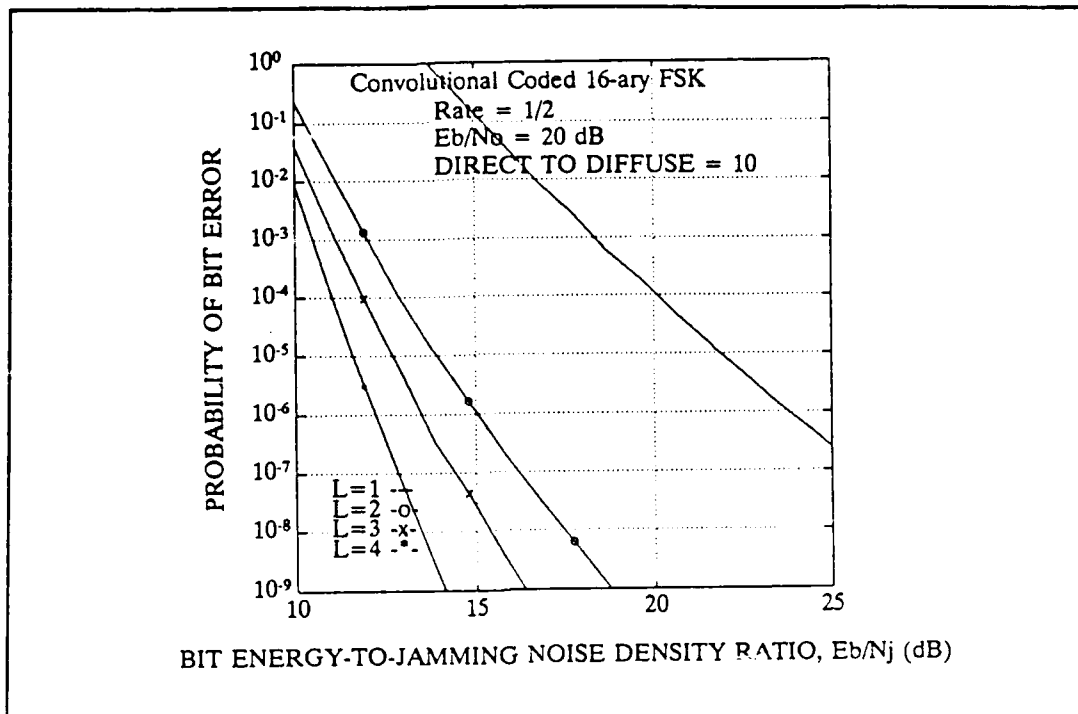


Figure C.40 Convolutional Code Rate 1/2 Performance for 16-ary FSK in a Rician channel with $E_b/N_0 = 20$ dB.

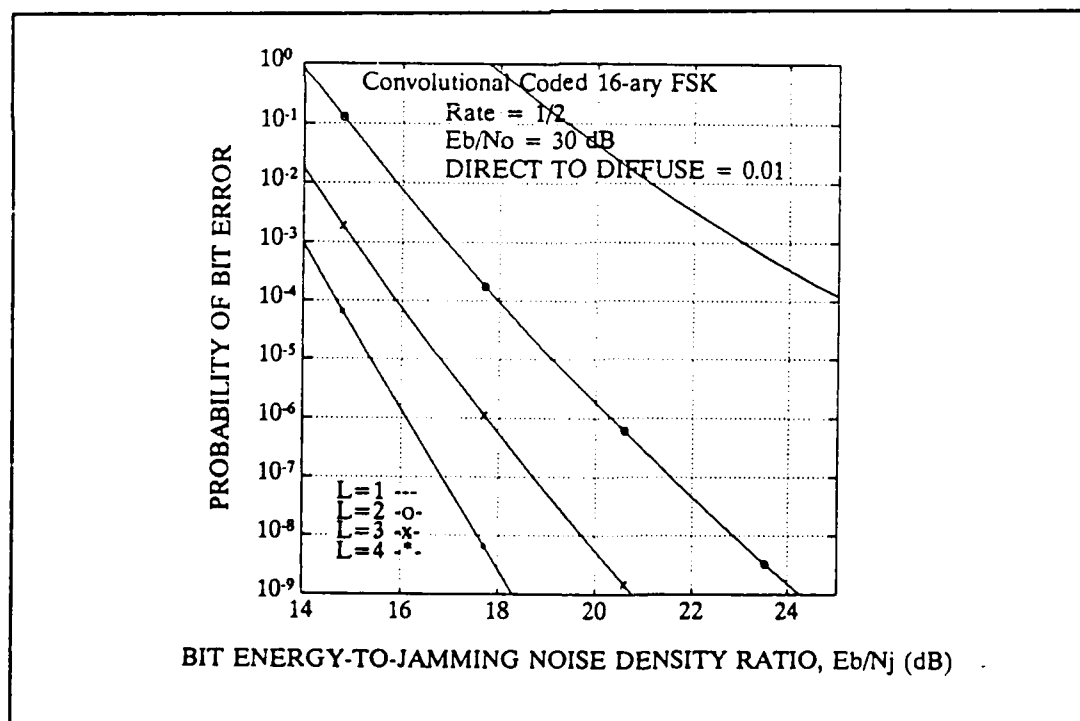


Figure C.41 Convolutional Code Rate 1/2 Performance for 16-ary FSK in a deeply-faded Rayleigh channel with $E_b/N_0 = 30$ dB.

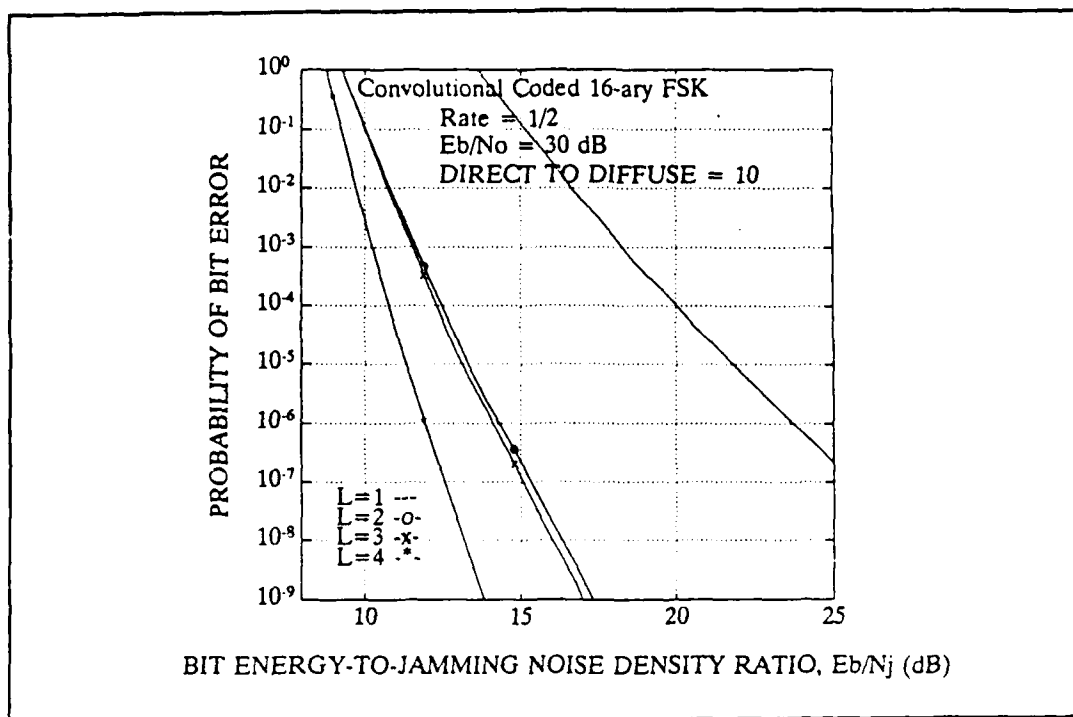


Figure C.42 Convolutional Code Rate 1/2 Performance for 16-ary FSK in a Rician channel with $E_b/N_o = 30$ dB.

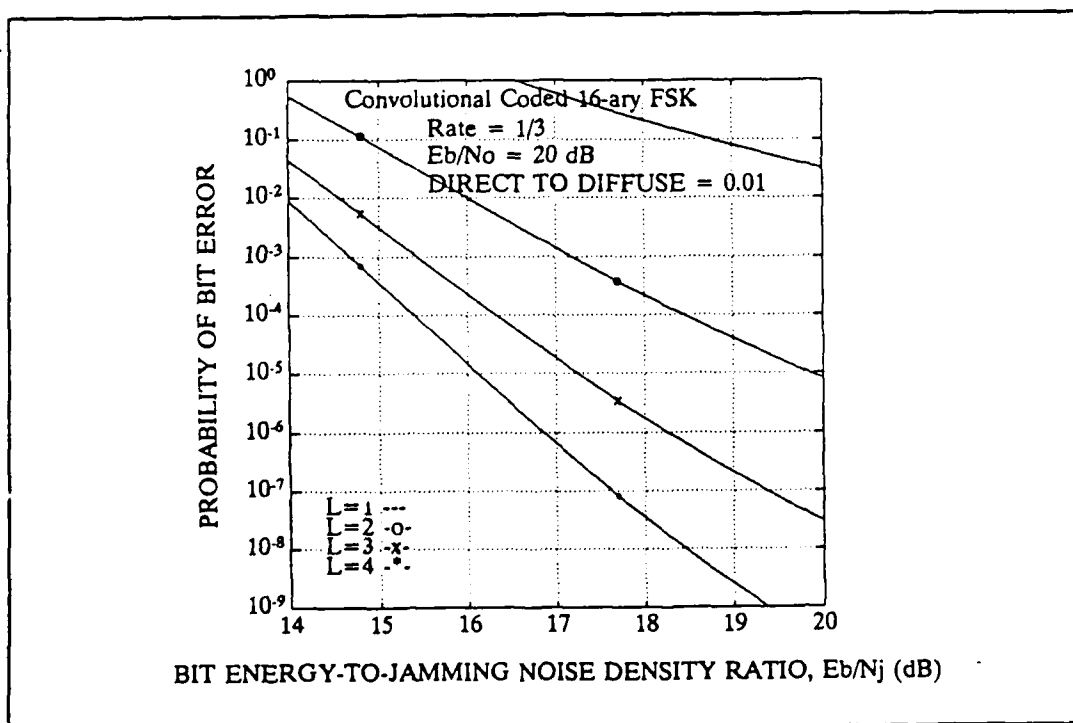


Figure C.43 Convolutional Code Rate 1/3 Performance for 16-ary FSK in a deeply faded Rayleigh channel with $E_b/N_o = 20$ dB.

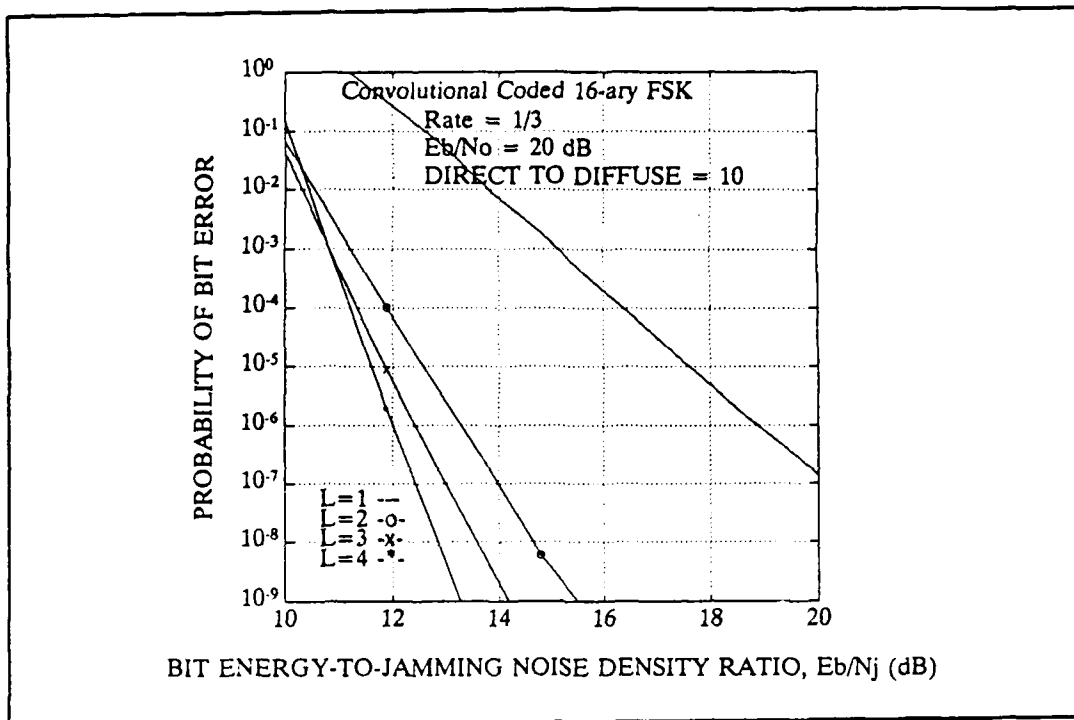


Figure C.44 Convolutional Code Rate 1/3 Performance for 16-ary FSK in a Rician channel with $E_b/N_o = 20$ dB.

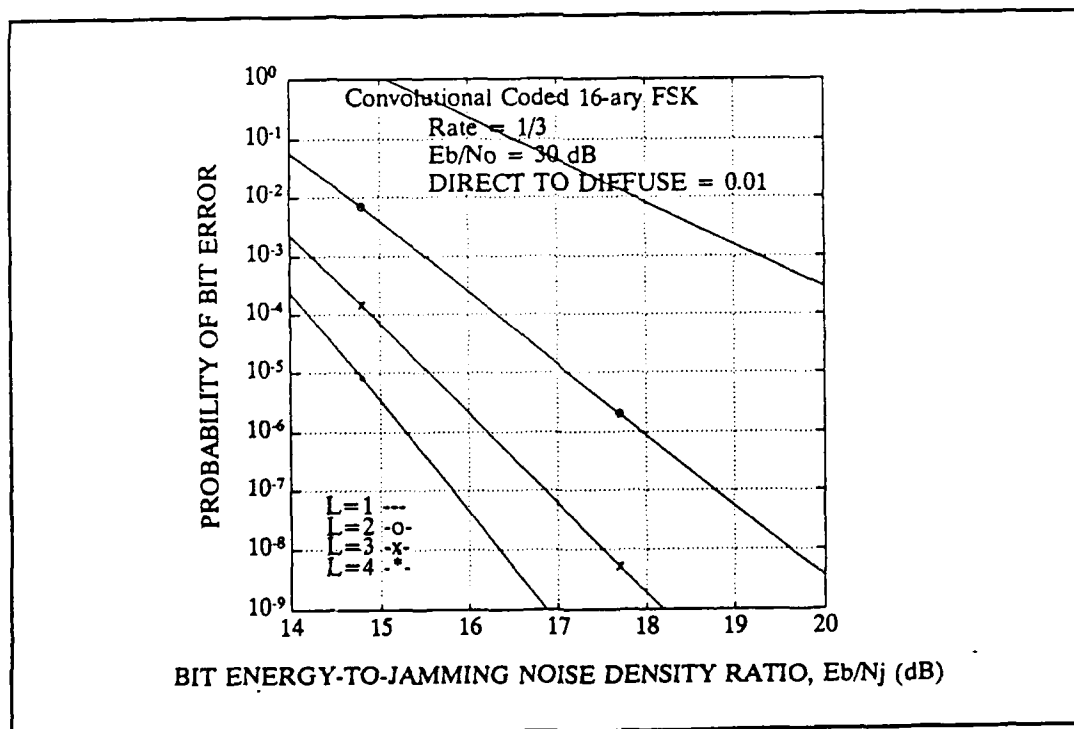


Figure C.45 Convolutional Code Rate 1/2 Performance for 16-ary FSK in a deeply-faded Rayleigh channel with $E_b/N_o = 30$ dB.

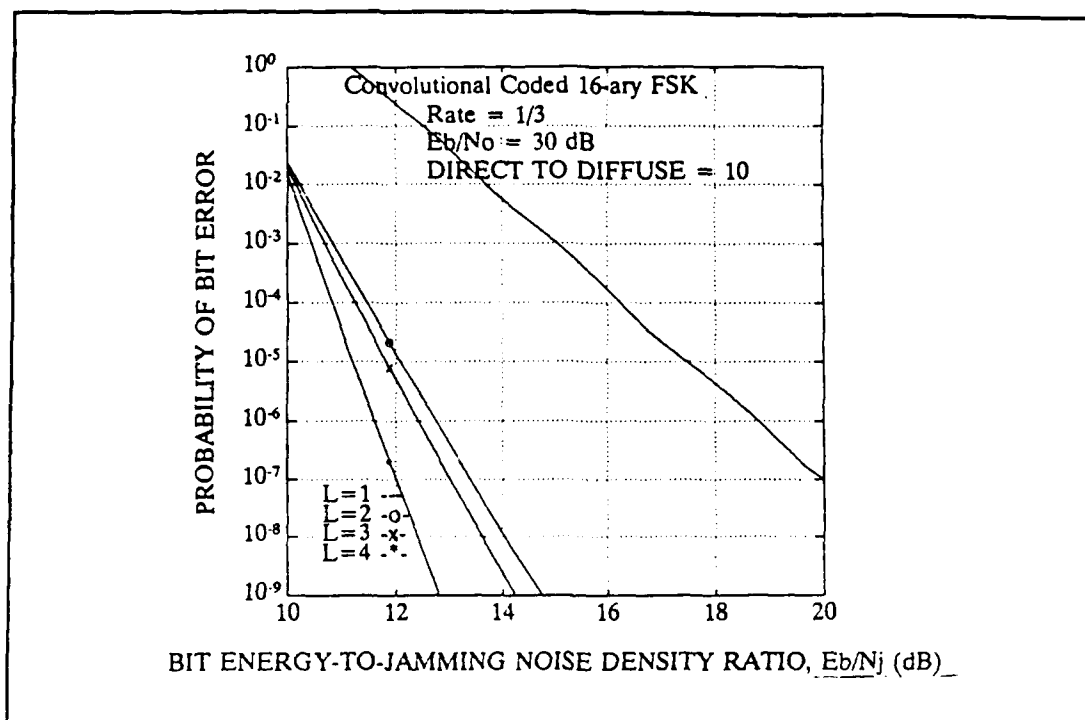


Figure C.46 Convolutional Coded Rate 1/3 Performance for 16-ary FSK in a Rician channel with $E_b/N_o = 30$ dB.

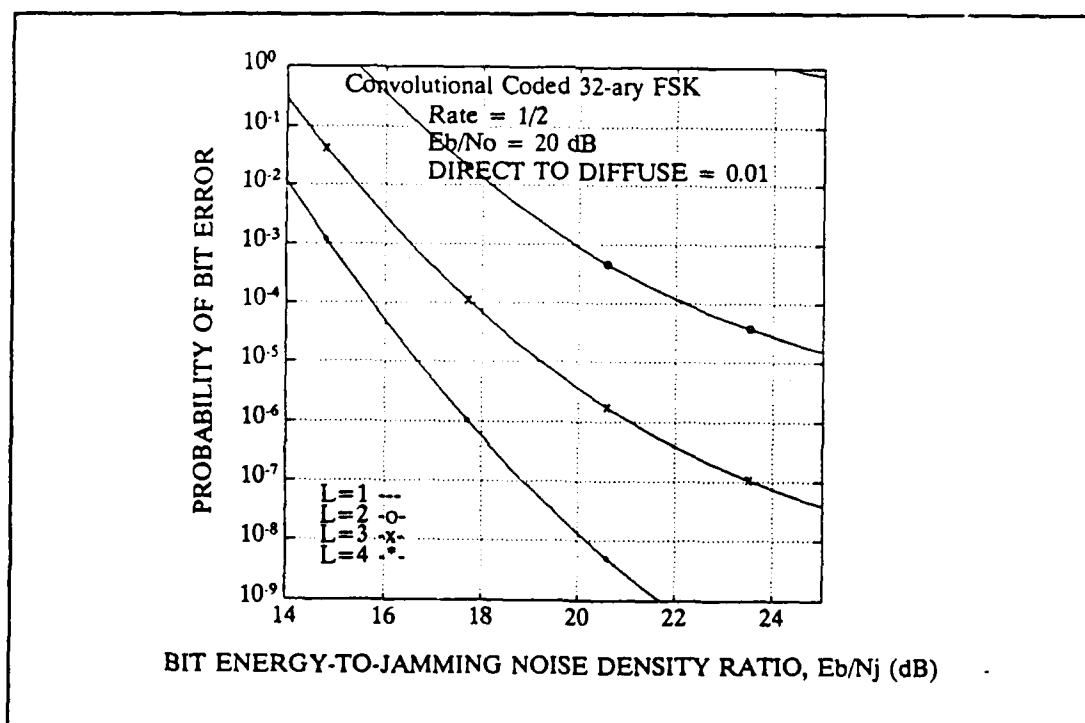


Figure C.47 Convolutional Code Rate 1/2 Performance for 32-ary FSK in a deeply-faded Rayleigh channel with $E_b/N_o = 20$ dB.

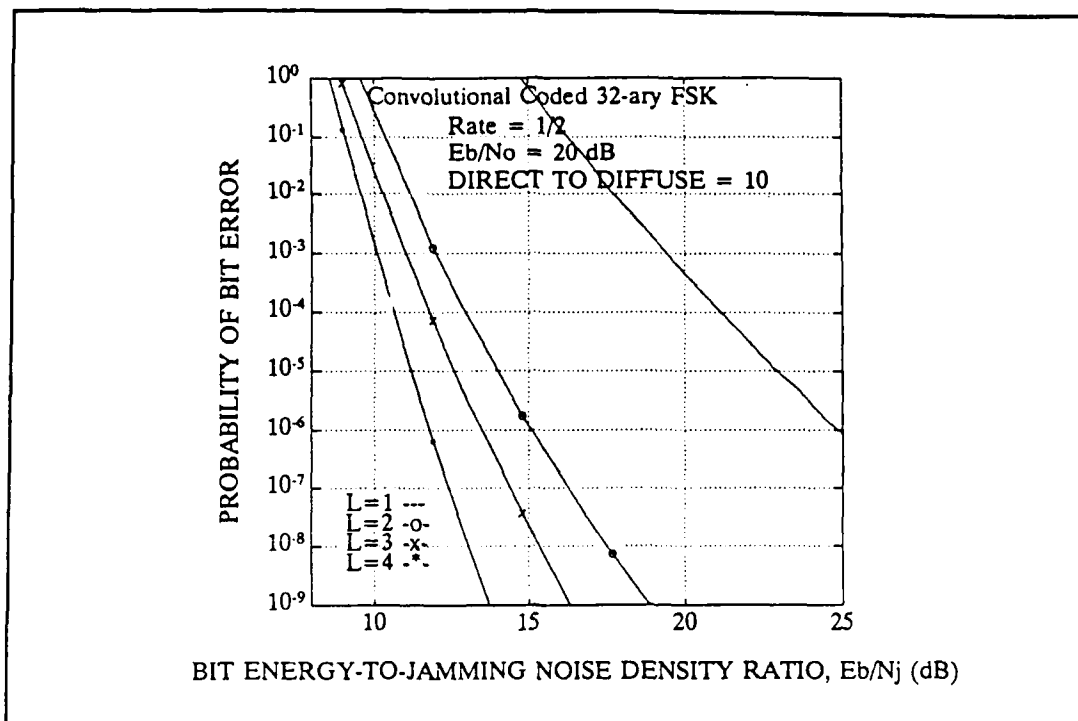


Figure C.48 Convolutional Code Rate 1/2 Performance for 32-ary FSK in a Rician channel with $E_b/N_o = 20$ dB.

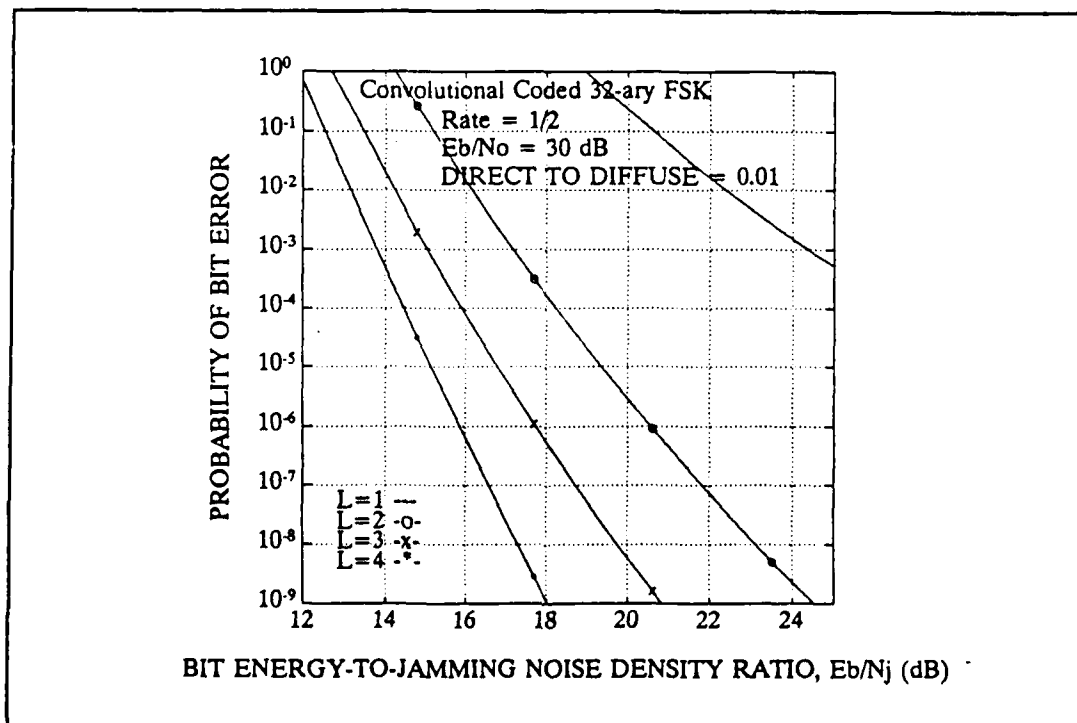


Figure C.49 Convolutional Code Rate 1/2 Performance for 32-ary FSK in a deeply-faded Rayleigh channel with $E_b/N_o = 30$ dB.

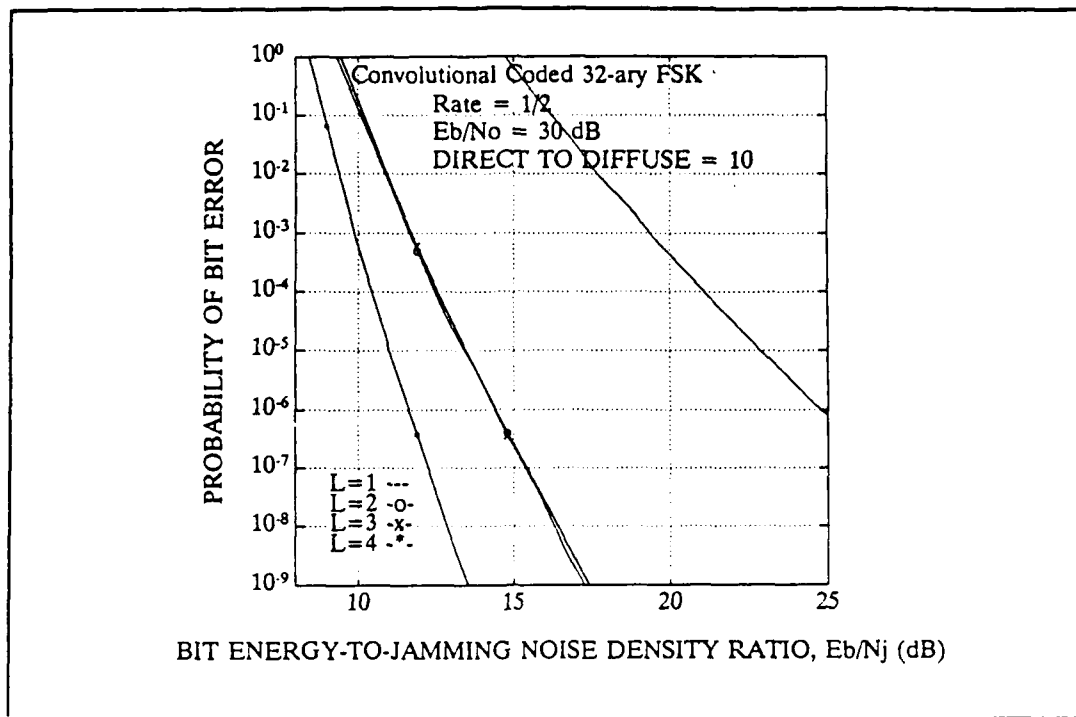


Figure C.50 Convolutional Code Rate 1/2 Performance for 32-ary FSK in a Rician channel with $E_b/N_o = 30$ dB.

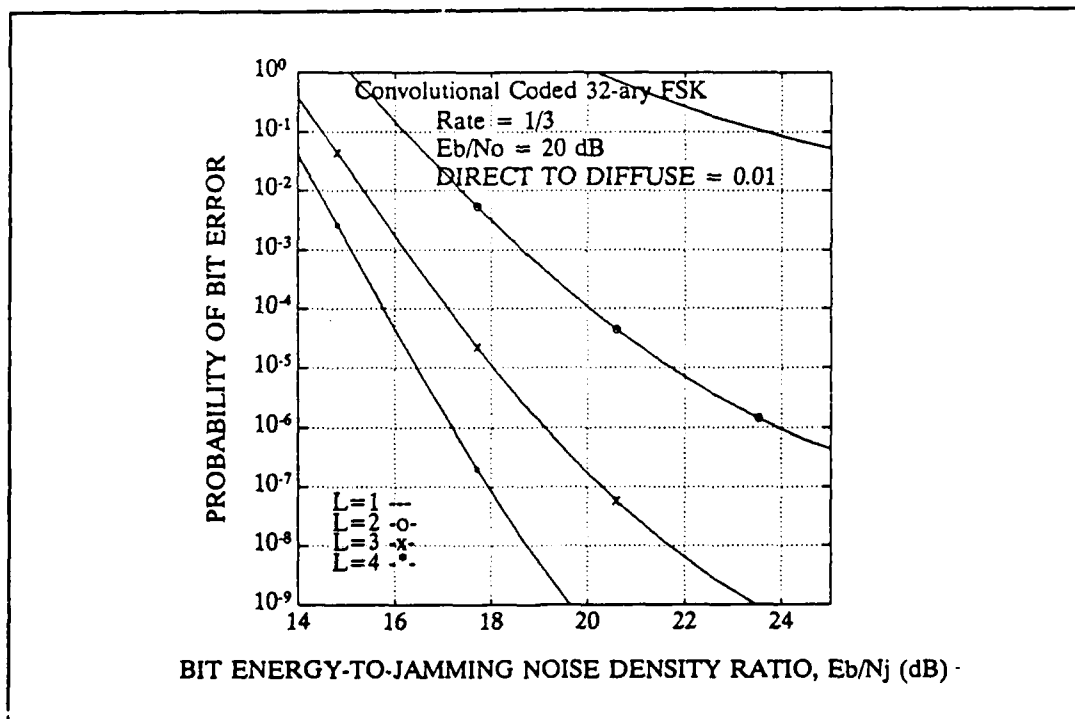


Figure C.51 Convolutional Code Rate 1/3 Performance for 32-ary FSK in a deeply-faded Rayleigh channel with $E_b/N_o = 20$ dB.

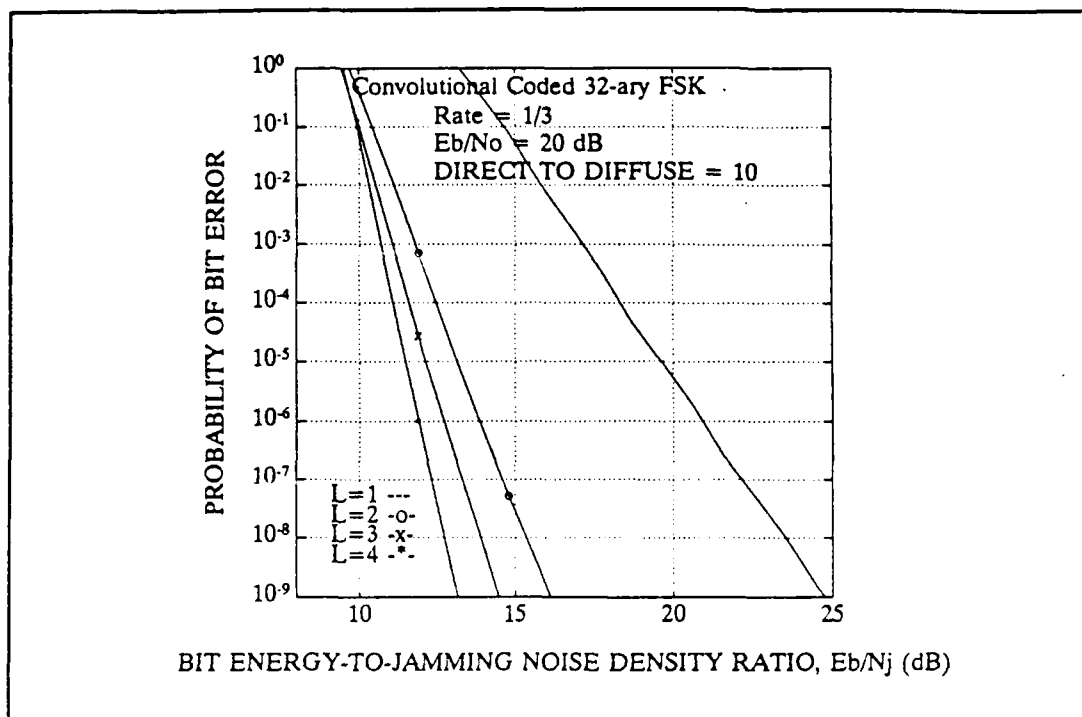


Figure C.52 Convolutional Code Rate 1/3 Performance for 32-ary FSK in a Rician channel with $E_b/N_o = 20$ dB.

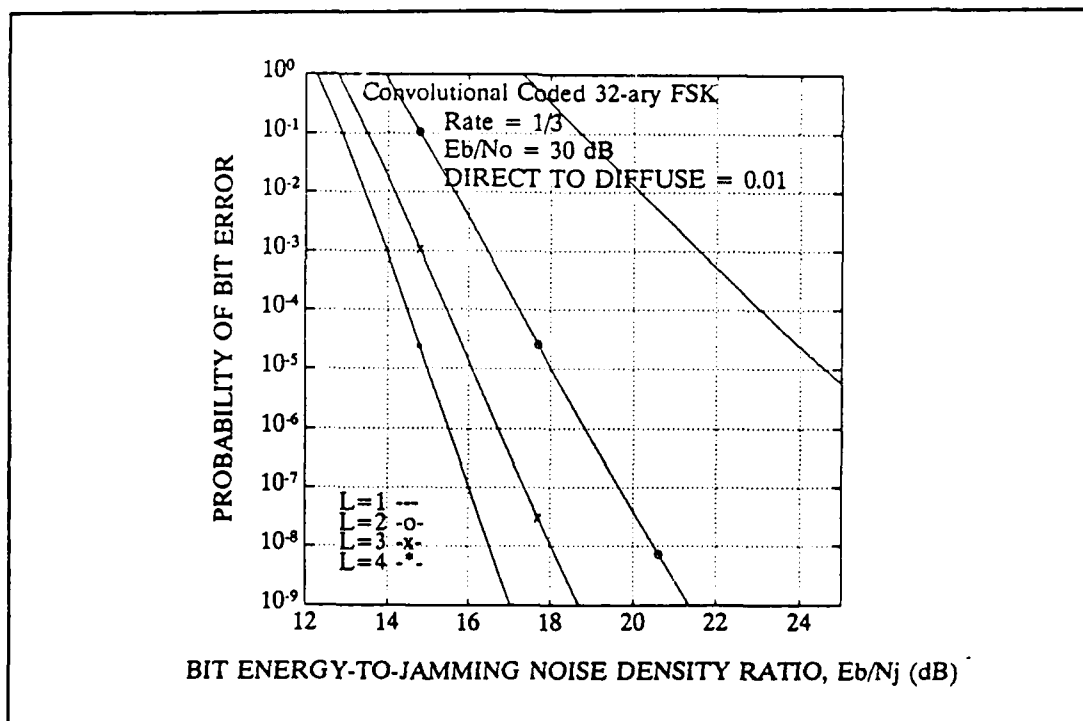


Figure C.53 Convolutional Code Rate 1/3 Performance for 32-ary FSK in a deeply-faded Rayleigh channel with $E_b/N_o = 30$ dB.

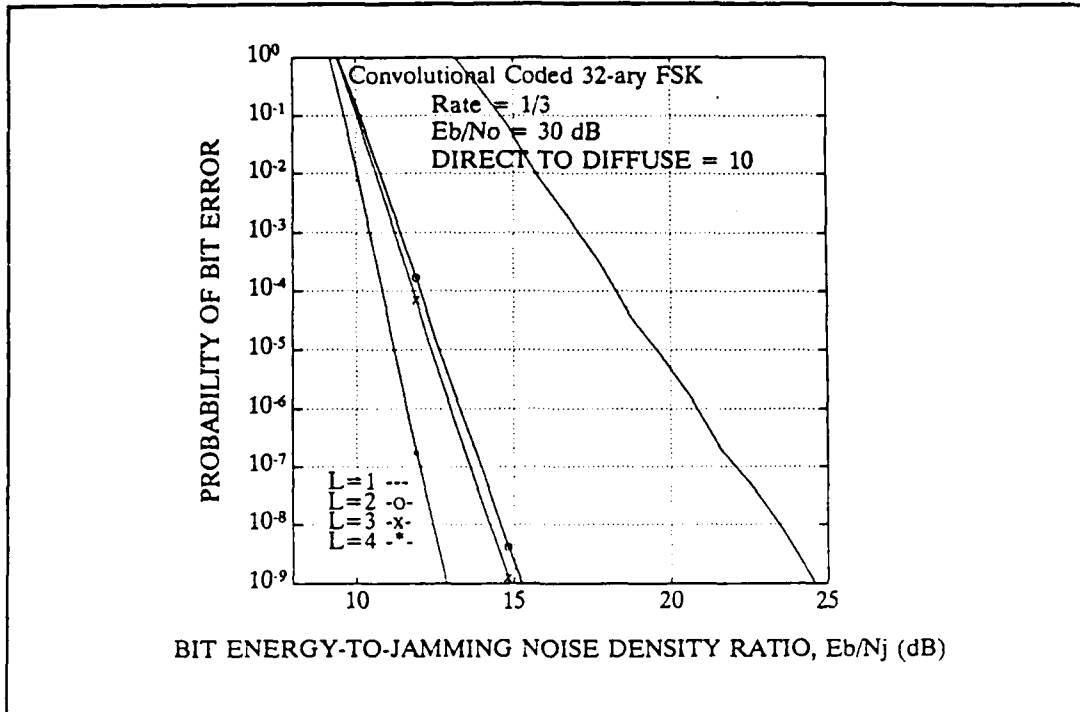


Figure C.54 Convolutional Coded Rate 1/3 Performance for 32-ary FSK in a Rician channel with $E_b/N_o = 30$ dB.

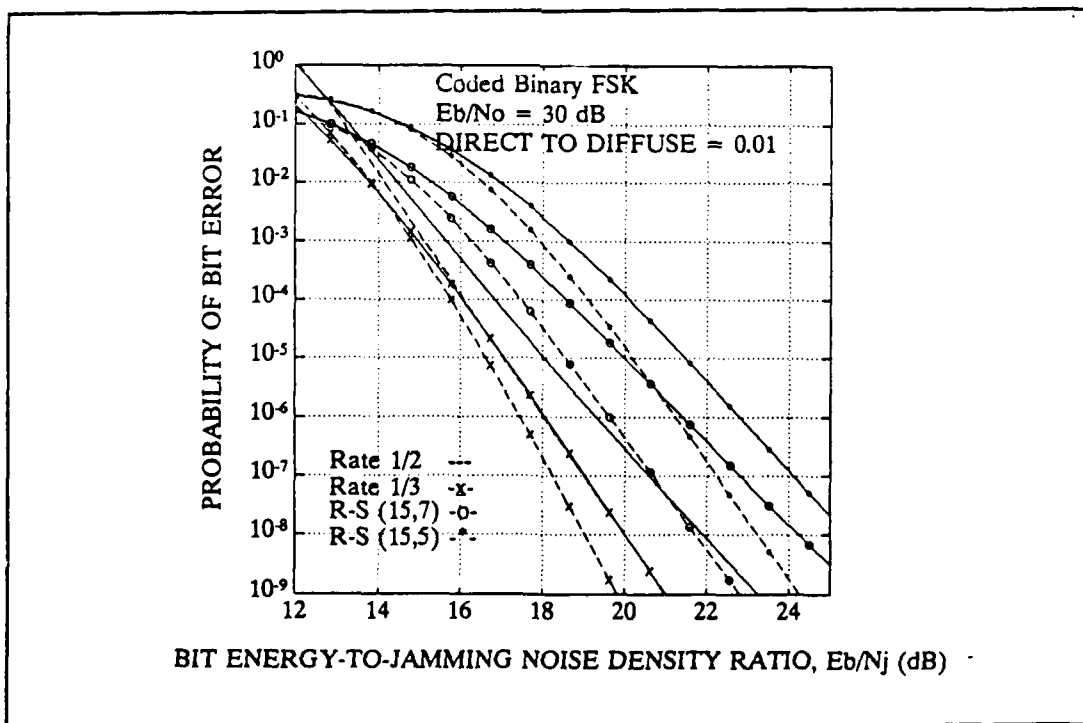


Figure C.55 Coded Performance for BFSK in a deeply-faded Rayleigh channel with $E_b/N_o = 30$ dB.

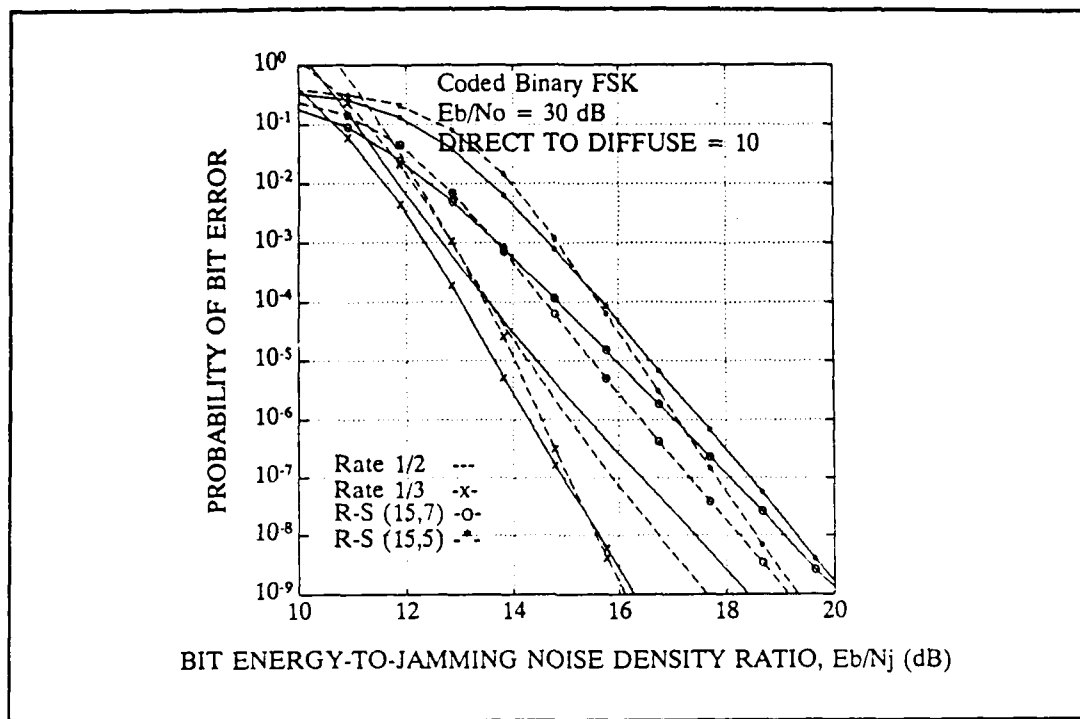


Figure C.56 Coded Performance for BFSK in a Rician channel with $E_b/N_o = 30 \text{ dB}$.

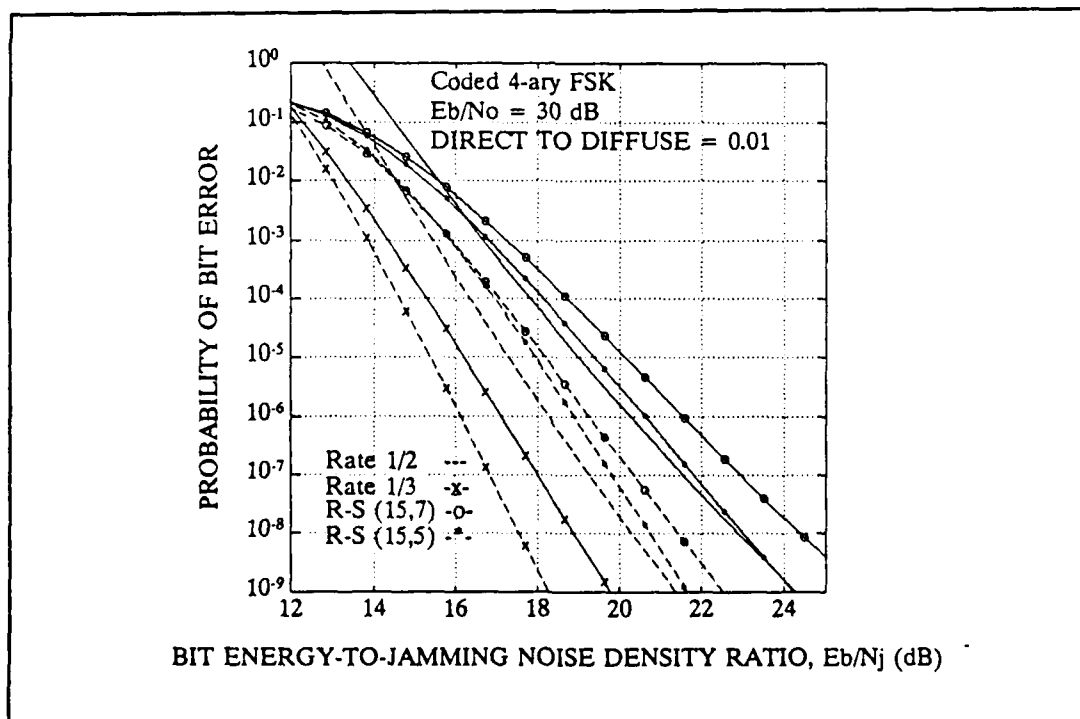


Figure C.57 Coded Performance for 4-ary FSK in a deeply-faded Rayleigh channel with $E_b/N_o = 30 \text{ dB}$.

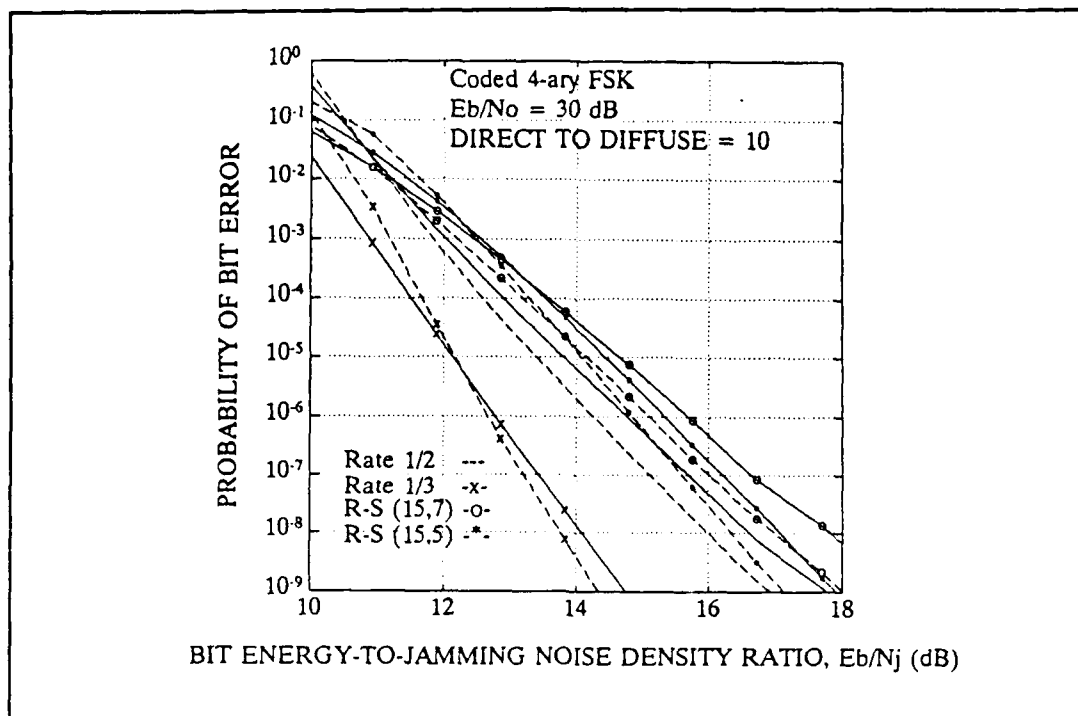


Figure C.58 Coded Performance for 4-ary FSK in a Rician channel with $E_b/N_o = 30$ dB.

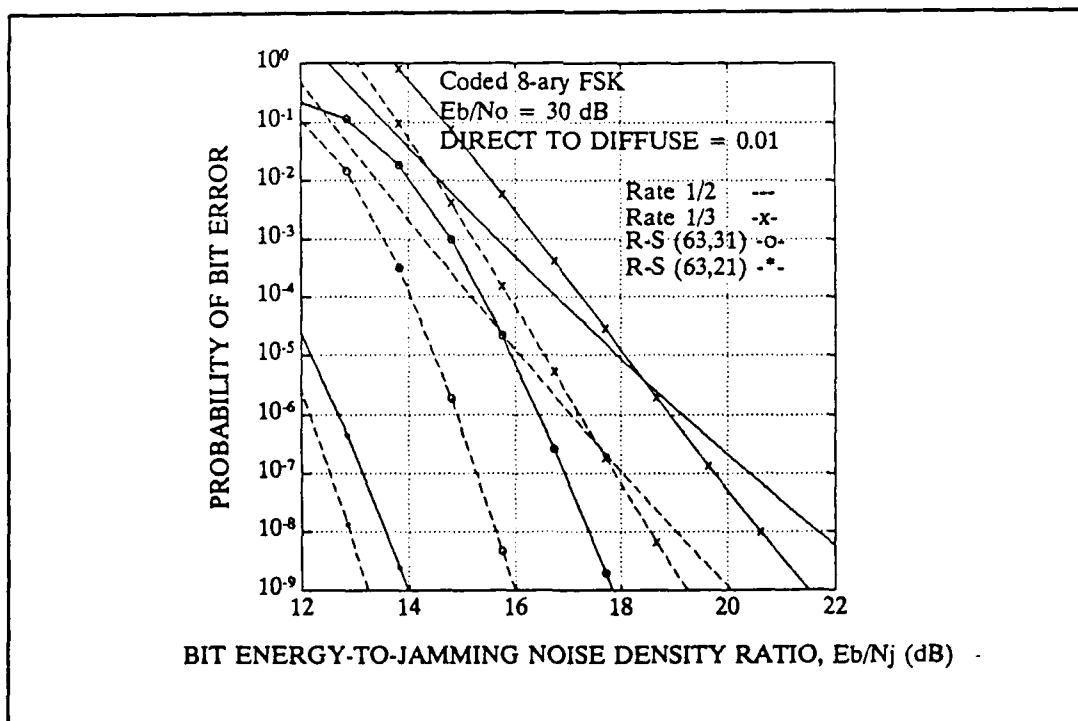


Figure C.59 Coded Performance for 8-ary FSK in a deeply-faded Rayleigh channel with $E_b/N_o = 30$ dB.

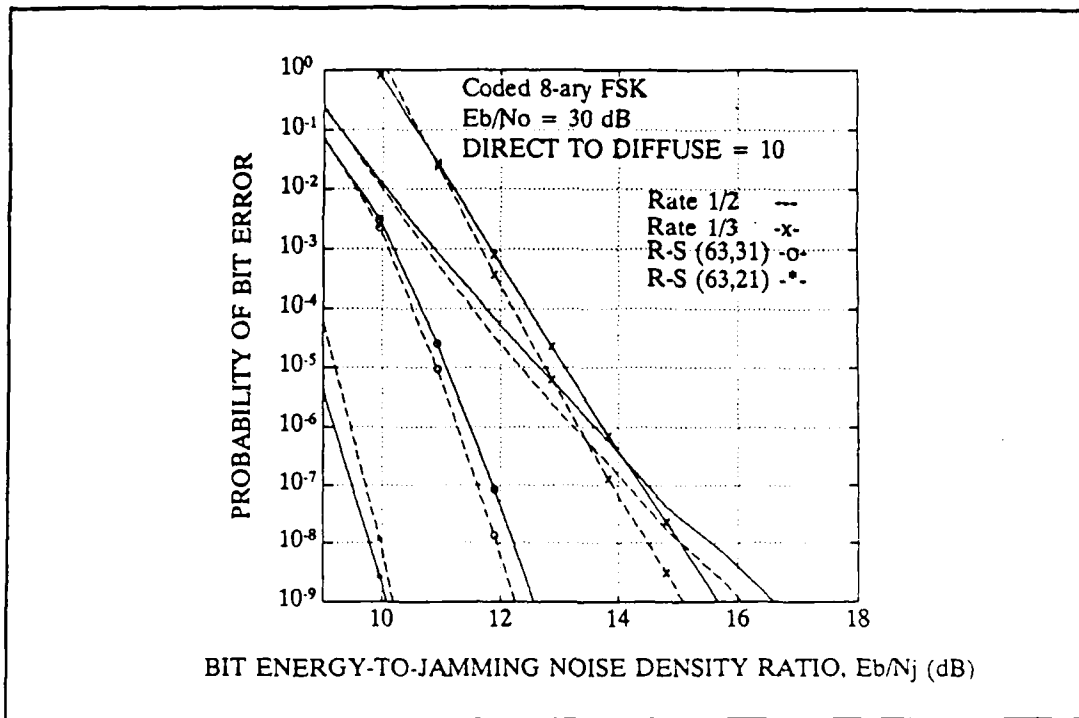


Figure C.60 Coded Performance for 8-ary FSK in a Rician channel with $E_b/N_o = 30$ dB.

REFERENCES

1. Ha, T. T., *Digital Satellite Communications*, Macmillan Publishing Co., New York, NY, 1986.
2. Ha, T. T. and Myers, G. A., *System Analysis of a Tactical Multi-Satellite Communication System*, Technical Report to be published, Naval Postgraduate School, Monterey, CA, 1990.
3. Proakis, J. G., *Digital Communications*, McGraw-Hill Book Co., New York, NY, 1983.
4. Whalen, A. D., *Detection of Signals in Noise*, Academic Press, Inc., Harcourt, Brace, Jovanovich Publishing Co., San Diego, CA, 1971.
5. Ziemer, R. E. and Peterson, R. L., *Digital Communications and Spread Spectrum Systems*, Macmillan Publishing Co., New York, NY, 1985.
6. Sklar, B., *Digital Communications Fundamentals and Applications*, Prentice Hall Inc., Englewood Cliffs, NJ, 1988.
7. Lin, S. and Costello, D. J., *Error Control Coding*, Prentice Hall Inc., Englewood Cliffs, NJ, 1983.
8. Lee, J. S., French, R. H., and Miller, L. E., "The Analyses of Uncoded Performances for Certain ECCM Receiver Design Strategies for Multihops/Symbol FH/MFSK Waveforms", *IEEE Journal on Sel. Areas in Comms.*, vol. SAC-3, no. 5, pp. 611-620, September 1985.
9. Miller, L. E., Lee, J. S. and Kadrichu, A. P., "Probablility of Error Analysis of a BFSK Frequency-Hopped System with Diversity Under Partial-Band Jamming Interference - Part III: Performance of a Square-Law Self-Normalizing Soft Decision Receiver", *IEEE Trans. on Comms.*, vol. 34, no. 7, pp. 669-675, July 1986.
10. Simon, M. K., Omura, J. K., et.al., *Spread Spectrum Commnications*, Computer Science Press, Rockville, MD, 1985.
11. Peebles P. Z., *Probability, Random Variables, and Random Signal Principles*, MacGraw-Hill Book Co., New York, NY, 1987.
12. Strum, R. D. and Kirk, D. E., *First Principles of Discrete Systems and Digital Signal Processing*, Addison-Wesley Publishing Co., Reading, MA, 1988.

13. Stark, W. E, "Coding for Frequency-Hopped Spread Spectrum Communication with Partial-Band Interference - Part I. Capacity and Cutoff Rate", *IEEE Trans. on Comms.*, vol. COM-33, no. 10, pp. 1045-1057, October 1985.
14. Lee, J. S., French, R. H., and Miller, L. E., "Error-Correcting Codes and Nonlinear Diversity Combining Against Worst-Case Partial-Band Noise Jamming of FH-MFSK Systems", *IEEE Trans. on Comms.*, vol. 36, no. 4, pp. 471-478, April 1988.
15. Odenwalder, J. P., "Optimal Decoding of Convolutional Codes", Ph.D Dissertation, University of California, Los Angeles, 1970, Univ. Microfilm # 70-19,875.
16. Robertson, R. C., "Error Probabilities of Frequency Hop MFSK with Noise-Normalization Combining in a Fading Channel with Partial-Band Interference", Technical Paper to be Published, Naval Postgraduate School, Monterey, CA, 1990.
17. Luke, Y. L., *Integrals of Bessel Functions*, MacGraw-Hill Publishing Co., New York, NY, 1962.
18. Gradshteyn, I. S. and Ryzhik, I. M., *Table of Integrals, Series and Products*, Academic Press, Inc., Harcourt, Brace, Jovanovich Publishing Co., San Diego, CA, 1980.

INITIAL DISTRIBUTION LIST

	No. Copies
1. Defense Technical Information Center Cameron Station Alexandria, VA 22304-6145	2
2. Library, Code 0142 Naval Postgraduate School Monterey, CA 93942-5000	2
3. Chairman, Code EC Department of Electrical and Computer Engineering Naval Postgraduate School Monterey, CA 93943-5000	1
4. Commander Naval Space Command Attn: Code N3 Dahlgren, VA 22448	1
5. Commander US Army Signal School and Fort Gordon Attn: Proponency Office Fort Gordon, GA 30907	1
6. Professor Tri T. Ha, Code EC/Ha Department of Electrical and Computer Engineering Naval Postgraduate School Monterey, CA 93943-5000	5
7. Professor Glen A. Myers, Code EC/Mv Department of Electrical and Computer Engineering Naval Postgraduate School Monterey, CA 93943-5000	1
8. Professor R. Clark Robertson, Code EC/Rc Department of Electrical and Computer Engineering Naval Postgraduate School Monterey, CA 93943-5000	2
9. Captain Michael W. Briske USAISEC-FE (Korea) APO, SF 96301-0075	2